



**NAVAL  
POSTGRADUATE  
SCHOOL**

**MONTEREY, CALIFORNIA**

**THESIS**

**REAL-TIME OPTIMAL SLEW MANEUVER DESIGN AND  
CONTROL**

by

Andrew Fleming

December 2004

Thesis Advisor:  
Second Reader:

I. Michael Ross  
Barry Leonard

**Approved for public release; distribution is unlimited.**

THIS PAGE INTENTIONALLY LEFT BLANK

REPORT DOCUMENTATION PAGE			Form Approved OMB No. 0704-0188	
Public reporting burden for this collection of information is estimated to average 1 hour per response, including the time for reviewing instruction, searching existing data sources, gathering and maintaining the data needed, and completing and reviewing the collection of information. Send comments regarding this burden estimate or any other aspect of this collection of information, including suggestions for reducing this burden, to Washington headquarters Services, Directorate for Information Operations and Reports, 1215 Jefferson Davis Highway, Suite 1204, Arlington, VA 22202-4302, and to the Office of Management and Budget, Paperwork Reduction Project (0704-0188) Washington DC 20503.				
1. AGENCY USE ONLY (Leave blank)		2. REPORT DATE December 2004	3. REPORT TYPE AND DATES COVERED Engineer's Thesis	
4. TITLE AND SUBTITLE Title (Mix case letters) Real-time Optimal Slew Maneuver Design and Control			5. FUNDING NUMBERS	
6. AUTHOR(S) Andrew Fleming			8. PERFORMING ORGANIZATION REPORT NUMBER	
7. PERFORMING ORGANIZATION NAME(S) AND ADDRESS(ES) Naval Postgraduate School Monterey, CA 93943-5000			10. SPONSORING/MONITORING AGENCY REPORT NUMBER	
9. SPONSORING /MONITORING AGENCY NAME(S) AND ADDRESS(ES) N/A			11. SUPPLEMENTARY NOTES The views expressed in this thesis are those of the author and do not reflect the official policy or position of the Department of Defense or the U.S. Government.	
12a. DISTRIBUTION / AVAILABILITY STATEMENT Approved for public release; distribution is unlimited.			12b. DISTRIBUTION CODE	
13. ABSTRACT (maximum 200 words) This thesis considers the problem of time-optimal spacecraft slew maneuvers. Since the work of Bilimoria and Wie it has been known that the time-optimal reorientation of a symmetric rigid body was not the eigenaxis maneuver once thought to be correct. Here, this concept is extended to axisymmetric and asymmetric rigid body reorientations with idealized independent torque generating devices. The premise that the time-optimal maneuver is not, in general, an eigenaxis maneuver, is shown to hold for all spacecraft configurations. The methodology is then extended to include spacecraft control systems employing magnetic torque rods, a combination of pitch bias wheel with magnetic torque rods, and finally to control systems employing single gimbal control moment gyros. The resulting control solutions, designed within the limitations of the actuators, eliminate the requirement to avoid actuator singularities. Finally, by employing sampled-state feedback the viability of real-time optimal closed loop control is demonstrated.				
14. SUBJECT TERMS Optimal Control, Time-optimal Control, Real-time Optimal Control, Slew Maneuver Optimization, DIDO, Dynamic Optimization, Sampled-data Feedback Control			15. NUMBER OF PAGES 179	
			16. PRICE CODE	
17. SECURITY CLASSIFICATION OF REPORT Unclassified	18. SECURITY CLASSIFICATION OF THIS PAGE Unclassified	19. SECURITY CLASSIFICATION OF ABSTRACT Unclassified	20. LIMITATION OF ABSTRACT UL	

NSN 7540-01-280-5500

Standard Form 298 (Rev. 2-89)  
Prescribed by ANSI Std. Z39-18

THIS PAGE INTENTIONALLY LEFT BLANK

**Approved for public release; distribution is unlimited**

**REAL-TIME OPTIMAL SLEW MANEUVER DESIGN AND CONTROL**

Andrew Fleming  
Commander, United States Navy  
B.S., Rensselaer Polytechnic Institute, 1988

Submitted in partial fulfillment of the  
requirements for the degree of

**ASTRONAUTICAL ENGINEER  
AND  
MASTER OF SCIENCE IN ASTRONAUTICAL ENGINEERING**

from the

**NAVAL POSTGRADUATE SCHOOL  
December 2004**

Author: Andrew Fleming

Approved by: I. Michael Ross  
Thesis Advisor

Barry Leonard  
Second Reader

Anthony J. Healey  
Chairman  
Department of Mechanical and Astronautical  
Engineering

THIS PAGE INTENTIONALLY LEFT BLANK

## **ABSTRACT**

This thesis considers the problem of time-optimal spacecraft slew maneuvers. Since the work of Bilimoria and Wie it has been known that the time-optimal reorientation of a symmetric rigid body was not the eigenaxis maneuver once thought to be correct. Here, this concept is extended to axisymmetric and asymmetric rigid body reorientations with idealized independent torque generating devices. The premise that the time-optimal maneuver is not, in general, an eigenaxis maneuver, is shown to hold for all spacecraft configurations. The methodology is then extended to include spacecraft control systems employing magnetic torque rods, a combination of pitch bias wheel with magnetic torque rods, and finally to control systems employing single gimbal control moment gyros. The resulting control solutions, designed within the limitations of the actuators, eliminate the requirement to avoid actuator singularities. Finally, by employing sampled-state feedback the viability of real-time optimal closed loop control is demonstrated.

THIS PAGE INTENTIONALLY LEFT BLANK

# TABLE OF CONTENTS

I.	INTRODUCTION.....	1
	A. MOTIVATION .....	1
	B. THE PROBLEM.....	1
	C. HISTORICAL BACKGROUND .....	2
	D. CONCLUSION .....	3
II.	OPTIMAL CONTROL PROBLEM FORMULATION .....	5
	A. INTRODUCTION.....	5
	B. METHODOLOGY .....	5
	C. OPTIMAL CONTROL PROBLEM FORMULATION .....	6
III.	IDEALIZED TORQUE ACTUATOR CONTROL PROBLEM.....	11
	A. INTRODUCTION.....	11
	B. INERTIALLY SYMMETRIC RIGID-BODIES.....	11
	1. Notation and Transformations .....	12
	2. Problem Formulation .....	14
	2. Time Optimal Maneuvers .....	18
	3. Numerical Considerations and Notes .....	28
	4. Conclusions .....	30
	C. AXISYMMETRIC SPACECRAFT REORIENTATIONS .....	30
	1. Problem Formulation .....	31
	2. Time Optimal Maneuvers .....	33
	a. <i>Non-spinning Axisymmetric Reorientations About             the Axis of Symmetry .....</i>	<i>33</i>
	b. <i>Non-spinning Axisymmetric Reorientations of the             Axis of Symmetry.....</i>	<i>43</i>
	c. <i>Reorientations of the Spinning Axis of Symmetry ...</i>	<i>45</i>
	3. Numerical Considerations and Notes .....	54
	4. Conclusions .....	54
	D. ASYMMETRIC SPACECRAFT REORIENTATION MANEUVERS....	54
	1. Problem Formulation .....	55
	2. Time Optimal Maneuvers .....	56
	3. Numerical Considerations and Notes .....	64
	4. Conclusions .....	65
IV.	MAGNETIC TORQUE CONTROL .....	69
	A. INTRODUCTION.....	69
	B. BASIC MAGNETIC TORQUE ATTITUDE CONTROL .....	69
	C. TIME-OPTIMAL MAGNETIC TORQUE CONTROLLED SLEW.....	73
	1. Problem Formulation .....	73
	2. Solving the Optimal Control Problem .....	75
	a. <i>Hamiltonian Minimization .....</i>	<i>76</i>
	b. <i>Hamiltonian Evolution and Final Value.....</i>	<i>77</i>

3.	Numerical Results .....	78
4.	Numerical Considerations and Scaling .....	85
5.	Conclusions .....	86
V.	NPSAT 1 CONTROL SYSTEM.....	89
A.	INTRODUCTION.....	89
B.	PROBLEM FORMULATION.....	90
C.	TIME-OPTIMAL NPSAT 1 SLEW.....	92
1.	Problem Statement.....	93
2.	Solving the Optimal Control Problem .....	95
3.	Numerical Results .....	96
4.	Numerical Considerations and Scaling .....	105
5.	Conclusions .....	105
VI.	CONTROL MOMENT GYRO CONTROL SYSTEMS.....	107
A.	INTRODUCTION.....	107
B.	CONTROL MOMENT GYRO BASICS.....	107
C.	PROBLEM FORMULATION.....	108
D.	CMG TIME-OPTIMAL SLEW MANEUVERS.....	111
1.	Problem Statement.....	112
2.	Solving the Optimal Control Problem .....	113
3.	Numerical Results .....	115
4.	Numerical Considerations.....	124
5.	Conclusions .....	125
VII.	CLOSED LOOP CONTROL .....	127
A.	INTRODUCTION.....	127
B.	CLASSICAL CLOSED LOOP CONTROL .....	127
1.	Error Signal Command Generation.....	128
2.	Singularity Issues .....	129
C.	BELLMAN'S PRINCIPLE OF OPTIMALITY.....	134
D.	REAL-TIME OPTIMAL CONTROL.....	138
1.	Asymmetric Spacecraft with Idealized Actuator Control..	138
a.	<i>Numerical Considerations and Notes .....</i>	<i>148</i>
2.	Asymmetric Spacecraft with Magnetic Torque Rod Control.....	148
E.	CONCLUSIONS.....	154
VIII.	FUTURE WORK .....	157
A.	ALGORITHM IMPROVEMENT AND OPTIMIZATION .....	157
B.	COMPUTATIONAL DELAY MODELING .....	158
C.	EXTENSION TO HARDWARE.....	159
	INITIAL DISTRIBUTION LIST .....	161

## LIST OF FIGURES

Figure 1	Inertial Symmetric Body .....	14
Figure 2	Inertial Symmetric Quaternion Solution .....	21
Figure 3	Inertial Symmetric Angular Rate Solution .....	21
Figure 4	Inertial Symmetric Quaternion Transformed Solution .....	22
Figure 5	Inertial Symmetric Angular Rate Transformed Solution.....	22
Figure 6	Inertial Symmetric Optimal Control Solution.....	23
Figure 7	Quaternion Propagated Solution.....	24
Figure 8	Angular Rate Propagated Solution.....	24
Figure 9	Inertial Symmetric Spacecraft Control and Switching Function About X-body Axis .....	25
Figure 10	Inertial Symmetric Spacecraft Control and Switching Function About Y-body Axis .....	26
Figure 11	Inertial Symmetric Spacecraft Control and Switching Function About Z-body Axis.....	26
Figure 12	Inertial Symmetric Problem Hamiltonian Evolution.....	28
Figure 13	Inertial Axisymmetric Body.....	31
Figure 14	Case 1 – Axisymmetric Spacecraft Time-optimal Control Solution .....	35
Figure 15	Case I – Axisymmetric Spacecraft Time-Optimal Quaternion History.	36
Figure 16	Case I – Axisymmetric Spacecraft Time-Optimal Angular Rate History.....	36
Figure 17	Axisymmetric Spacecraft Quaternion Solution Validation by Propagation.....	37
Figure 18	Axisymmetric Spacecraft Angular Rate Solution Validation.....	37
Figure 19	Axisymmetric Spacecraft x-axis Switching Structure and Control .....	38
Figure 20	Axisymmetric Spacecraft y-axis Switching Structure and Control .....	39
Figure 21	Axisymmetric Spacecraft z-axis Switching Structure and Control .....	39
Figure 22	Case 1 – Axisymmetric Hamiltonian Evolution and Transversality.....	40
Figure 23	Constant Mass Prolate Spacecraft Moment of Inertia versus Length of Symmetry Axis .....	41
Figure 24	Axisymmetric Reorientation Maneuvers About Symmetry Axis versus Symmetry Axis Length .....	42
Figure 25	Prolate Axisymmetric Spacecraft Case III – Switching function.....	43
Figure 26	Axisymmetric Spacecraft Optimal Control Solution for X-axis Large Angle Rotation (135 Degree Rotation) .....	44
Figure 27	Axisymmetric Spacecraft Optimal Control Solution for X-axis Small Angle Rotation (60 Degree Rotation) .....	44
Figure 28	Angular Rate History for Constant Spin Rate Time-optimal Maneuver.....	47
Figure 29	Time Histories of $w_1$ and $w_2$ for Constant Spin Time-optimal Maneuver.....	48

Figure 30	Angular Rate History for Time-optimal Spinning Reorientation Maneuver.....	48
Figure 31	Time Histories of $w_1$ and $w_2$ for Spinning Spacecraft Time-optimal Maneuver.....	49
Figure 32	Spinning Axisymmetric Spacecraft Time-optimal Control Solution.....	50
Figure 33	Spinning Axisymmetric Spacecraft Angular Rate Solution Validation by Propagation.....	50
Figure 34	Spinning Axisymmetric Spacecraft W History Solution Validation by Propagation.....	51
Figure 35	Spinning Axisymmetric Spacecraft X-axis Switching Function and Normalized Control.....	52
Figure 36	Spinning Axisymmetric Spacecraft Y-axis Switching Function and Normalized Control.....	52
Figure 37	Spinning Axisymmetric Spacecraft Z-axis Switching Function and Normalized Control.....	53
Figure 38	Spinning Axisymmetric Spacecraft Time-optimal Solution Hamiltonian.....	53
Figure 39	Asymmetric Spacecraft Time-optimal Maneuver Control Solution.....	59
Figure 40	Asymmetric Spacecraft Time-optimal Maneuver Quaternion History..	60
Figure 41	Asymmetric Spacecraft Time-optimal Maneuver Angular Rate History.....	60
Figure 42	Asymmetric Spacecraft Quaternion Solution Validation by Propagation.....	61
Figure 43	Asymmetric Spacecraft Angular Rate Solution Validation by Propagation.....	61
Figure 44	Asymmetric Spacecraft X-axis Switching Function and Control Solution.....	62
Figure 45	Asymmetric Spacecraft Y-axis Switching Function and Control Solution.....	62
Figure 46	Asymmetric Spacecraft Z-axis Switching Function and Control Solution.....	63
Figure 47	Asymmetric Spacecraft Time-optimal Hamiltonian Evolution and Transversality.....	64
Figure 48	Earth Magnetic Field.....	71
Figure 49	Time-optimal Control Solution for Magnetic Torque Problem.....	79
Figure 50	Quaternion Solution and Validation by Propagation.....	80
Figure 51	Angular Rate Solution and Validation by Propagation.....	81
Figure 52	Magnetic Torque Slew Time-optimal Quaternion History.....	81
Figure 53	Magnetic Torque Slew Time-optimal Angular Rate History.....	82
Figure 54	Magnetic Torque Control X-axis Switching Function and Control Solution.....	82
Figure 55	Magnetic Torque Control Y-axis Switching Function and Control Solution.....	83
Figure 56	Magnetic Torque Control Z-axis Switching Function and Control Solution.....	83

Figure 57	Magnetic Torque Solution Hamiltonian and Final Value .....	84
Figure 58	Constant Magnetic Field Approximation Hamiltonian Solution.....	85
Figure 59	NPSAT1 Conceptual Image courtesy of Dan Sakoda .....	89
Figure 60	NPSAT 1 Torque Rod & Wheel Time-optimal Control Solution (1) .....	97
Figure 61	NPSAT 1 Pitch Wheel Torque Time-optimal Control Solution (2).....	97
Figure 62	Quaternion Solution and Validation by Propagation .....	98
Figure 63	Angular Rate Solution and Validation by Propagation.....	99
Figure 64	Pitch Wheel Momentum Solution and Validation by Propagation.....	99
Figure 65	NPSAT 1 Slew Time-optimal Quaternion History .....	100
Figure 66	NPSAT 1 Slew Time-optimal Angular Rate History.....	100
Figure 67	NPSAT 1 Slew Time-optimal Pitch Wheel Angular Momentum History.....	101
Figure 68	NPSAT 1 Control Switching Function and Control Solution (1).....	101
Figure 69	NPSAT 1 Control Switching Function and Control Solution (2).....	102
Figure 70	NPSAT 1 Control Switching Function and Control Solution (3).....	102
Figure 71	NPSAT 1 Control Switching Function and Control Solution (4).....	103
Figure 72	NPSAT 1 Torque Rod & Wheel Problem Hamiltonian Evolution .....	104
Figure 73	NPSAT 1 Control Switching Function for Wheel Torque (Close up) .	104
Figure 74	Single-Gimbal Control Moment Gyro (After Ref.[5]).....	107
Figure 75	Pyramid Mounting Arrangement of Four Single Gimbal CMGs (from Ref.[8]) .....	110
Figure 76	CMG Time-optimal Control Solution.....	117
Figure 77	CMG Solution Quaternion History Validation by Propagation .....	117
Figure 78	CMG Solution Angular Rate History Validation by Propagation.....	118
Figure 79	CMG Solution Gimbal Angle History Validation by Propagation .....	118
Figure 80	CMG Slew Time-optimal Quaternion History.....	119
Figure 81	CMG Slew Time-optimal Angular Rate History.....	119
Figure 82	CMG Slew Time-optimal Gimbal Angle History .....	120
Figure 83	CMG Control Switching Function and Control Solution.....	121
Figure 84	CMG Control Switching Function and Control Solution (2).....	121
Figure 85	CMG Control Switching Function and Control Solution (3).....	122
Figure 86	CMG Control Switching Function and Control Solution (4).....	122
Figure 87	CMG Time-optimal Slew Solution Hamiltonian.....	123
Figure 88	Condition Number of CMG Control Solution Jacobian Matrix .....	124
Figure 89	Classic Closed Loop Spacecraft Attitude Control System.....	128
Figure 90	Asymmetric Eigenaxis Rotation Torque Control Solution.....	130
Figure 91	Spacecraft Model with CMG Actuators.....	131
Figure 92	Condition Number of CMG Jacobian Matrix with Independent Torque Solution .....	132
Figure 93	Gimbal Angle Rates From Pseudoinverse Steering Logic .....	132
Figure 94	Gimbal Angle Rates from Pseudoinverse Steering Logic (Close-up)	133
Figure 95	Principle of Optimality.....	135
Figure 96	Asymmetric Time-optimal Quaternion Solution – Bellman’s Principle of Optimality .....	136
Figure 97	Effect of Increasing Nodes on Quaternion Solution .....	137

Figure 98	Closed Loop Simulation Model .....	138
Figure 99	Asymmetric Spacecraft Time-optimal State Solution and Propagation.....	139
Figure 100	Asymmetric Spacecraft Quaternion Propagation Interval 1 .....	140
Figure 101	Asymmetric Spacecraft Angular Rate Propagation Interval 1 .....	140
Figure 102	Asymmetric Spacecraft Quaternion Propagation Interval 2 .....	141
Figure 103	Asymmetric Spacecraft Angular Rate Propagation Interval 2 .....	141
Figure 104	Asymmetric Spacecraft Quaternion Propagation Interval 3 .....	142
Figure 105	Asymmetric Spacecraft Angular Rate Propagation Interval 3 .....	142
Figure 106	Asymmetric Spacecraft Quaternion Propagation Interval 4 .....	143
Figure 107	Asymmetric Spacecraft Angular Rate Propagation Interval 4 .....	143
Figure 108	Asymmetric Spacecraft Quaternion Propagation Interval 5 .....	144
Figure 109	Asymmetric Spacecraft Angular Rate Propagation Interval 5 .....	144
Figure 110	Asymmetric Spacecraft Quaternion Propagation Interval 6 .....	145
Figure 111	Asymmetric Spacecraft Angular Rate Propagation Interval 6 .....	145
Figure 112	Asymmetric Spacecraft Quaternion Propagation Interval 7 .....	146
Figure 113	Asymmetric Spacecraft Angular Rate Propagation Interval 7 .....	146
Figure 114	Asymmetric Spacecraft Idealized Actuator Time-optimal Solution Computation Time.....	147
Figure 115	Magnetic Torque Open Loop Solution Propagated with Disturbance Torque .....	149
Figure 116	Magnetic Torque Open Loop Solution Propagated with Disturbance Torque (2).....	150
Figure 117	Magnetic Torque Quaternion Propagation Interval 2 .....	152
Figure 118	Magnetic Torque Quaternion Propagation – Maneuver Completion .	152
Figure 119	Magnetic Torque Angular Rate Propagation – Maneuver Completion .....	153
Figure 120	Magnetic Torque Time-optimal Maneuver Computation Time .....	154
Figure 121	Conceptual Computational Delay Model.....	158

## LIST OF TABLES

Table 1	Comparison of symmetric spacecraft reorientation time for time-optimal and eigenaxis maneuvers .....	29
Table 2	Cost reduction for inertial symmetric time-optimal reorientations over eigenaxis maneuvers.....	30
Table 3	Prolate Spacecraft Characteristics .....	34
Table 4	Asymmetric Maneuver Comparison.....	64
Table 5	NPSAT 1 Parameters for Numerical Simulations .....	79
Table 6	Effects of Scaling on Solution Fidelity.....	86
Table 7	NPSAT 1 Simulation Component Characteristics.....	92
Table 8	Simulated CMG Characteristics.....	115
Table 9	Bellman Principle Effect on Computational Time.....	137
Table 10	State Trajectory Propagation Error with Disturbance.....	150
Table 11	Closed Loop State Propagation Results .....	153

THIS PAGE INTENTIONALLY LEFT BLANK

## **ACKNOWLEDGMENTS**

I would be remiss if I did not acknowledge the help and support of my family and friends. Without whose constant support and direction this work would not have been possible.

To my wife and son who, without complaint, gave up countless hours of time we could have spent together. Not many men are lucky enough to have a wife who is both beautiful and a talented mechanical engineer, nor a son who patiently accepts homework as a reason dad can't play until later.

To Dr. Mike Ross, my advisor, who tolerated my numerous logical leaps and missteps. Your unlimited patience and sense of humor made this an enjoyable experience.

THIS PAGE INTENTIONALLY LEFT BLANK

# I. INTRODUCTION

## A. MOTIVATION

Modern satellites require more precision and agility than ever before. In both military and commercial applications the ability to rapidly maneuver represents an increase in mission effectiveness and productivity. Rapid retargeting maneuvers translate directly into more time on the intended object and more observations per orbit. With commercial Earth-imaging satellites like Ikonos and research into agile microsattellites<sup>1</sup> on the rise, the need for time-optimal satellite control is greater than ever. Planned future satellite missions in support of missile-defense and Earth observation will rely on satellite agility and minimum-time maneuvers for mission success.

## B. THE PROBLEM

Spacecraft time-optimal attitude maneuvers have held the interest of engineers and mathematicians for decades. In their paper, "Survey of Time-Optimal Attitude Maneuvers," Scrivener and Thompson provide a summary of work in this and related areas<sup>2</sup>. They also present the principal difficulties associated with solving the time-optimal attitude maneuver problem.

Unlike the pointing problem which lends itself well to linearization techniques, slew problems, especially large angle slew maneuvers are highly nonlinear. Euler's equations, which represent the rotational motion of a rigid body, consist of three, coupled, nonlinear differential equations.

$$I_x \dot{w}_x + (I_z - I_y) w_z w_y = u_1$$

$$I_y \dot{w}_y + (I_x - I_z) w_x w_z = u_2$$

$$I_z \dot{w}_z + (I_y - I_x) w_y w_x = u_3$$

Additionally, the high angular velocities associated with time-optimal maneuvering cause significant gyroscopic stiffness through the non-linear terms.

While these equations completely describe the rotational motion of the body with respect to an inertial frame they do not determine the spacecraft's attitude. To describe the attitude of the spacecraft Euler parameters are generally used since they provide singularity free kinematics:

$$\begin{bmatrix} \dot{q}_1 \\ \dot{q}_2 \\ \dot{q}_3 \\ \dot{q}_4 \end{bmatrix} = \frac{1}{2} \begin{bmatrix} 0 & w_1 & -w_2 & w_3 \\ -w_3 & 0 & w_1 & w_2 \\ w_2 & -w_1 & 0 & w_3 \\ -w_1 & -w_2 & -w_3 & 0 \end{bmatrix} \begin{bmatrix} q_1 \\ q_2 \\ q_3 \\ q_4 \end{bmatrix}$$

These non-linear ordinary differential equations have no closed-form solutions except for a small number of cases involving simple rotations or simple geometry (i.e., torque free motion of an axisymmetric body<sup>3,4</sup>).

The time-optimal nature of the problem adds additional difficulties. Major problems are encountered in solving the boundary value problem that arises from the application of the Minimum Principle. The problem, formulated in Chapter II, has no known numerical or analytical solution except when certain restrictions are applied. These assumptions have taken the form of specific configurations or restricted motions<sup>5</sup>.

### C. HISTORICAL BACKGROUND

A short summary of the historical work that influenced this research is presented here. Beginning with their landmark work in 1993, Bilimoria and Wie demonstrated with extensive analytical modeling and numerical analysis that the time-optimal maneuver was not the long-assumed eigenaxis maneuver<sup>6</sup>. Their methods and results are examined in detail in Chapter III. Bilimoria and Wie later extended this work to an axisymmetric body and observed the same characteristic precession they had noted earlier<sup>7</sup>. Beyers and Vadali<sup>8</sup> reproduced the results of Bilimoria and Wie but focused on developing a control algorithm. They used linearization and the switch time optimization (STO) algorithm developed by Meier and Bryson<sup>9</sup> to produce an algorithm that could be implemented in real-time.

In the context of magnetic control, Junkins et al.<sup>10</sup> modeled a single controller aligned with the spin axis of a spin-stabilized symmetric spacecraft. The time-optimal solutions were found through an interactive graphical technique. These results were eventually implemented for open loop control on the NOVA-1 spacecraft<sup>11</sup>.

#### **D. CONCLUSION**

Solving the problem of spacecraft time-optimal control has occupied the interest of engineers and mathematicians for years. The problem is simple to formulate and yet solutions have been difficult to obtain. In this thesis we extend the present body of work to all spacecraft moment of inertia configurations. The ideal actuators often studied to simplify the problem formulation are replaced with magnetic torque rods and a combination of torque rods and a pitch-bias wheel. Finally, the control moment gyro configuration most studied for its singularity problems is examined and shown to be singularity free in the time-optimal result. This unpredicted benefit of the formulation has the potential to make future work in actuator singularity avoidance moot. Finally, computational speeds are shown to be such so as to allow time-optimal solutions to the nonlinear plant to be generated in real-time.

---

## ENDNOTES

<sup>1</sup> Lappas, V.J. (2003). "Experimental Testing of a CMG Cluster for Agile Microsatellites." *Proceedings of the 54<sup>th</sup> International Congress of the International Astronautical Federation, the International Academy of Astronautics and the International Institute of Space Law*. 29 September – 03 October, Bremen, Germany.

<sup>2</sup> Scrivener, S.L., and Thompson, R.C. (1994). "Survey of Time-Optimal Attitude Maneuvers." *The Journal of Guidance, Control, and Dynamics*, Vol. 17, No. 2. American Institute of Aeronautic and Astronautics. Reston, VA.

<sup>3</sup> Ibid.

<sup>4</sup> Wiesel, W.E. (1997). *Spaceflight Dynamics*. Irwin/McGraw-Hill. Boston, MA.

<sup>5</sup> Scrivener, S.L., and Thompson, R.C. (1994). "Survey of Time-Optimal Attitude Maneuvers." *The Journal of Guidance, Control, and Dynamics*, Vol. 17, No. 2. American Institute of Aeronautic and Astronautics. Reston, VA.

<sup>6</sup> Bilimoria, K.D. and Wie, B. (1993). "Time-Optimal Reorientation of Rigid Spacecraft." *The Journal of Guidance, Control, and Dynamics*, Vol. 16, No. 3. American Institute of Aeronautic and Astronautics. Reston, VA.

<sup>7</sup> Bilimoria, K.D., and Wie, B. (1993). "Time-Optimal Reorientation of a Rigid Axisymmetric Spacecraft." *Proceedings of the AIAA Guidance, Navigation, and Control Conference*. AIAA Paper No. 91-2644

<sup>8</sup> Beyers, R.M., and Vadali, S.R. (1993). "Quasi-Closed Form Solution to the Time-Optimal Rigid Spacecraft Reorientation Problem." *The Journal of Guidance, Control, and Dynamics*, Vol. 16, No. 3. American Institute of Aeronautic and Astronautics. Reston, VA.

<sup>9</sup> Meier, E.B. and Bryson, A.E. (1990). "Efficient Algorithm for Time Optimal Control of a Two-Link Manipulator," *Journal of Guidance, Control, and Dynamics*, Vol. 13, No. 5. American Institute of Aeronautic and Astronautics. Reston, VA.

<sup>10</sup> Junkins, J.L., Carrington, C., and Williams, C. (1981). "Time Optimal Magnetic Attitude Maneuvers." *The Journal of Guidance and Control*, Vol. 4, No. 4. American Institute of Aeronautic and Astronautics. Reston, VA.

<sup>11</sup> Junkins, J.L., and Turner, J.D. (1986). *Optimal Spacecraft Rotational Maneuvers*. Elsevier Publishing, New York, NY.

## **II. OPTIMAL CONTROL PROBLEM FORMULATION**

### **A. INTRODUCTION**

In this section the optimal control problem formulation is developed. This formulation will be referred to throughout the remainder of this work. There are numerous excellent books and papers on optimal control theory which explain these concepts in much greater detail. Interested readers are referred to the references [1, 2, 3, & 4] for further information.

### **B. METHODOLOGY**

Over the years many different methods of solving optimal control problems have been developed. These are broadly grouped into two categories: indirect and direct methods. In indirect methods, the necessary conditions for optimality are derived from Pontryagin's Minimum Principle and solved to obtain the optimal trajectory. These methods are notoriously labor intensive. In direct methods, the optimal control problem is discretized into a parameter optimization problem. The resulting nonlinear programming problem can then be solved by standard nonlinear programming means.

In this work we will employ a Legendre Pseudospectral method encoded in the reusable software package DIDO<sup>5</sup>. Pseudospectral methods are well known in the field of fluid dynamics where they are used to numerically solve partial differential equations. Unlike other methods which employ piecewise-continuous polynomials Pseudospectral methods are unique in their application of global orthogonal polynomials as trial functions.

In the Legendre Pseudospectral method the time domain of the problem is discretized at a special set of Legendre-Gauss-Lobatto (LGL) points. Polynomial approximations of the state and control variables are considered where Lagrange polynomials are the trial functions and the unknown coefficients are the values of the state and control variables at the LGL points (nodes). Using the properties of the Lagrange polynomials the nonlinear differential state equations are

transformed to nonlinear algebraic equations. These equations are then posed as a nonlinear programming problem and a sparse numerical optimizer is used to solve the problem. In addition, a relationship between the costate variables and the Lagrange multipliers called the Covector Mapping Theorem, allows for determination of the costates at the LGL points<sup>6</sup>. This provides numerical information that is used to validate the solution's optimality. Interested readers should refer to references 7, 8, 9, and 10 for details regarding Pseudospectral Methods.

Numerical results throughout this work are specified in terms of the number of LGL points used to obtain the solution. Initial solutions were generally based on 30 LGL points with initial guesses restricted to two vectors representing the initial and final conditions. Initial control solution guesses were arbitrary. Where greater accuracy was desired the 30 LGL point state and control solution was used as a guess for a second solution based on 100 LGL points.

### C. OPTIMAL CONTROL PROBLEM FORMULATION

In an attempt to develop the notation and methodology that will be used throughout this work we consider the following optimal control problem. Determine the control function  $\underline{u}^*(t)$  and the corresponding state trajectory  $\underline{x}^*(t)$  that minimize the Bolza cost functional\*

$$J(\underline{x}(\cdot), \underline{u}(\cdot), t_f) = E(\underline{x}(t_f), t_f) + \int_{t_0}^{t_f} F(\underline{x}(t), \underline{u}(t), t) dt$$

where  $\underline{x} \in \mathbb{R}^n$  and  $\underline{u} \in \mathbb{R}^m$  are subject to the differential constraint

$$\dot{\underline{x}} = f(\underline{x}(t), \underline{u}(t)) \quad t \in [t_0, t_f]$$

and the boundary conditions

$$\begin{aligned} \underline{e}_0(\underline{x}(t_0), t_0) &= 0 & \underline{e}_0 &\in \mathbb{R}^p & \text{and } p &\leq n+1 \\ \underline{e}_f(\underline{x}(t_f), t_f) &= 0 & \underline{e}_f &\in \mathbb{R}^q & \text{and } q &\leq n+1 \end{aligned}$$

---

\*  $(\cdot)$  : Functional dependence not specified.

and control inequality constraints of the form

$$\underline{h}(u, t) \leq 0 \quad h \in \mathbb{R}^r$$

where  $\partial h / \partial u$  has full rank.

The Lagrange multiplier theory allows us to adjoin the state equations and constraints to the cost functional to form an augmented cost functional as follows

$$\bar{J} = E(x(t_f), t_f) + \mathbf{u}_0^T \mathbf{e}_0((x(t_0), t_0) + \mathbf{u}_f^T \mathbf{e}_f((x(t_f), t_f) + \int_{t_0}^{t_f} \{F(x, u, t) + \mathbf{I}(t)^T (f(x, u, t) - \dot{x}) + \mathbf{m}(t)^T h(u, t)\} dt$$

Defining the Hamiltonian as,

$$H(\mathbf{I}, x, u, t) = F(x, u, t) + \mathbf{I}^T f(x, u, t)$$

Pontryagin's Minimum Principle provides the following necessary conditions for  $u^*$  to be an optimal control.

$$H(\mathbf{I}^*, x^*, u^*, t) \leq H(\mathbf{I}^*, x^*, u, t) \rightarrow \text{Hamiltonian Minimization}$$

$$\dot{\mathbf{I}}^* = -\frac{\partial H}{\partial x} \rightarrow \text{Adjoint equations}$$

$$\mathbf{I}(t_0) = -\mathbf{u}^T \frac{\partial \mathbf{e}_0}{\partial x_0} \rightarrow \text{Initial transversality}$$

$$\mathbf{I}(t_f) = \frac{\partial E}{\partial x_f} + \mathbf{u}^T \frac{\partial \mathbf{e}_f}{\partial x_f} \rightarrow \text{Terminal transversality}$$

$$H[t_f] + \frac{\partial E}{\partial t} + \mathbf{u}^T \frac{\partial \mathbf{e}_f}{\partial t} = 0 \rightarrow \text{Hamiltonian Value}$$

For the case in which the cost function and constraints are linear in the state and control variables, no minimum exists for the Hamiltonian minimization unless inequality constraints are imposed on the state and/or control variables.<sup>11</sup> In the case, where the inequality constraints are linear and placed only on the control variables the problem is a special case of linear programming problem covered in detail by Bryson<sup>12</sup> and others<sup>13</sup>. The important result is the application of the Karush-Kuhn-Tucker (KKT) Theorem and complementarity conditions. Then, if a minimum exists, it will require the control variable to be at a boundary

of the feasible control region. Since the Hamiltonian is subject to an inequality constraint on the control variable we apply the Karush-Kuhn-Tucker Theorem and form the Lagrangian of the Hamiltonian:

$$\bar{H} = H + \mathbf{m}^T h \quad (2.1)$$

where  $\mathbf{m}_i$  is a KKT multiplier. Then the KKT Theorem gives the following necessary conditions for the optimal trajectory

$$\frac{\partial \bar{H}}{\partial u_i} = \frac{\partial H}{\partial u} + \left( \frac{\partial h}{\partial u} \right)^T \mathbf{m} = 0 \quad (2.2)$$

In addition, the multiplier-constraint pair must satisfy the complementarity conditions of the KKT Theorem which states:

$$\mathbf{m}_i \begin{cases} \leq 0 & h_i(u, t) = h_i^L(t) \\ = 0 & \text{if } h_i^L(t) < h_i(u, t) < h_i^U(t) \\ \geq 0 & h_i(u, t) = h_i^U(t) \\ \text{unrestricted} & h_i^L(t) = h_i^U(t) \end{cases} \quad (2.3)$$

In subsequent chapters, once the state dynamics of the problem have been established, the optimal control problem will be presented in this format. The candidate optimal control solution will then be propagated through the state dynamics to verify the feasibility of the solution. Verifying that this candidate solution is optimal is more difficult. Recall that the Minimum Principle supplies necessary conditions not sufficient conditions for optimality. However, since the Legendre Pseudospectral Method, through the covector mapping theorem, provides costate information at the nodes we can evaluate the necessary conditions for optimality. Where available, results will be compared to published works. Finally, engineering and physical insight will be used to establish that the solutions obtained are optimal.

---

## ENDNOTES

<sup>1</sup> Bryson, Arthur, E. & Ho, Y. (1975). *Applied Optimal Control*. Taylor & Francis Publishing. New York, NY.

<sup>2</sup> Pinch, E.R. (1993). *Optimal Control and the Calculus of Variations*. Oxford Science Publications, Oxford, England.

<sup>3</sup> Kirk, D.E. (1998). *Optimal Control Theory – An Introduction*. Prentice-Hall, Englewood Cliffs, NJ.

<sup>4</sup> Gregory, J. and Lin, C. (1992). *Constrained Optimization in the Calculus of Variations and Optimal Control Theory*. Van Nostrand Reinhold, New York, NY.

<sup>5</sup> Ross, I.M., and Fahroo, F. (2001). "User's Manual for DIDO 2001: A MATLAB Application Package for Dynamic Optimization," Tech. Rep. NPS Technical Report AA-01-003, Department of Aeronautics and Astronautics, Naval Postgraduate School, Monterey, CA.

<sup>6</sup> Fahroo & Ross. (2001). "Costate Estimation by a Legendre Pseudospectral Method," *Journal of Guidance, Control, and Dynamics*, Vol. 24, No. 2. American Institute of Aeronautic and Astronautics. Reston, VA.

<sup>7</sup> Ibid.

<sup>8</sup> Fahroo, F., and Ross, I.M. (2000). "A Spectral Patching Method for Direct Trajectory Optimization," *The Journal of the Astronautical Sciences*, Vol. 48, No. 2/3. American Institute of Aeronautic and Astronautics. Reston, VA.

<sup>9</sup> Fahroo, F., and Ross, I.M. (2001). "A Direct Method for Solving Nonsmooth Optimal Control Problems," *Proceedings of the International Federation on Automatic Control, 15<sup>th</sup> World Congress*, Barcelona, Spain.

<sup>10</sup> Ross, I.M. (2004). "How to Find Minimum Fuel Controllers," *Proceedings of the AIAA Guidance, Navigation, and Control Conference*, Providence, RI. AIAA Paper No. 2004-5346.

<sup>11</sup> Bryson, Arthur, E. & Ho, Y. (1975). *Applied Optimal Control*. Taylor & Francis Publishing. New York, NY.

<sup>12</sup> Ibid.

<sup>13</sup> Stengel, R.F. (1994). *Optimal Control and Estimation*. Dover Publications. New York, NY.

THIS PAGE INTENTIONALLY LEFT BLANK

### III. IDEALIZED TORQUE ACTUATOR CONTROL PROBLEM

#### A. INTRODUCTION

In this section, we develop the time-optimal rotational maneuver for a rigid-body with ideal, bounded actuators. The idealized actuator will be defined by:

$$\text{Torque}_{\text{out}} = [I]u$$

where  $|u| \leq 1$ , is the control vector and  $I$  is the identity matrix. In the case of the ideal actuator, the control vector is equal to the output torque vector. This distinction allows for later definition of the control vector  $u$  as, for example, magnetic dipole moment (See Chapter IV). In this case the actuator is *not* considered ideal. The closest physical approximation to the idealized actuator is a thruster.

Bilimoria and Wie showed that the time-optimal solution for the reorientation of an inertial symmetric body was not necessarily an eigenaxis maneuver.<sup>1</sup> Shen and Tsiotras examined time-optimal reorientations of axisymmetric spacecraft using two controls.<sup>2</sup> Finally, Proulx and Ross examined the control structure and evaluated time-optimal reorientations of asymmetric spacecraft<sup>3</sup>. We begin with a reexamination of the inertial symmetric reorientation problem in order to establish the methodology. Then the principles are extended to axisymmetric and finally to asymmetric spacecraft in the orbital frame.

#### B. INERTIALLY SYMMETRIC RIGID-BODIES

Inertial symmetric rigid-body reorientations represent the simplest problem that we can pose. Yet, prior to the work of Bilimoria and Wie the solution was misunderstood. The eigenaxis maneuver about the control axis was thought to be the time-optimal maneuver for symmetric bodies and near time-optimal for other configurations.<sup>4</sup> Through analytical analysis and numerical simulation

Bilimoria and Wie demonstrated that this was not true for symmetric bodies. They showed that all three control components cannot be simultaneously zero on the time-optimal trajectory.

## 1. Notation and Transformations

In order to progress with the problem formulation we establish the standard notation and rotation sequences used in the development. The spacecraft will have an assumed standard orbit frame defined as:

$Z_o$  – Nadir pointing

$X_o$  – Velocity vector

$Y_o$  – completes the right hand set

We choose the rotation sequence for the body to orbit frame transformation, represented as Euler angles as  $\mathbf{y} \rightarrow \mathbf{q} \rightarrow \mathbf{j}$  with axes order of rotation  $3 \rightarrow 2 \rightarrow 1$ . Therefore,  $\mathbf{y}$  is the first angular rotation about the zbody axis. The second rotation is about the once displaced ybody axis by an angle  $\mathbf{q}$ . The final angular rotation  $\mathbf{j}$  is about the x-body axis.

Then, following the notation convention of Kane<sup>5</sup> the following angular velocities are defined:

$${}^N\bar{\mathbf{w}}_B^b \triangleq \begin{bmatrix} \mathbf{w}_x \\ \mathbf{w}_y \\ \mathbf{w}_z \end{bmatrix} \rightarrow \text{Angular rate of body with respect to inertial in body frame. (3.1)}$$

$${}^N\bar{\mathbf{w}}_O^o \triangleq \begin{bmatrix} 0 \\ -\mathbf{w}_o \\ 0 \end{bmatrix} \rightarrow \text{Angular rate of orbit with respect to inertial in orbit frame. (3.2)}$$

$${}^o\bar{\mathbf{w}}_B^b \triangleq \begin{bmatrix} \mathbf{w}_1 \\ \mathbf{w}_2 \\ \mathbf{w}_3 \end{bmatrix} \rightarrow \text{Angular rate of body with respect to orbit in body frame. (3.3)}$$

and:

$${}^N\bar{\mathbf{w}}_B^b = {}^N\bar{\mathbf{w}}_B^o + {}^o\bar{\mathbf{w}}_B^b \quad (3.4)$$

The rotational transformation from the orbit frame to the body frame is referred to as the direction cosine matrix (DCM). It is defined from the rotation sequence above and represented in terms of the quaternion vector as,<sup>6</sup>

$${}^B\bar{\mathbf{C}}^o = \begin{bmatrix} q_1^2 - q_2^2 - q_3^2 + q_4^2 & 2(q_1q_2 - q_3q_4) & 2(q_1q_3 - q_2q_4) \\ 2(q_1q_2 - q_3q_4) & q_2^2 - q_1^2 - q_3^2 + q_4^2 & 2(q_2q_3 - q_1q_4) \\ 2(q_1q_3 - q_2q_4) & 2(q_2q_3 - q_1q_4) & q_3^2 - q_1^2 - q_2^2 + q_4^2 \end{bmatrix} \quad (3.5)$$

Therefore, the angular velocity of the body with respect to the Newtonian frame may be written as:

$${}^N\bar{\mathbf{w}}_B^b = {}^o\bar{\mathbf{w}}_B^b + {}^B\bar{\mathbf{C}}^o {}^N\bar{\mathbf{w}}_O^o \quad (3.6)$$

Then substituting from equation (3.2) we have,

$${}^N\bar{\mathbf{w}}_B^b = {}^o\bar{\mathbf{w}}_B^b - w_o C_{i2} \quad (3.7)$$

where  $w_o$  is the magnitude of the orbital angular velocity\* and  $C_{i2}$  is the second column of the DCM. Then by substituting the values established in equation (3.5) we obtain the following relationships,

$$\begin{bmatrix} w_x \\ w_y \\ w_z \end{bmatrix} = \begin{bmatrix} w_1 \\ w_2 \\ w_3 \end{bmatrix} - w_o \begin{bmatrix} 2(q_1q_2 + q_3q_4) \\ q_2^2 - q_1^2 - q_3^2 + q_4^2 \\ 2(q_2q_3 + q_1q_4) \end{bmatrix} \quad (3.8)$$

---

\* Orbital angular velocity  $w_o$  is sometimes referred to as “mean motion” for circular or elliptical orbits.

and,

$$\begin{bmatrix} w_1 \\ w_2 \\ w_3 \end{bmatrix} = \begin{bmatrix} w_x \\ w_y \\ w_z \end{bmatrix} + w_o \begin{bmatrix} 2(q_1q_2 + q_3q_4) \\ q_2^2 - q_1^2 - q_3^2 + q_4^2 \\ 2(q_2q_3 + q_1q_4) \end{bmatrix} \quad (3.9)$$

## 2. Problem Formulation

The inertial symmetric body is shown in Figure 1. The state of the system can be completely defined by its attitude and the time-rate-of-change of attitude.

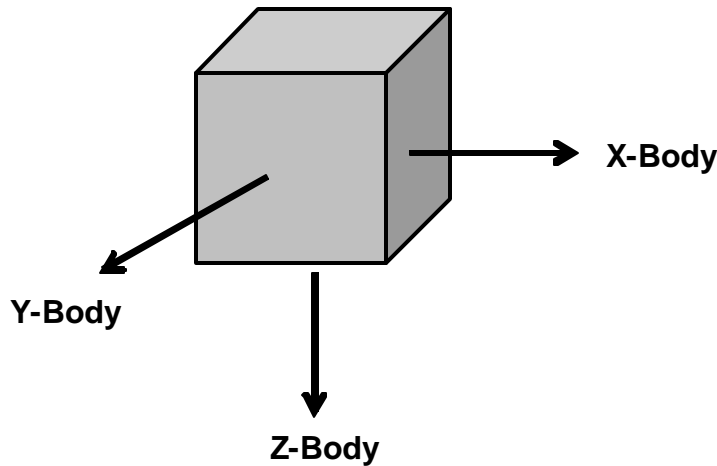


**Figure 1 Inertial Symmetric Body**

For mathematical simplicity in extension to future work, the attitude is represented as a quaternion. Quaternions have none of the inherent singularities that are well known in other representations of spacecraft attitude. Additionally, they are computationally more suited for on-board real-time processing since there are no trigonometric functions to be evaluated in the quaternion kinematics equations.

Euler's rotation theorem states that a rigid body can be changed from any given initial orientation to an arbitrary final orientation by a single rotation about an axis that is fixed to the body and stationary in an inertial reference frame.<sup>7</sup> This axis which remains unchanged in both the body and reference frames is called the *eigenaxis* or Euler Axis.<sup>8</sup>

Defining the eigenaxis in the body frame as:

$$\bar{e} = e_1 \hat{i} + e_2 \hat{j} + e_3 \hat{k} \quad (3.10)$$

allows us to define the quaternion vector as follows:

$$\begin{aligned} q_1 &\doteq e_1 \sin\left(\frac{f}{2}\right) \\ q_2 &\doteq e_2 \sin\left(\frac{f}{2}\right) \\ q_3 &\doteq e_3 \sin\left(\frac{f}{2}\right) \\ q_4 &\doteq \cos\left(\frac{f}{2}\right) \end{aligned} \quad (3.11)$$

where  $f$  is the rotation angle about the eigenaxis. The state of the spacecraft is then represented by:<sup>†</sup>

$$\underline{x} = \begin{bmatrix} \underline{q} \\ \underline{w} \end{bmatrix} \in \mathbb{R}^7$$

The state dynamics include both quaternion kinematics and rotational dynamics. The quaternion kinematics are well known and are repeated here for completeness.

$$\dot{\underline{q}} = \frac{1}{2} \underline{\Omega} \underline{q} \quad \text{with,} \quad \underline{\Omega} \triangleq \begin{bmatrix} 0 & w_3 & -w_2 & w_1 \\ -w_3 & 0 & w_1 & w_2 \\ w_2 & -w_1 & 0 & w_3 \\ -w_1 & -w_2 & -w_3 & 0 \end{bmatrix} \quad (3.12)$$

Termwise, we have,

---

<sup>†</sup> We have adopted the convention that  $q_4$  is the scalar quantity of the quaternion vector.

$$\begin{aligned}
\dot{q}_1 &= \frac{1}{2}[\mathbf{w}_1 q_4 - \mathbf{w}_2 q_3 + \mathbf{w}_3 q_2] \\
\dot{q}_2 &= \frac{1}{2}[\mathbf{w}_1 q_3 + \mathbf{w}_2 q_4 - \mathbf{w}_3 q_1] \\
\dot{q}_3 &= \frac{1}{2}[-\mathbf{w}_1 q_2 + \mathbf{w}_2 q_1 + \mathbf{w}_3 q_4] \\
\dot{q}_4 &= \frac{1}{2}[-\mathbf{w}_1 q_1 - \mathbf{w}_2 q_2 - \mathbf{w}_3 q_3]
\end{aligned} \tag{3.13}$$

In order to maintain consistent notation throughout this work we have used the subscripts indicating that the angular velocities are of the body with respect to the orbit in the body frame. For this example, we consider the spacecraft located in inertial space. Mathematically, orbital angular velocity is zero and we have,

$$\begin{bmatrix} \mathbf{w}_1 \\ \mathbf{w}_2 \\ \mathbf{w}_3 \end{bmatrix} = \begin{bmatrix} \mathbf{w}_x \\ \mathbf{w}_y \\ \mathbf{w}_z \end{bmatrix}$$

This distinction will become important for the later case where the spacecraft is in orbit about the Earth centered inertial frame.

The rotational dynamics of a rigid body are obtained by equating the applied torque about the center of mass to the time rate of change of the angular momentum.<sup>9</sup> This well-known fact is expressed as:

$$\vec{M} = \frac{d}{dt}(\vec{H})$$

where  $\vec{H}$  is the angular momentum vector of the rigid-body about its center of mass with respect to an inertial frame and  $\vec{M}$  is the external moment acting on the body about its center of mass.

Since this is the logical extension of Newton's 2<sup>nd</sup> law it follows that the time-derivative of angular momentum must be with respect to an inertial frame. The angular momentum is the product of the moment of inertia and the angular velocity,

$$\vec{H} = I\vec{\omega}$$

This allows us to express Euler's rotational equations of motion for a rigid-body in matrix notation.

$$I\dot{\mathbf{w}} + \mathbf{w} \times I\mathbf{w} = M_{\text{ext}}$$

If we express the moment of inertia and angular velocity in the principal axis frame as:

$$I = \begin{bmatrix} I_x & 0 & 0 \\ 0 & I_y & 0 \\ 0 & 0 & I_z \end{bmatrix}$$

$$\vec{\mathbf{w}} = w_1 \hat{\mathbf{b}}_1 + w_2 \hat{\mathbf{b}}_2 + w_3 \hat{\mathbf{b}}_3$$

Then Euler's equations can be expanded to:

$$\begin{aligned} M_1 &= I_x \dot{w}_x + (I_z - I_y) w_y w_z \\ M_2 &= I_y \dot{w}_y + (I_x - I_z) w_x w_z \\ M_3 &= I_z \dot{w}_z + (I_y - I_x) w_x w_y \end{aligned} \quad (3.14)$$

These equations are well known and generally referred to as Euler's Moment Equations.<sup>10</sup> For the case of a symmetric body the gyroscopic terms in equations (3.14) are zero and the rotational dynamics can be written as:

$$\dot{w}_x = \frac{M_1}{I_x} \quad \dot{w}_y = \frac{M_2}{I_y} \quad \dot{w}_z = \frac{M_3}{I_z}$$

This reduces Euler's Moment Equations from three-coupled non-linear ordinary differential equations to three uncoupled linear ordinary differential equations. Then normalizing the moment by the inertia, without any loss of generality we have,

$$\dot{w}_x = M_1 \quad \dot{w}_y = M_2 \quad \dot{w}_z = M_3 \quad (3.15)$$

Taken together, equations (3.13) and (3.15) form the system dynamic constraints. The normalized external torque,  $M_i$ , is chosen as the control parameter and it is limited somewhat arbitrarily to unity.

## 2. Time Optimal Maneuvers

With the dynamic constraints defined and presuming initial conditions and desired final conditions are known, we can formally state the time-optimal control problem for the rest-to-rest maneuver as follows:

$$\begin{aligned} \text{Minimize } J(\underline{x}(\cdot), \underline{u}(\cdot), t_f) &= t_f - t_0 \\ \text{s.t. } \dot{\underline{q}} &= \frac{1}{2} \Omega \underline{q} \\ \dot{\underline{w}} &= \underline{u}, \quad |\underline{u}| \leq 1 \end{aligned} \quad (3.16)$$

In order to allow a comparison with published results, we choose our initial and final conditions as:

$$\begin{aligned} \underline{x} &= [q_1 \quad q_2 \quad q_3 \quad q_4 \quad w_1 \quad w_2 \quad w_3]^T \\ \underline{x}_0 &= [0 \quad 0 \quad 0 \quad 1 \quad 0 \quad 0 \quad 0]^T \\ \underline{x}_f &= [0 \quad 0 \quad 1 \quad 0 \quad 0 \quad 0 \quad 0]^T \end{aligned} \quad (3.17)$$

Referring to equations (3.10) and (3.11) these conditions represent a rest-to-rest rotation maneuver of 180 degrees about the z-body axis.

As our first step in determining the control  $\underline{u}^*$  that will drive the dynamic system we write the Hamiltonian in standard form. Since we have written the cost functional in the Mayer form it will not appear in the Hamiltonian. Thus the Hamiltonian will be a linear combination of the state dynamics and take the form:

$$H(\underline{I}, \underline{x}, \underline{u}, t) = \underline{I}^T f(\underline{x}, \underline{u}) \quad (3.18)$$

Substituting equations (3.13) and (3.15) into the Hamiltonian equation (3.18) we have:

$$\begin{aligned} H &= \frac{I_{q_1}}{2} (w_1 q_4 - w_2 q_3 + w_3 q_2) + \frac{I_{q_2}}{2} (w_1 q_3 + w_2 q_4 - w_3 q_1) + \\ &\frac{I_{q_3}}{2} (-w_1 q_2 + w_2 q_1 + w_3 q_4) + \frac{I_{q_4}}{2} (-w_1 q_1 - w_2 q_2 - w_3 q_3) + \\ &I_{w_x} u_1 + I_{w_y} u_2 + I_{w_z} u_3 \end{aligned} \quad (3.19)$$

where the subscripts on the Lagrange multipliers have been selected to aid in bookkeeping.

In order to minimize the Hamiltonian we form the Lagrangian of the Hamiltonian by adjoining the constraint equations to the Hamiltonian in the form:

$$\bar{H} = H + \underline{\mathbf{m}}^T h \quad (3.20)$$

where  $\underline{\mathbf{m}}$  are the KKT multipliers and  $h(u(t), t)$  is the control constraint function in the standard form. On substituting the Hamiltonian equation (3.19) and the control constraint equation as defined above into equation (3.20) the inertial symmetric problem has necessary conditions,

$$\underline{\mathbf{l}}_w + \underline{\mathbf{m}} = 0 \quad (3.21)$$

with the complementarity condition,

$$\underline{\mathbf{m}} \begin{cases} \leq 0 \\ = 0 \\ \geq 0 \end{cases} \quad \text{if} \quad \begin{cases} u_i = -1 \\ -1 < u_i < 1 \\ u_i = 1 \end{cases} \quad (3.22)$$

The quantity  $\partial H / \partial \underline{\mathbf{u}}$  is called the “switching function” in the literature. The case when the switching function equals zero for a non-zero period of time was rigorously examined by Bilimoria and Wie and shown not to be time optimal. Thus we are left with a switching function that determines when the optimal control  $\underline{\mathbf{u}}^*$  will switch between its extreme values. For this reason the control profile is called bang-bang.<sup>11</sup>

In order to validate their results, Bilimoria and Wie used a multiple-shooting algorithm to solve the two-point boundary value problem resulting from the state and adjoint equations. This, in conjunction with the state and adjoint equations allowed them to determine and evaluate candidate optimal control solutions and the resulting trajectories.<sup>12</sup> Here we employ a pseudospectral approximation to arrive at the optimal solution.

A careful comparison of previous results with the ones obtained here (Figure 2 and Figure 3) reveals that for this case there are at least two and potentially four equally optimal solutions. For the symmetric spacecraft the precession that is characteristic of the optimal solution may proceed in either direction for a 180 degree reorientation. A simple transformation of the controls as follows:

Current  $\rightarrow$  Previous

$$u_1 \rightarrow (-1) \times u_2$$

$$u_2 \rightarrow u_1$$

$$u_3 \rightarrow u_3$$

will transform the current quaternion and angular rate histories (Figure 2 and Figure 3) to an exact match with those of Bilimoria and Wie. These transformed results are shown in Figure 4 and Figure 5. For the 180 degree maneuver under consideration one could argue that the entire maneuver could proceed in the opposite direction and still result in the same cost and hence be equally optimal. This, while true, is precluded by the quaternion definition convention employed.

Therefore, the results obtained correspond to the published results and clearly show that the solution is not an eigenaxis maneuver. This is evident from both the non-zero quaternion histories of  $q_1$  and  $q_2$  (Figure 2) and the non-zero angular velocities about the x and y axes (Figure 3).

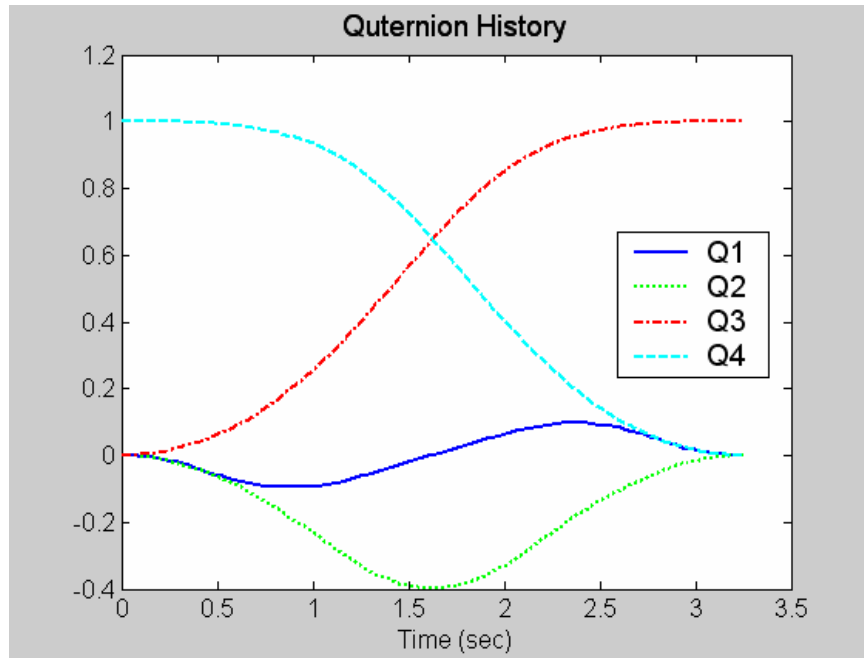


**Figure 2** *Inertial Symmetric Quaternion Solution*

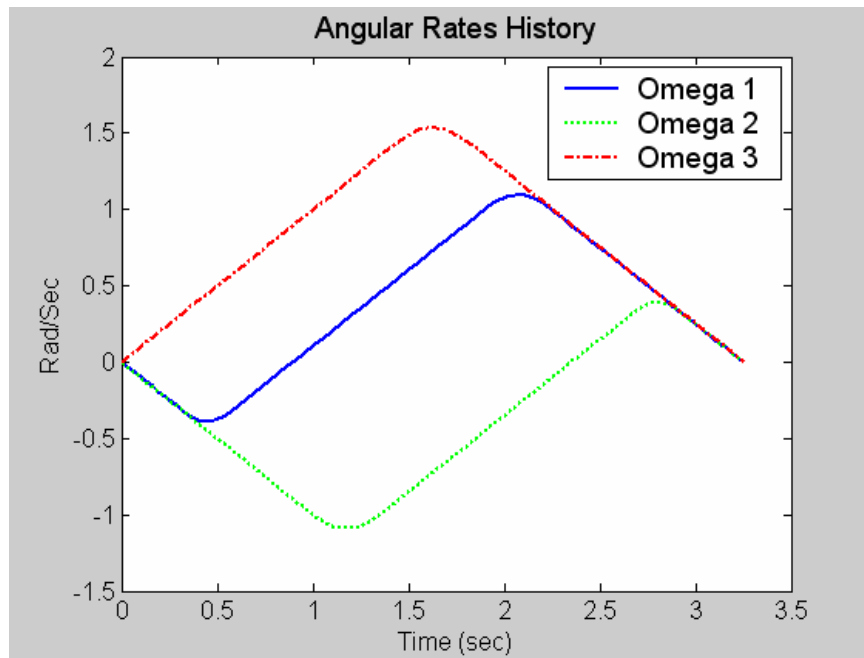


**Figure 3** *Inertial Symmetric Angular Rate Solution*

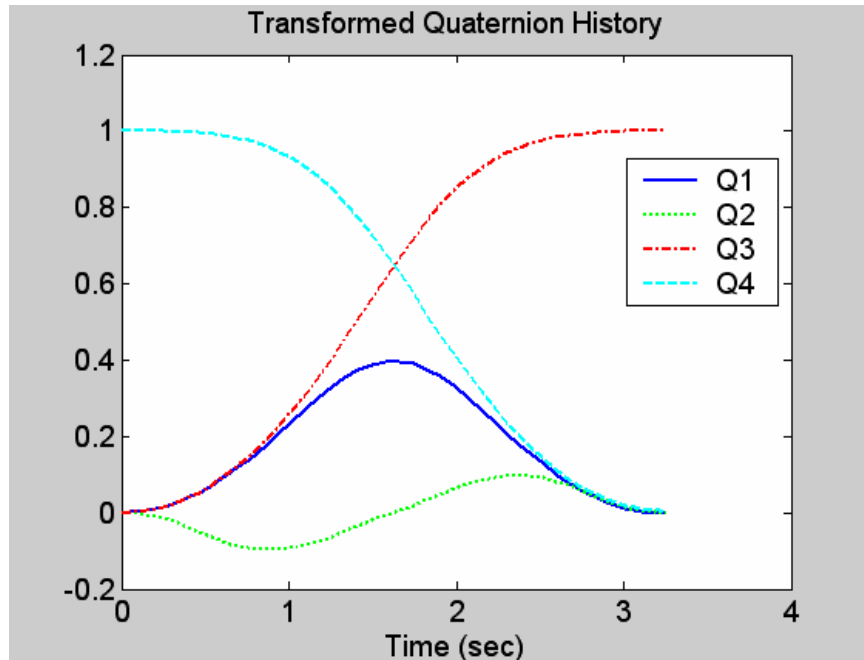


**Figure 4** *Inertial Symmetric Quaternion Transformed Solution*

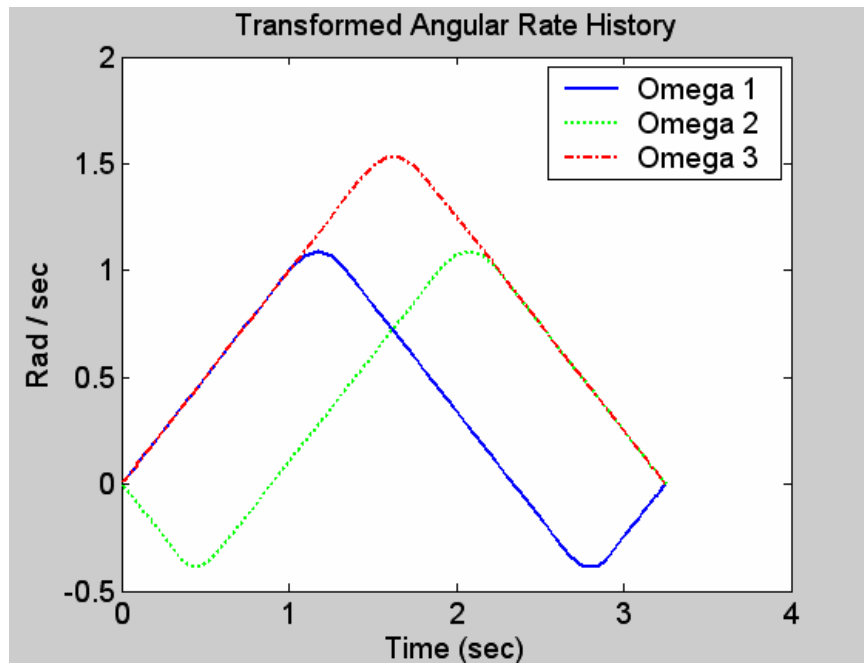


**Figure 5** *Inertial Symmetric Angular Rate Transformed Solution*

The optimal control solution is shown in Figure 6. This solution matches the previous work of Bilimoria and Wie and exhibits the five control switch, bang-bang structure that they observed.

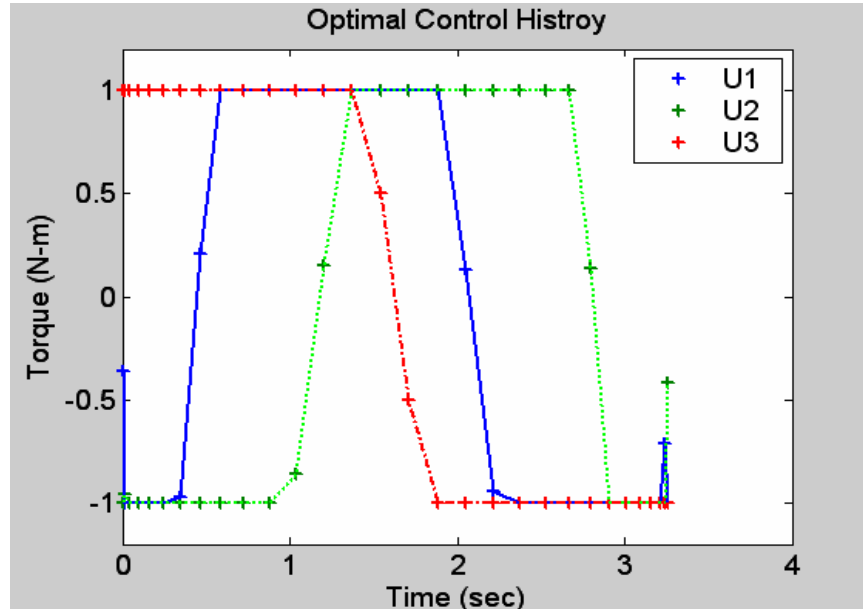


**Figure 6** *Inertial Symmetric Optimal Control Solution*

The control vector obtained is verified as a feasible control through propagation of the state dynamics. The initial conditions and control solution are used as input to a MATLAB<sup>®</sup> ODE45 propagation subroutine which uses an explicit one-step Runge-Kutta medium order (4<sup>th</sup> - to 5<sup>th</sup> -order) solver<sup>13</sup> to verify that the control solution drives the system from the given initial condition to the desired final condition. A linear interpolation was used to approximate the control values between LGL points. Propagation results are shown in Figure 7 and Figure 8. The original solution obtained is shown in solid lines overlaid with the propagated states shown as '+' marks below.

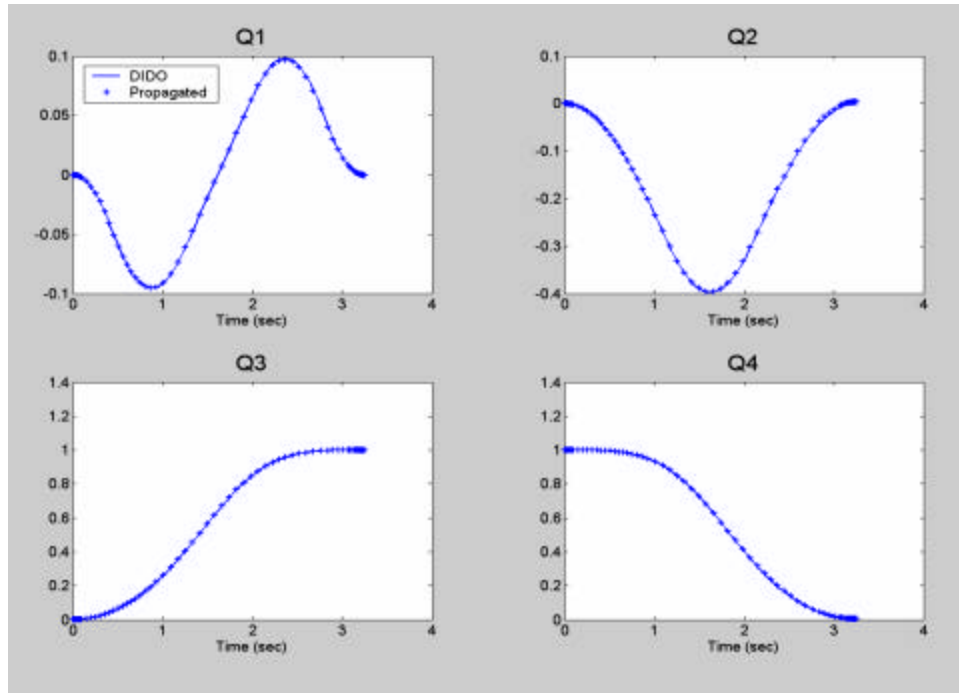


**Figure 7 Quaternion Propagated Solution**

It is easy to see that not only does the dynamic system propagate to the desired end state but that the pseudospectral approximation of the states closely matches the propagated results.

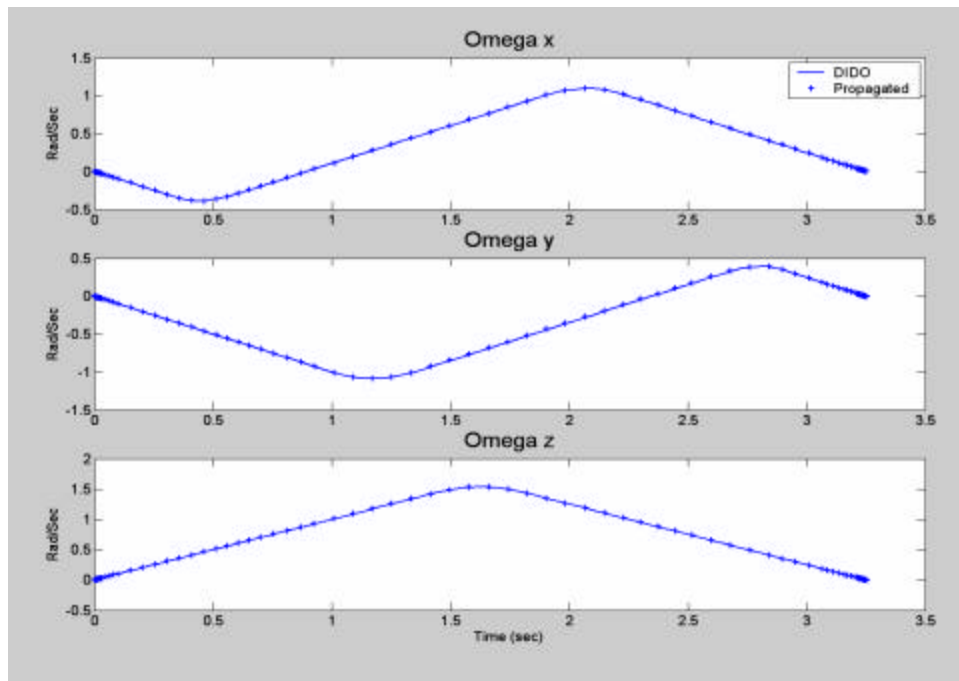


**Figure 8 Angular Rate Propagated Solution**

Next we examine the necessary conditions for optimality. Recall that equation (3.21) and the complementarity conditions of equation (3.22) define the switching structure of the control vector and define a relationship between the costate dynamics and KKT multipliers. An inspection of the switching functions and their relationship to the control behavior verifies that the control-constraint pair meet the KKT conditions. Switching functions for each axis are shown (Figure 9, Figure 10, and Figure 11).

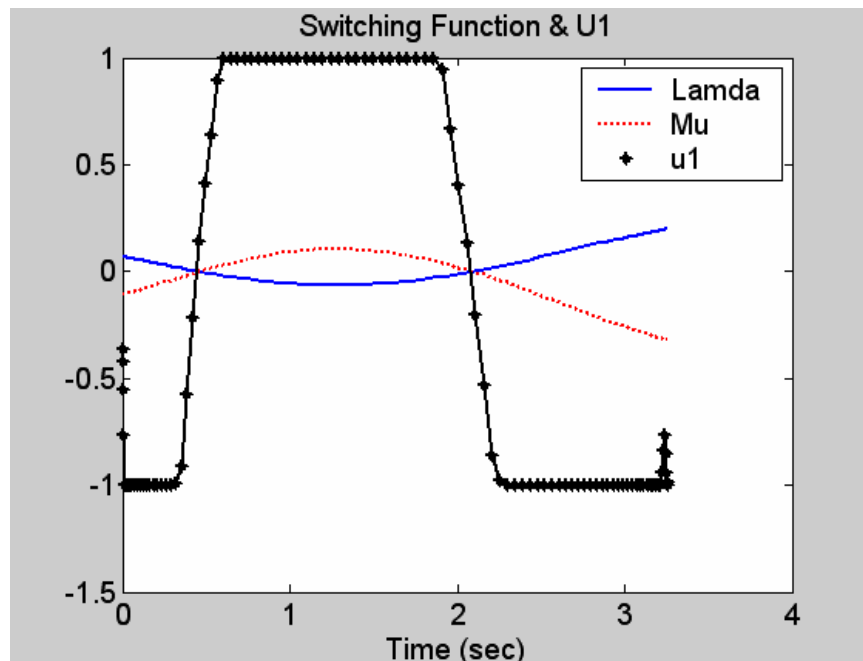


**Figure 9** *Inertial Symmetric Spacecraft Control and Switching Function About X-body Axis*

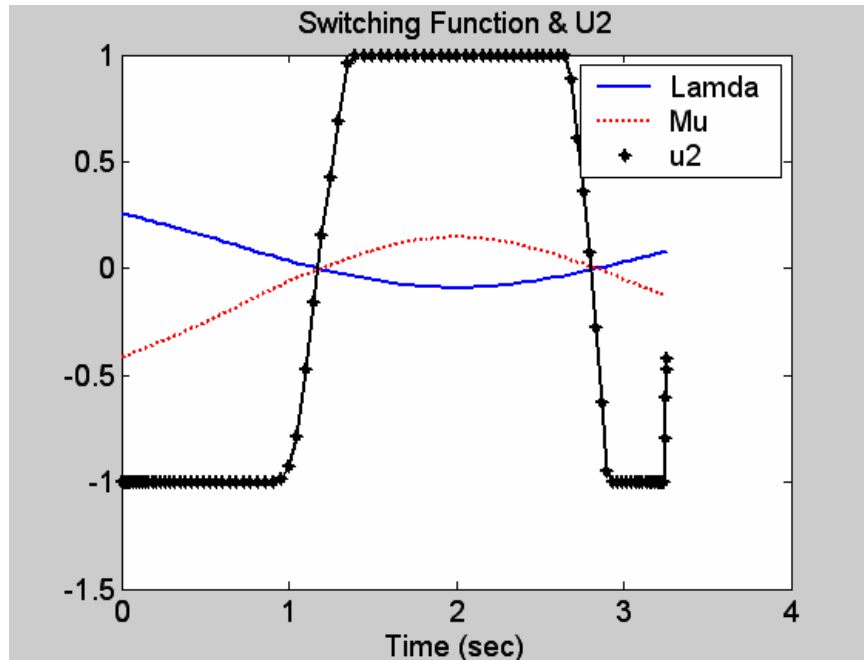


**Figure 10** *Inertial Symmetric Spacecraft Control and Switching Function About Y-body Axis*

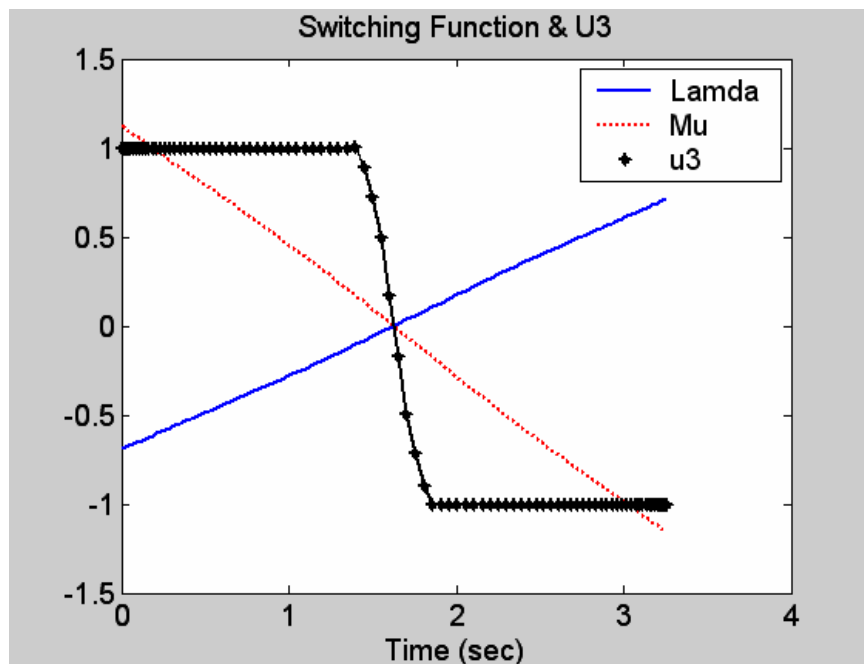


**Figure 11** *Inertial Symmetric Spacecraft Control and Switching Function About Z-body Axis*

Turning to the Hamiltonian equation (3.19) there is no explicit dependence on time and therefore the Hamiltonian will have a constant value along the optimal trajectory.

$$\frac{\partial H}{\partial t} = 0$$

Recall the Hamiltonian value condition allows us to determine the final value of the Hamiltonian from the end-point Lagrangian. The end manifold, in standard form, is given by:

$$\underline{e}(x_f, t_f) = \begin{bmatrix} q_{1_f} \\ q_{2_f} \\ q_{3_f} - 1 \\ q_{4_f} \\ w_{1_f} \\ w_{2_f} \\ w_{3_f} \end{bmatrix} = 0 \quad (3.23)$$

Then the end-point Lagrangian, previously defined as:

$$\bar{E} = E + \mathbf{u}^T \underline{e} \quad (3.24)$$

allows us to determine the final value of the Hamiltonian as:

$$\begin{aligned} H[t_f] + \frac{\partial \bar{E}}{\partial t_f} &= 0 \\ \rightarrow H[t_f] &= -1 \end{aligned} \quad (3.25)$$

Thus, the value of the Hamiltonian will be -1 at all times along the optimal trajectory. The resultant Hamiltonian, shown in Figure 12, meets the necessary conditions with some small numerical variation.

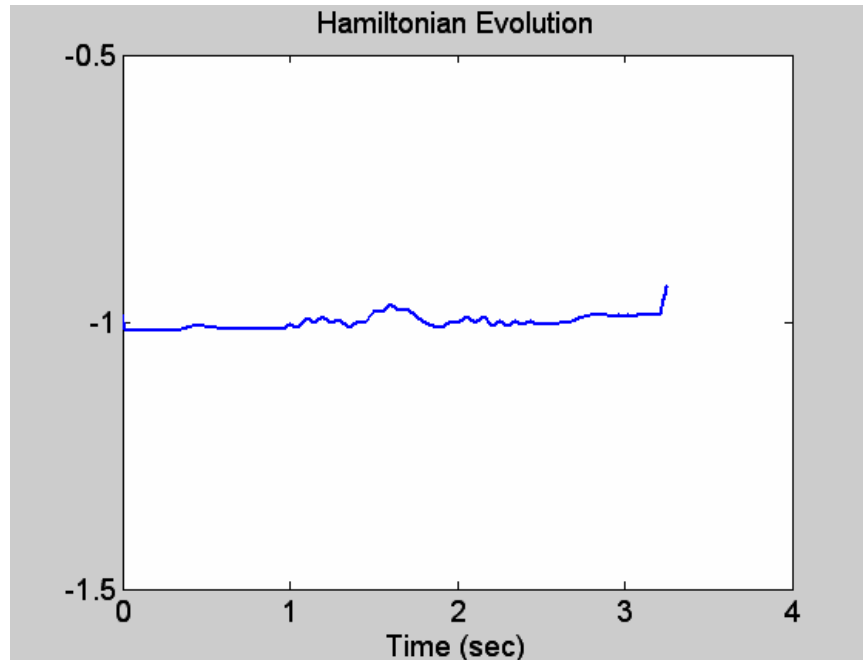


**Figure 12** *Inertial Symmetric Problem Hamiltonian Evolution*

The Adjoint equations can be formed by differentiation of the Hamiltonian. However, since the state variables are specified at both the initial and final conditions the adjoint variables will be free or unspecified at both initial and final conditions. Therefore, the adjoint equations and terminal transversality of the adjoint variables provide no new information which will aid in our solution to the problem.

### **3. Numerical Considerations and Notes**

We have shown that the optimal control solution is feasible and meets the necessary conditions derived from Pontryagin's Minimum Principle. Additionally, we have shown that the results obtained closely match those previously obtained by Bilimoria and Wie. Next we compare the time required for optimal reorientation with that required for a comparable eigenaxis rotation.

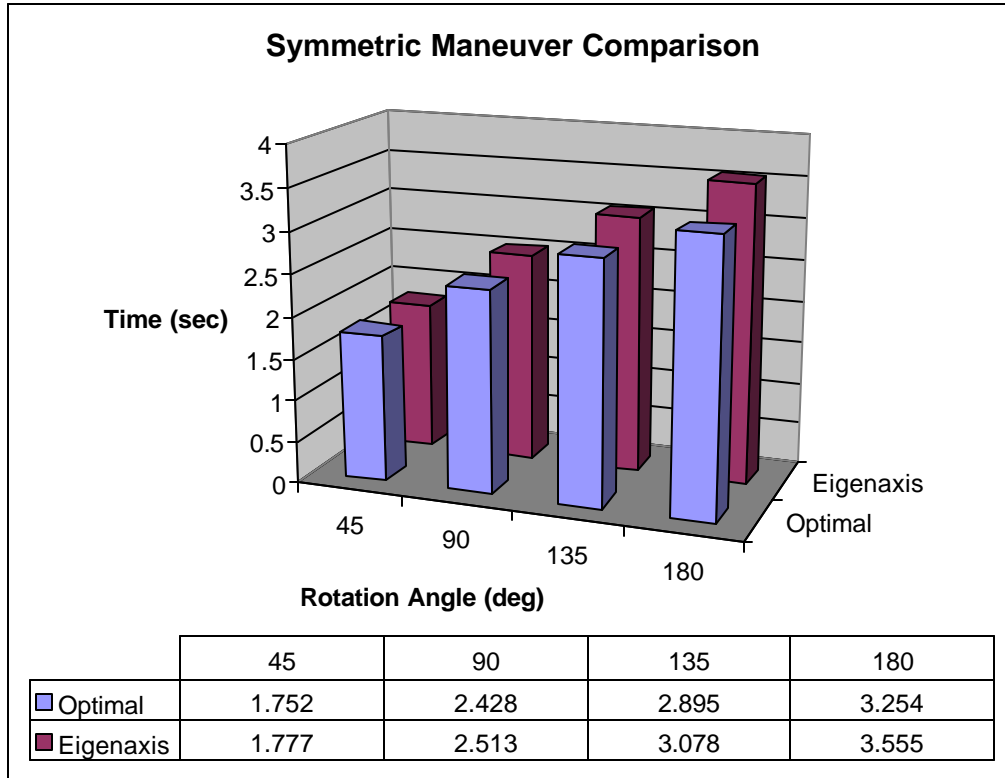


Table 1 **Comparison of symmetric spacecraft reorientation time for time-optimal and eigenaxis maneuvers**

A comparison of the time required for reorientations is shown in Table 1. These results indicate that the time-optimal maneuver is always faster than the optimal eigenaxis maneuver except as noted by Bilimoria and Wie<sup>14</sup>. The cost reduction is shown below in Table 2. It is clear that larger reorientation maneuvers represent a larger cost benefit.

Proper scaling of numerical problems is important to both the accuracy of the result and the computation time required in obtaining the result. No numerical scaling was employed in this algorithm. The nature of the problem is such that for reasonably large rotational maneuvers all numerical values are of the same order of magnitude.

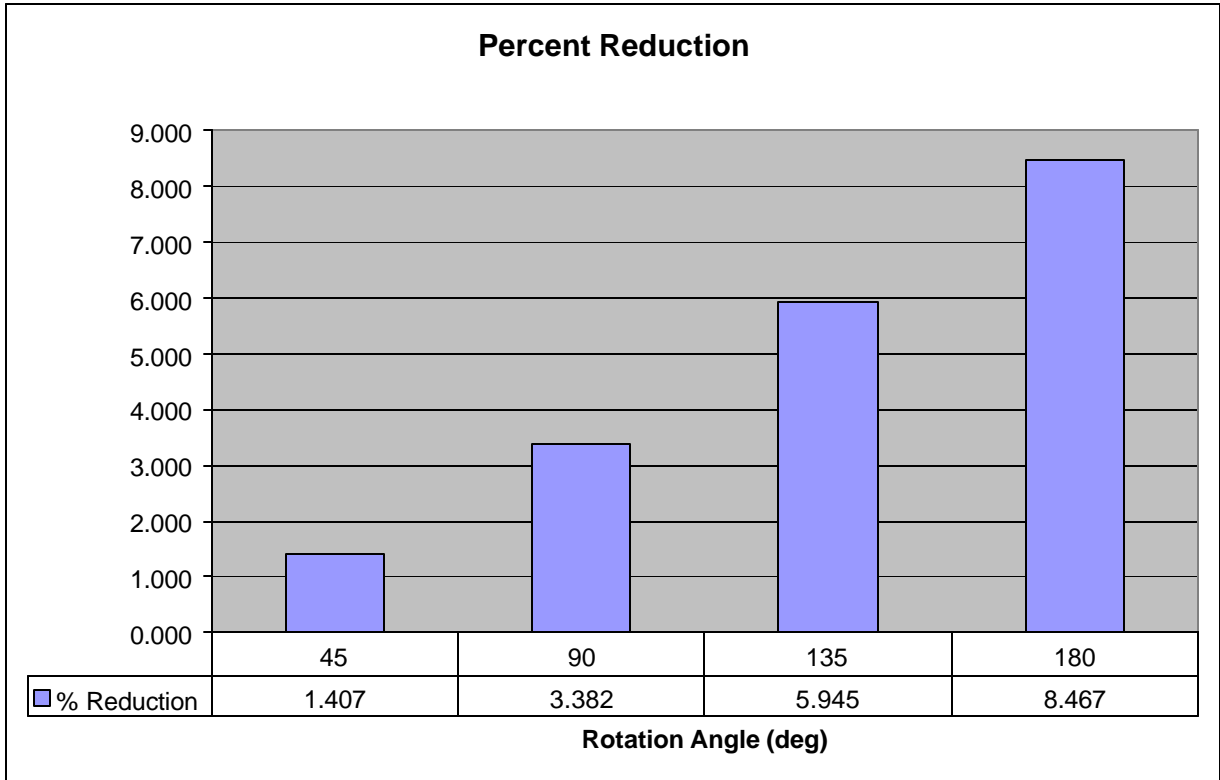


Table 2 ***Cost reduction for inertial symmetric time-optimal reorientations over eigenaxis maneuvers***

#### 4. Conclusions

The published work by Bilimoria and Wie represents a landmark achievement in the application of optimal control theory. Their basic result, that the time-optimal maneuver is not, in general, an eigenaxis maneuver will be shown to extend to a wide variety of spacecraft moments of inertia and control configurations.

#### C. AXISYMMETRIC SPACECRAFT REORIENTATIONS

In this section we will examine the time-optimal reorientation of axisymmetric spacecraft. Shen and Tsiotras<sup>15</sup> examined the problem of axisymmetric reorientations using two control torques. They used a combination of direct and indirect methods to numerically evaluate several representative maneuvers<sup>16</sup>. We begin with reorientations about the axis of symmetry before

examining the general reorientation case. Finally, we will examine the reorientation of the axis of symmetry of a spacecraft spinning about its axis of symmetry. For the spinning spacecraft we will examine the case where the spin rate is held constant throughout the maneuver. This amounts to the two-control reorientation of Shen and Tsiotras. Additionally, we will examine the case where the spin rate is allowed to vary during the maneuver from a given initial condition to a known final condition. We will show that adding this third control torque results in the time-optimal maneuver for a spinning spacecraft.

### 1. Problem Formulation

The inertial axisymmetric body is shown in Figure 13. The axis of symmetry is chosen as the z-body axis somewhat arbitrarily though this is not an

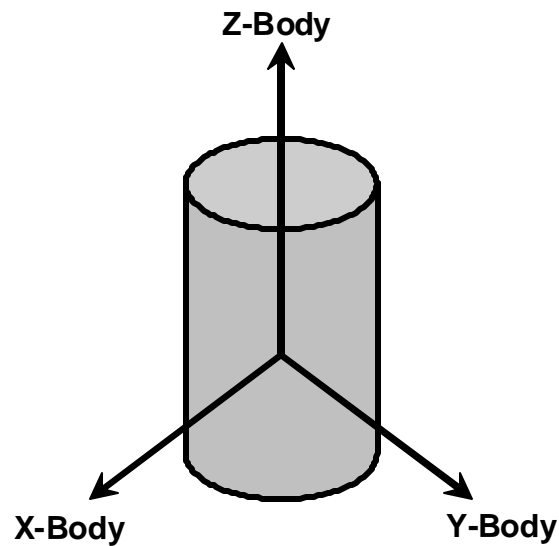


**Figure 13** *Inertial Axisymmetric Body*

uncommon configuration. As before the state of the spacecraft will be defined as:

$$\underline{x} = \begin{bmatrix} \underline{q} \\ \underline{w} \end{bmatrix} \in \mathbb{R}^7$$

The quaternion kinematics remain as previously defined in equation (3.12). However, the rotational dynamics in the principal axis frame given in equation (3.14) now take the following form:

$$\begin{aligned}
 M_1 &= I_x \dot{\mathbf{w}}_x + (I_z - I_y) \mathbf{w}_y \mathbf{w}_z \\
 M_2 &= I_y \dot{\mathbf{w}}_y + (I_x - I_z) \mathbf{w}_x \mathbf{w}_z \\
 M_3 &= I_z \dot{\mathbf{w}}_z
 \end{aligned} \tag{3.26}$$

Note that the gyroscopic term about the zbody axis has been eliminated by the equal moments of inertia about the x and ybody axes. Thus, the time rate of change of angular rate is given by:

$$\begin{aligned}
 \dot{\mathbf{w}}_x &= \frac{M_1}{I_x} - \left( \frac{I_z - I_y}{I_x} \right) \mathbf{w}_y \mathbf{w}_z \\
 \dot{\mathbf{w}}_y &= \frac{M_2}{I_y} - \left( \frac{I_x - I_z}{I_y} \right) \mathbf{w}_x \mathbf{w}_z \\
 \dot{\mathbf{w}}_z &= \frac{M_3}{I_z}
 \end{aligned} \tag{3.27}$$

These, taken together with the quaternion kinematics equations defined earlier form the new dynamic constraints on the axisymmetric system. Once again the control parameter is chosen as external torque and is limited to unity.

## 2. Time Optimal Maneuvers

The formal statement of the optimal control problem is as follows:

$$\begin{aligned}
 &\text{Minimize } J(x(\cdot), u(\cdot), t_f) = t_f - t_0 \\
 &\text{s.t.} \quad \dot{\underline{q}} = \frac{1}{2} \Omega \underline{q} \\
 &\quad \dot{w}_x = \frac{u_1}{I_x} - \left( \frac{I_z - I_y}{I_x} \right) w_y w_z \\
 &\quad \dot{w}_y = \frac{u_2}{I_y} - \left( \frac{I_x - I_z}{I_y} \right) w_x w_z \\
 &\quad \dot{w}_z = \frac{u_3}{I_z} \\
 &\quad |\underline{u}| \leq 1
 \end{aligned} \tag{3.28}$$

### a. *Non-spinning Axisymmetric Reorientations About the Axis of Symmetry*

We will begin by considering a family of prolate spacecraft with characteristics as given (Table 3). Assuming the spacecraft has uniform mass distribution, the moments of inertia about the principal axes are given by:

$$\begin{aligned}
 I_z &= \frac{1}{2} m r^2 \\
 I_x = I_y &= \frac{1}{4} m r^2 + \frac{1}{12} m \ell^2
 \end{aligned} \tag{3.29}$$

where,  $\ell$  is the length of the axis of symmetry,  $m$  is the mass of the spacecraft and  $r$  is the radius. The effect of increasing length on moment of inertia is shown in Table 3.

Prolate Cylinder Spacecraft						
Case	Mass	Length	Radius	I <sub>x</sub>	I <sub>y</sub>	I <sub>z</sub>
I	1	1	1	0.33333	0.33333	0.5
II	1	5	1	2.33333	2.33333	0.5
III	1	10	1	8.58333	8.58333	0.5
IV	1	20	1	33.5833	33.5833	0.5
V	1	50	1	208.583	208.583	0.5
VII	1	100	1	833.583	833.583	0.5

Table 3 *Prolate Spacecraft Characteristics*

The initial and final conditions will define a rest-to-rest maneuver in inertial space representative of a 135 degree rotation about the axis of symmetry. The initial condition will be defined as nadir pointing therefore we have the following:

$$\begin{aligned}\underline{x} &= [q_1 \quad q_2 \quad q_3 \quad q_4 \quad w_1 \quad w_2 \quad w_3]^T \\ \underline{x}_0 &= [0 \quad 0 \quad 0 \quad 1 \quad 0 \quad 0 \quad 0]^T \\ \underline{x}_f &= \left[ 0 \quad 0 \quad \sin\left(\frac{135^\circ}{2}\right) \quad \cos\left(\frac{135^\circ}{2}\right) \quad 0 \quad 0 \quad 0 \right]^T\end{aligned}$$

Referring to equation (3.18) we can write the Hamiltonian for the axisymmetric system as follows:

$$\begin{aligned}H &= \frac{I_{q_1}}{2} (w_1 q_4 - w_2 q_3 + w_3 q_2) + \frac{I_{q_2}}{2} (w_1 q_3 + w_2 q_4 - w_3 q_1) + \\ & \frac{I_{q_3}}{2} (-w_1 q_2 + w_2 q_1 + w_3 q_4) + \frac{I_{q_4}}{2} (-w_1 q_1 - w_2 q_2 - w_3 q_3) + \\ & I_{w_x} \left( \frac{u_1}{I_x} - \left( \frac{I_z - I_y}{I_x} \right) w_x w_z \right) + I_{w_y} \left( \frac{u_2}{I_y} - \left( \frac{I_x - I_z}{I_y} \right) w_x w_z \right) + I_{w_z} \frac{u_3}{I_z}\end{aligned}\tag{3.30}$$

where we have followed the Lagrange multiplier subscript convention established earlier. Then minimizing the Hamiltonian by forming the Lagrangian of the Hamiltonian and evaluating the partial derivative of the Lagrangian with respect to the control as before we have,

$$\begin{aligned}\frac{\partial \bar{H}}{\partial u_1} &= \frac{I_{w_x}}{I_x} + \mathbf{m}_1 = 0 \\ \frac{\partial \bar{H}}{\partial u_2} &= \frac{I_{w_y}}{I_y} + \mathbf{m}_2 = 0 \\ \frac{\partial \bar{H}}{\partial u_3} &= \frac{I_{w_z}}{I_z} + \mathbf{m}_3 = 0\end{aligned}\tag{3.31}$$

as necessary conditions for optimal control solution. Turning our attention to the first prolate spacecraft case (Table 3) we find that the optimal solution exhibits characteristics similar to the symmetric spacecraft we examined previously. The optimal control solution is shown in Figure 14. It displays the same bang-bang switching structure that was previously observed in the symmetric case.

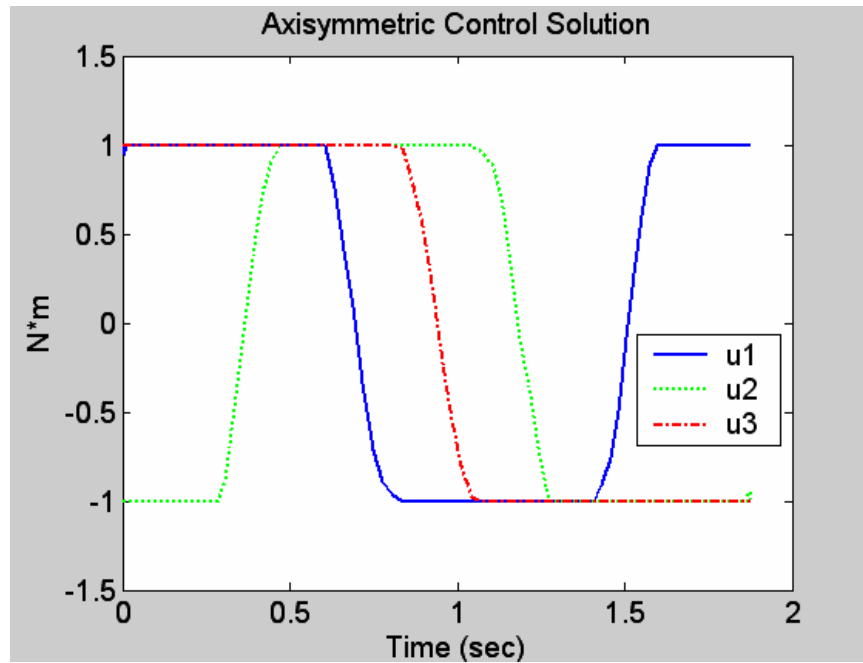


**Figure 14 Case 1 – Axisymmetric Spacecraft Time-optimal Control Solution**

The quaternion and angular rate histories are shown (Figure 15 and Figure 16) and clearly demonstrate that the time optimal maneuver is not an eigenaxis maneuver.

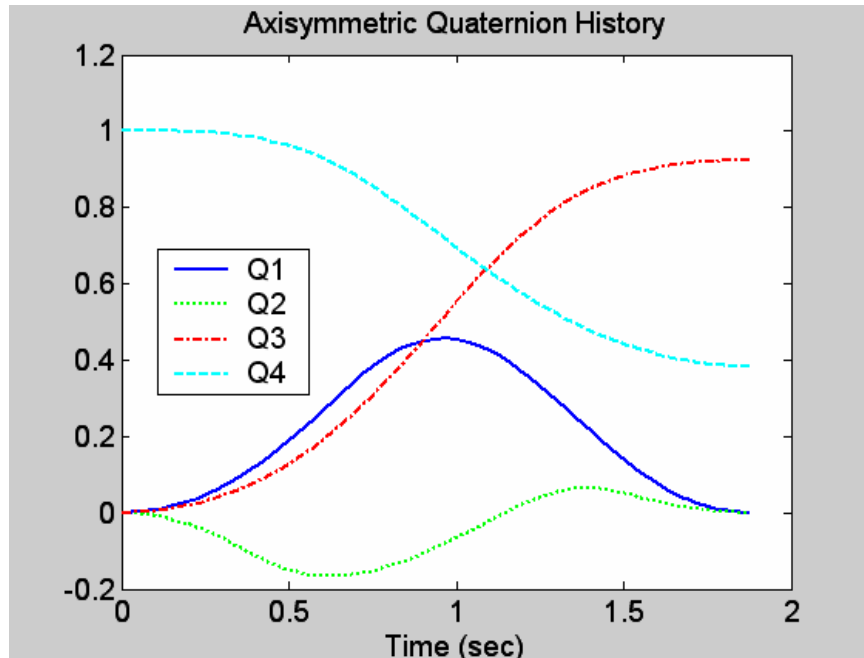


**Figure 15** Case I – Axisymmetric Spacecraft Time-Optimal Quaternion History

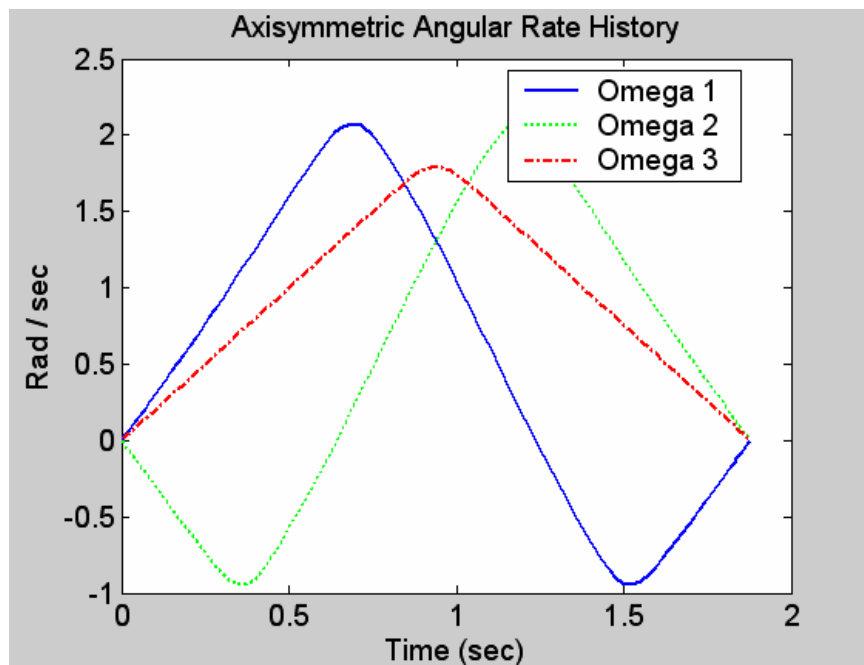


**Figure 16** Case I – Axisymmetric Spacecraft Time-Optimal Angular Rate History

The feasibility of the solution is verified by propagating the optimal control solution through the state dynamics. The propagation results, shown in Figure 17 and Figure 18, indicate that the solution does indeed drive the state from the

known initial conditions to the desired final conditions. The original solution obtained is shown in solid lines overlaid with the propagated states shown as '+' marks below.

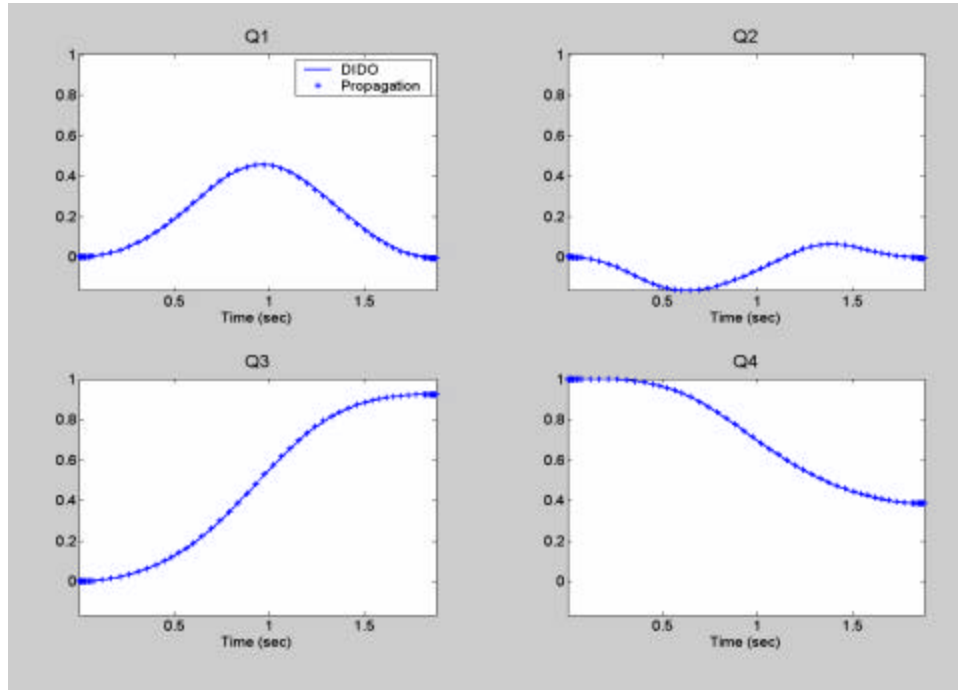


**Figure 17** *Axisymmetric Spacecraft Quaternion Solution Validation by Propagation*

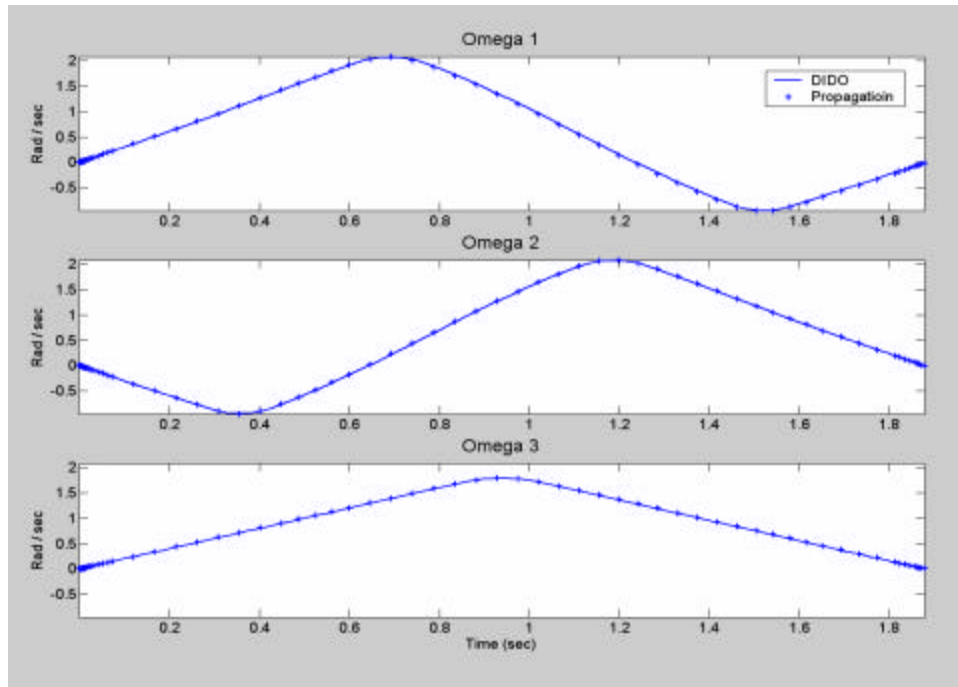


**Figure 18** *Axisymmetric Spacecraft Angular Rate Solution Validation*

The necessary conditions for optimality that we can evaluate directly include the switching structure obtained from the Hamiltonian minimization (Equation (3.31)), and the behavior of the Hamiltonian over time. The switching structure is shown in Figure 19 through Figure 21. The control solution has been overlaid to further illustrate the relationship between the switching function and the control solution.

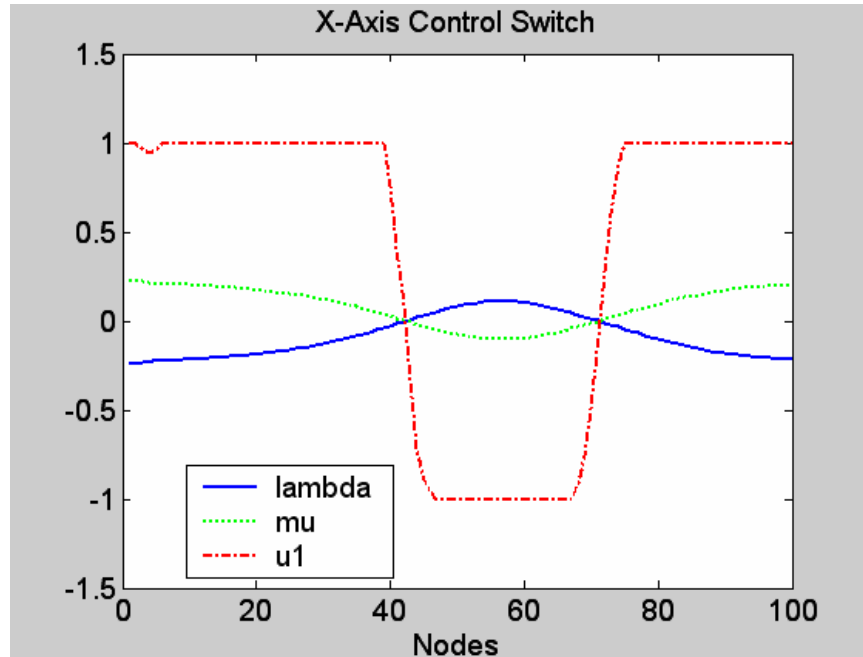


**Figure 19** Axisymmetric Spacecraft x-axis Switching Structure and Control

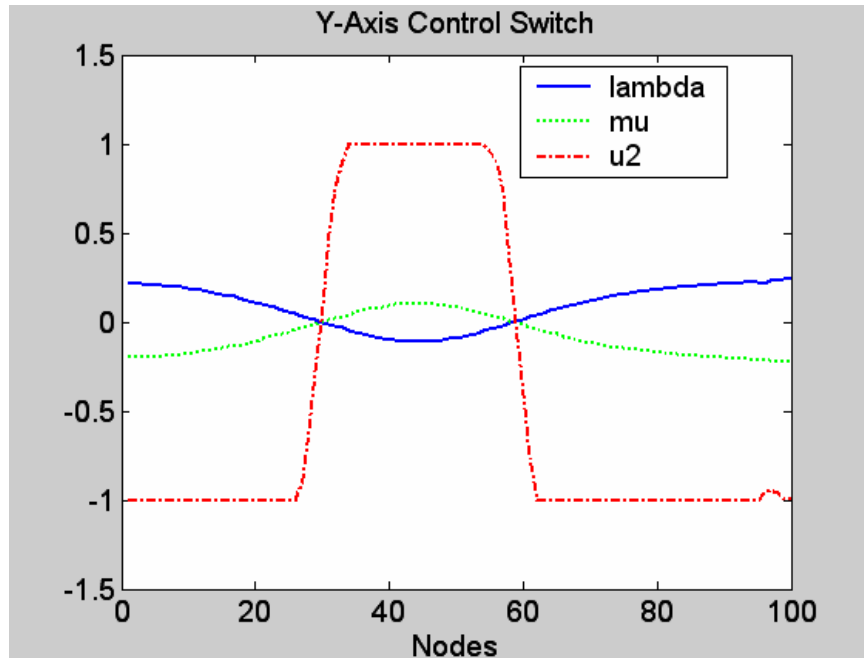


**Figure 20** Axisymmetric Spacecraft y-axis Switching Structure and Control

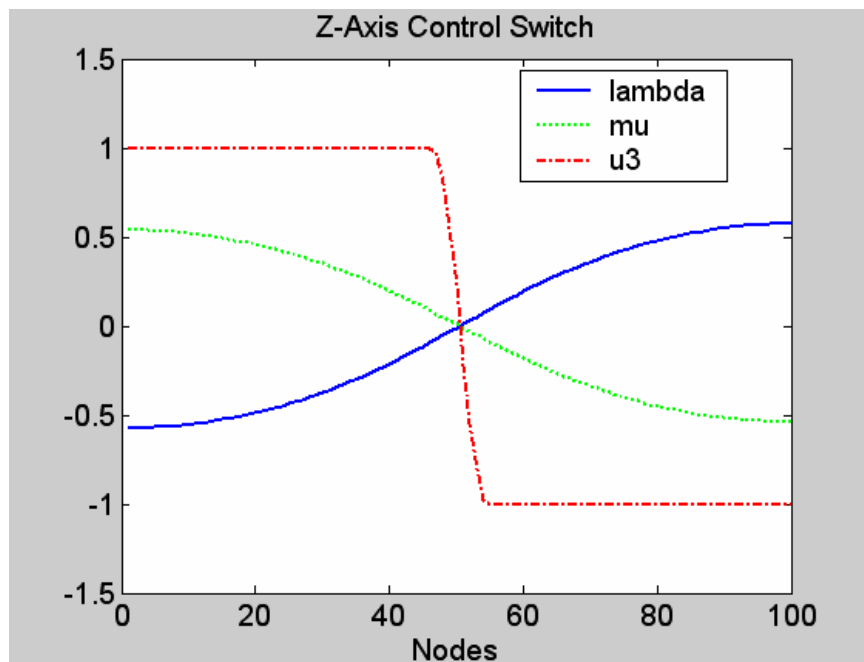


**Figure 21** Axisymmetric Spacecraft z-axis Switching Structure and Control

Inspecting the Hamiltonian for the axisymmetric case (Equation (3.30)) reveals no direct dependence on time. Therefore we can see that the Hamiltonian should be a constant over the interval under consideration. Additionally, forming the end-state Lagrangian as before in equation (3.24) gives the final value of the Hamiltonian. The evolution of the Hamiltonian over time is shown in Figure 22.

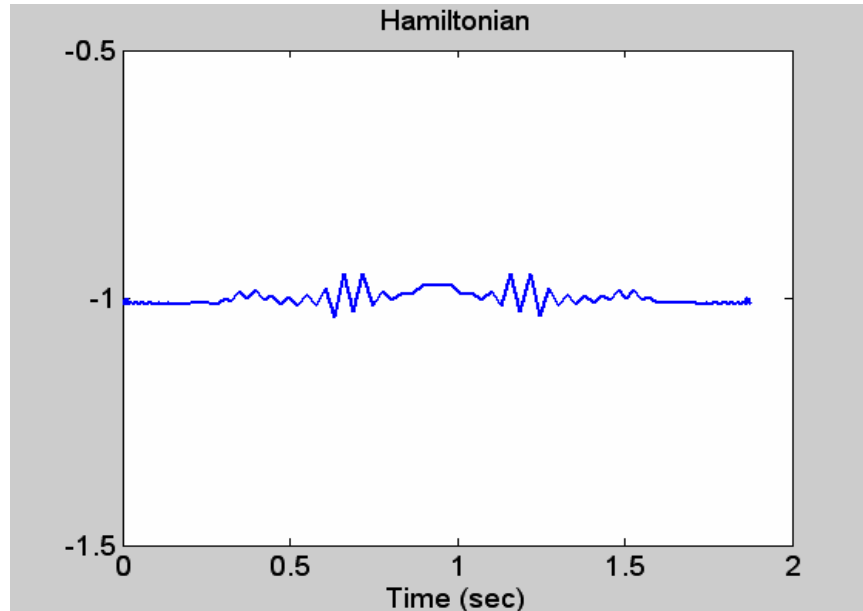


**Figure 22** *Case 1 – Axisymmetric Hamiltonian Evolution and Transversality*

Our analysis of the solution indicates that it is a feasible solution to the time-optimal reorientation problem. Additionally, the solution meets the necessary conditions for optimality derived from Pontryagin’s Minimum Principle.

Now examine the effects of increasing the length of the symmetry axis of a constant mass prolate spacecraft. From equations (3.29) and Table 3 we can see that the moment of inertia about the axis of symmetry remains constant while the remaining moments of inertia grow proportionally to length squared. This is shown in Figure 23. These increasing moments of inertia have two effects. First, the angular acceleration about the x & y-body axes is reduced proportional to the increase in moment of inertia. Physically, this is a decrease in the ability of a constant torque to cause an angular acceleration of an increasing

mass moment of inertia. However, in addition to the decreasing control effectiveness, we see that the switching functions of the controls about the x & y axes are numerically vanishing due to the increasing moment of inertia. The y axis switching function for case III illustrates this effect and is shown in Figure 25. Increasing the value of the control torque available is not sufficient to counter the vanishing switching function.

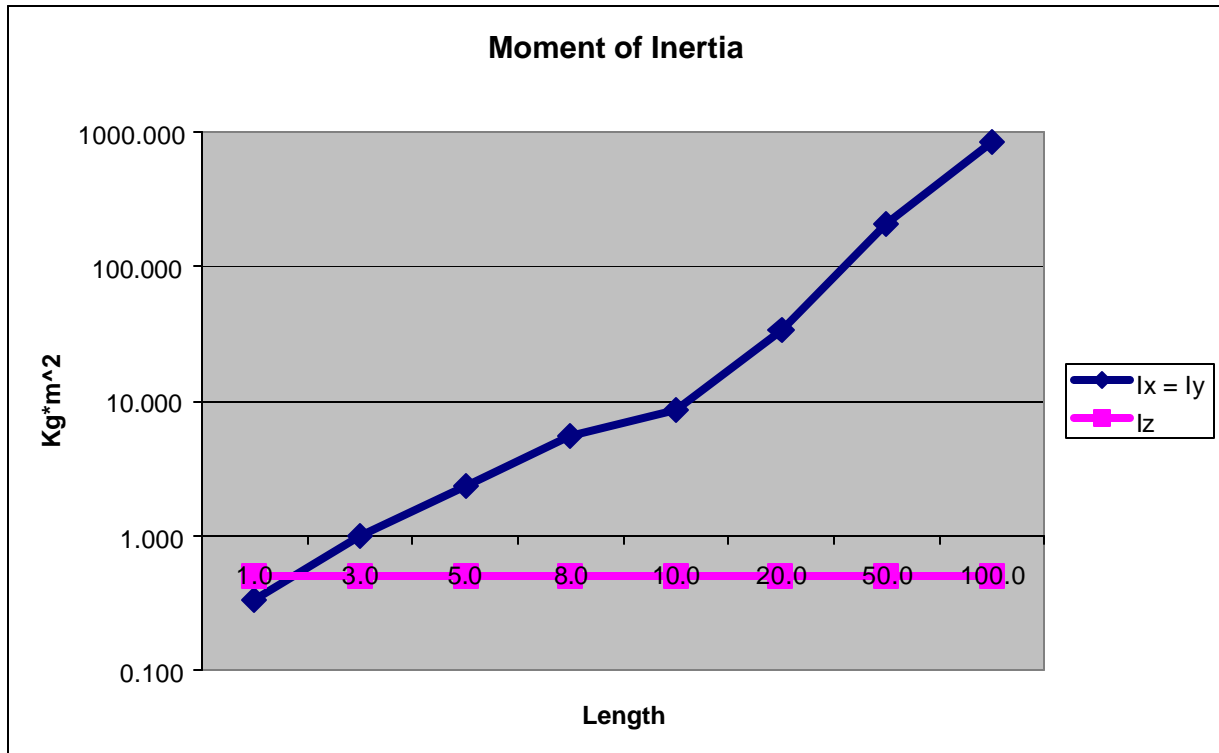


**Figure 23** *Constant Mass Prolate Spacecraft Moment of Inertia versus Length of Symmetry Axis*

Therefore the time-optimal reorientation maneuver about the symmetry axis approaches an eigenaxis maneuver as the length of the body grows in a constant mass spacecraft.

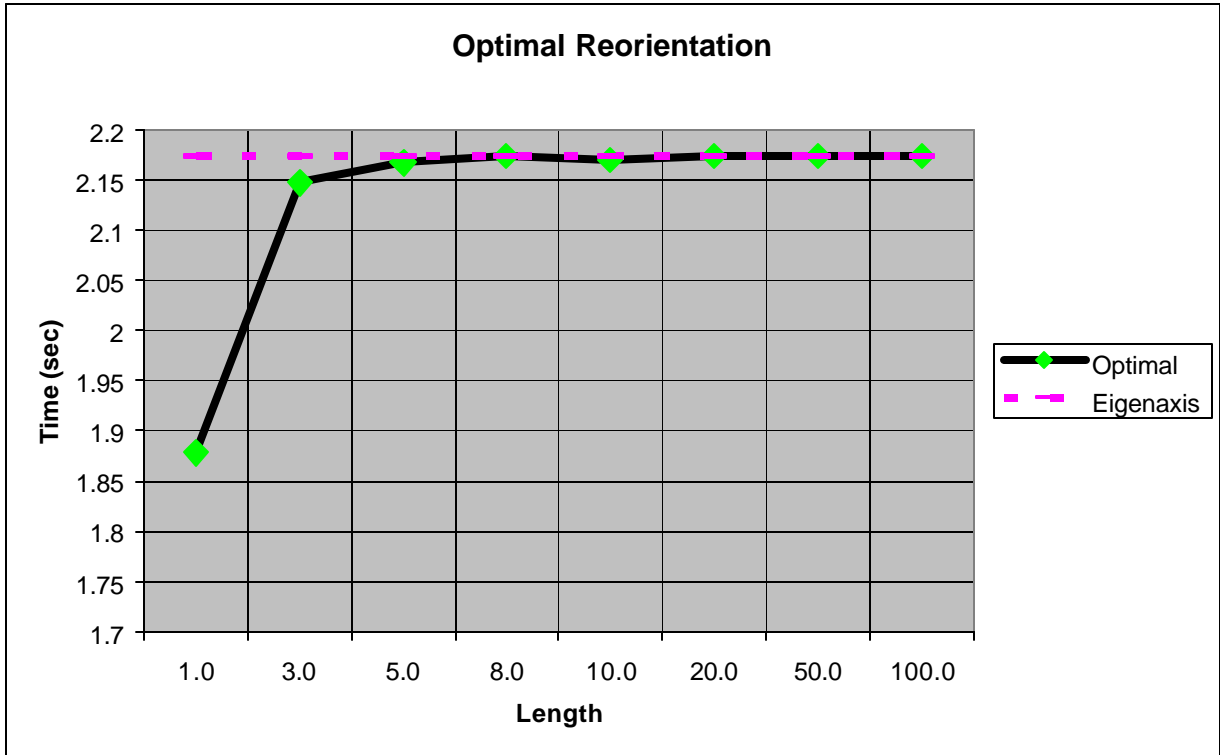


**Figure 24** *Axisymmetric Reorientation Maneuvers About Symmetry Axis versus Symmetry Axis Length*

It is interesting to note that the structure of switching function is not significantly affected by the increasing moments of inertia. The switching function for the prolate spacecraft of case III (Table 3), where the length of the symmetry axis is 10 times longer than the original, displays the same switching structure as the original. The magnitude is however, reduced by several orders of magnitude. The switching function for the y-axis control of Case III is included (Figure 25) for comparison to that of Case I (Figure 20).

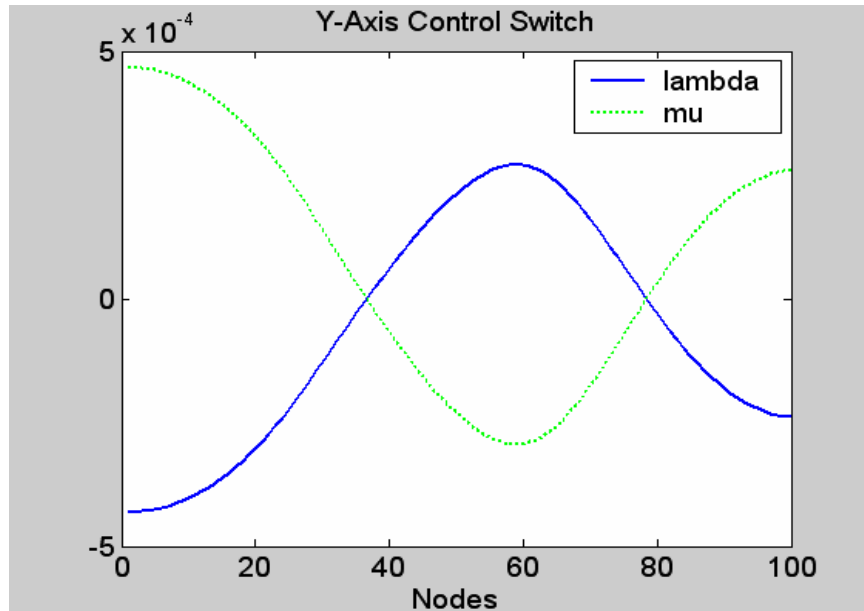


**Figure 25 Prolate Axisymmetric Spacecraft Case III – Switching function**

**b. Non-spinning Axisymmetric Reorientations of the Axis of Symmetry**

The case of non-spinning axisymmetric spacecraft reorientations of the axis of symmetry is mathematically no different from the previous section. The problem formulation and necessary conditions for optimality remain unchanged. The optimal maneuvers display the same characteristic precession about the eigenaxis and involve control torques about all three axes. It is interesting to note that the control switching structure behaves in a manner very similar to that observed by Bilimoria and Wie in their work on symmetric reorientations.<sup>17</sup> That is, for small angle reorientations we observe a sequential seven-switch structure and for large angle maneuvers we observe a sequential five-switch structure. The control solutions for two representative maneuvers are shown. In Figure 26, we see the control solution for a large angle maneuver about the x-axis. The representative maneuver is chosen as a 135 degree rotation. The five-switch-sequential structure is clearly evident. In Figure 27, the control solution for a representative small angle maneuver about the x-axis is

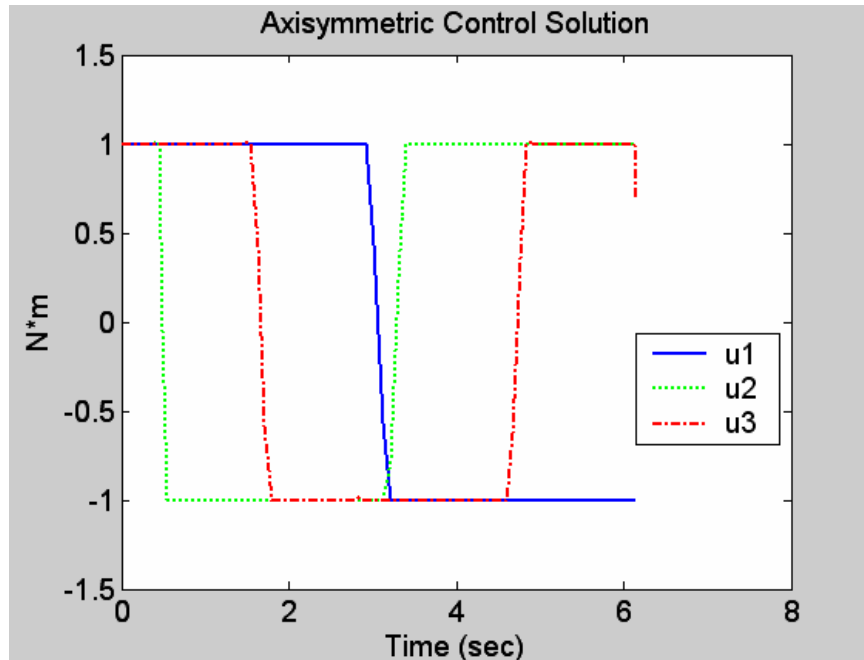


**Figure 26** Axisymmetric Spacecraft Optimal Control Solution for X-axis Large Angle Rotation (135 Degree Rotation)

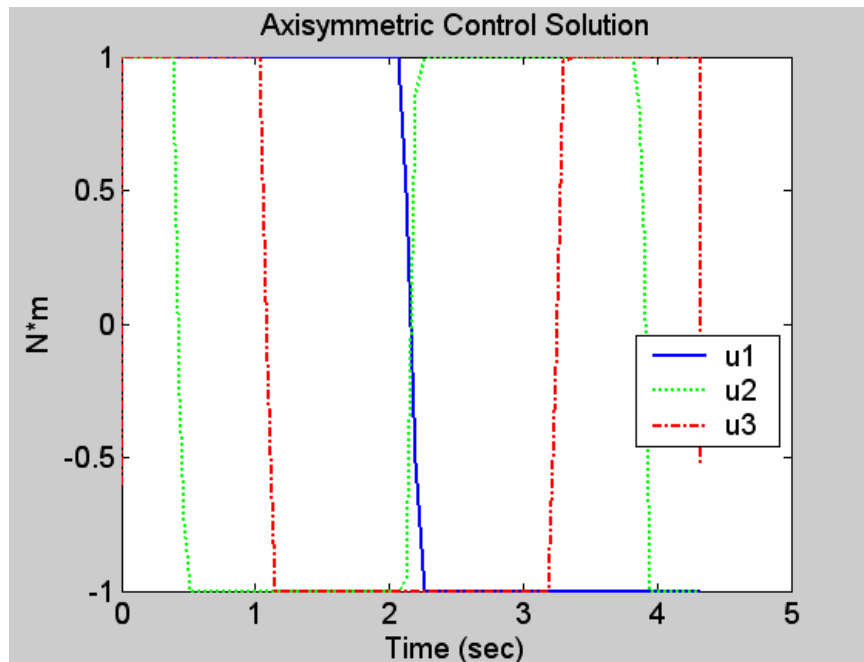


**Figure 27** Axisymmetric Spacecraft Optimal Control Solution for X-axis Small Angle Rotation (60 Degree Rotation)

shown. The maneuver, a 60 degree rotation results in a seven-switch-sequential solution. This suggests that there is a dividing point, as Bilimoria and Wie observed for the symmetric case, where the time-optimal solution changes from the seven-switch to the five-switch structure.

**c. Reorientations of the Spinning Axis of Symmetry**

Next we consider the reorientation of a spinning axisymmetric spacecraft. Shen and Tsiotras also considered this case where the rigid body was subject to only two control torques which spanned the plane perpendicular to the axis of symmetry. They concluded that two torques were sufficient to achieve a time-optimal maneuver.<sup>18</sup> In this section we will show that a third torque about the symmetry axis, if available, further reduces the objective function and is the true time-optimal solution.

Consider the axisymmetric spacecraft of Figure 13, which is spinning about the z-axis, the axis of symmetry. Euler' equations remain unchanged from equation (3.26) and are repeated here for the convenience of the reader:

$$\begin{aligned} M_1 &= I_x \dot{w}_x + (I_z - I_y) w_y w_z \\ M_2 &= I_y \dot{w}_y + (I_x - I_z) w_x w_z \\ M_3 &= I_z \dot{w}_z \end{aligned}$$

Using the formulation of Shen and Tsiotras suggested by Tsiotras and Longuski<sup>19</sup> the orientation of the  $\hat{n}_3$  inertial axis of the inertial frame given by  $\hat{n} = (\hat{n}_1, \hat{n}_2, \hat{n}_3)$  with respect to the body frame can be represented by two variables defined as:

$$w_1 = \frac{\mathbf{b}}{1 + \mathbf{g}} \quad w_2 = \frac{-\mathbf{a}}{1 + \mathbf{g}}$$

where  $w_1$  and  $w_2$  obey the differential equations:

$$\dot{w}_1 = w_z w_2 + w_y w_1 w_2 + \frac{w_x}{2} (1 + w_1^2 - w_2^2)$$

$$\dot{w}_2 = -w_z w_1 + w_x w_1 w_2 + \frac{w_y}{2} (1 + w_2^2 - w_1^2)$$

Readers are directed to the references [18,19] for a complete derivation of this parameterization. Using this formulation we can state the time-optimal reorientation of the spin axis as follows:

$$\text{Minimize } J(x(\cdot), u(\cdot), t_f) = t_f - t_0$$

s.t.

$$\dot{w}_x = \frac{u_1}{I_x} - \left( \frac{I_z - I_y}{I_x} \right) w_y w_z$$

$$\dot{w}_y = \frac{u_2}{I_y} - \left( \frac{I_x - I_z}{I_y} \right) w_x w_z$$

$$\dot{w}_z = \frac{u_3}{I_z}$$

$$\dot{w}_1 = w_z w_2 + w_y w_1 w_2 + \frac{w_x}{2} (1 + w_1^2 - w_2^2)$$

$$\dot{w}_2 = -w_z w_1 + w_x w_1 w_2 + \frac{w_y}{2} (1 + w_2^2 - w_1^2)$$

$$|u| \leq 1$$

Following the numerical example of Shen and Tsiotras we establish the following spacecraft parameters:

$$I_x = 4$$

$$I_y = 4$$

$$I_z = 2$$

$$|u_i| = \left| \frac{M_i}{I_i} \right| \leq 1$$

The Hamiltonian and necessary conditions are available in the reference and not repeated here. Using initial and final conditions given as:

$$\underline{x} = [w_1 \ w_2 \ w_3 \ w_1 \ w_2]^T$$

$$\underline{x}_0 = [0 \ 0 \ -0.5 \ 1.5 \ -0.5]^T$$

$$\underline{x}_f = [0 \ 0 \ -0.5 \ 0 \ 0]^T$$

we can duplicate the results of Shen and Tsiotras by setting the torque  $M_3 = 0$ . The results are shown in Figure 28 and Figure 29. The maneuver, defined as a 115.38 degree reorientation of  $\hat{b}_3$  to  $\hat{n}_3$ , and is completed in 2.6142 seconds. Published results indicated a minimum maneuver time of 2.61 seconds.<sup>20</sup>

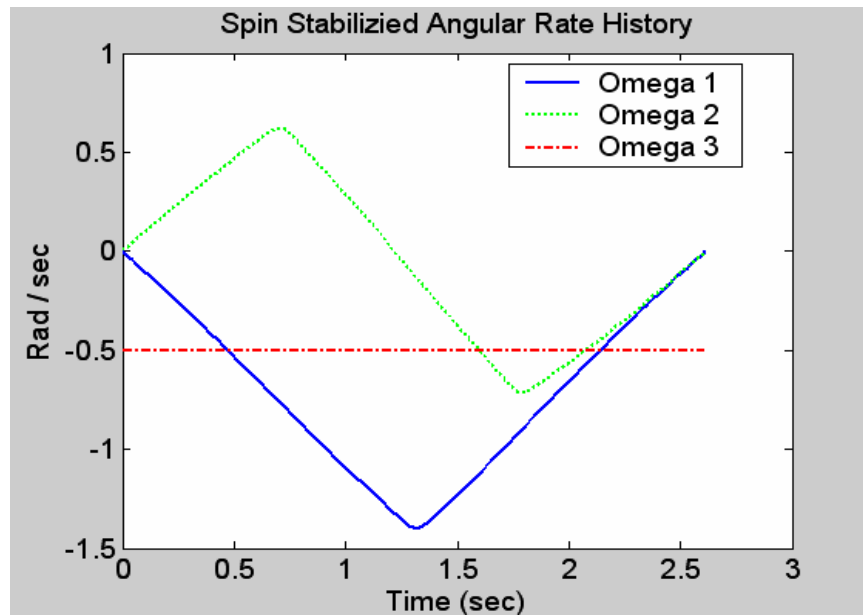


**Figure 28** Angular Rate History for Constant Spin Rate Time-optimal Maneuver

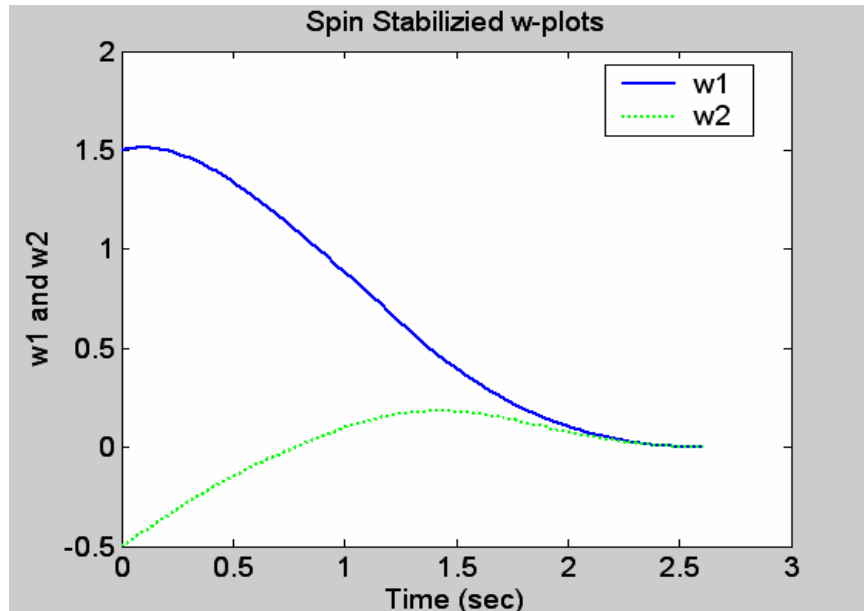


**Figure 29** Time Histories of  $w_1$  and  $w_2$  for Constant Spin Time-optimal Maneuver

However, if the control  $u_3$  is available, and the boundary conditions are enforced such that the spin rate is allowed to vary throughout the maneuver, then the true time-optimal solution is found.

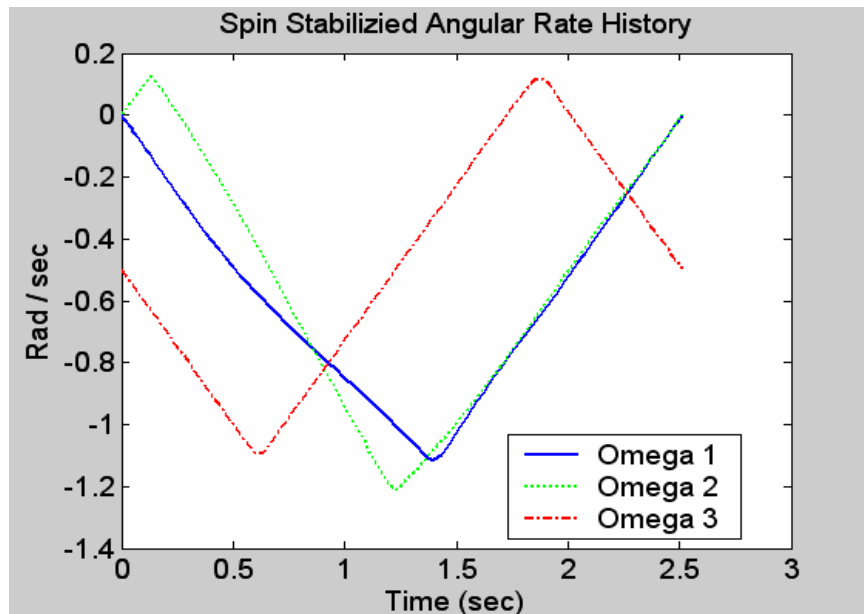


**Figure 30** Angular Rate History for Time-optimal Spinning Reorientation Maneuver

If spin rate of the z-axis is allowed to vary the time-optimal maneuver solution contains a significant change in spin rate as shown in Figure 30. The improved time for maneuver completion is now 2.513 seconds. This is a reduction of 3.87% from the previously assumed time-optimal solution. The three-axis control time-optimal  $w$  solution is shown in Figure 31.

The control solution obtained (Figure 32) is bang-bang in all three axes. As before the control solution is propagated through the state dynamics to verify that the solution is feasible. The original solution obtained is shown in solid lines overlaid with the propagated states shown as '+' marks below. It is clear (Figure 33 and Figure 34) that the spacecraft states properly propagate from the given initial conditions to the desired final conditions.

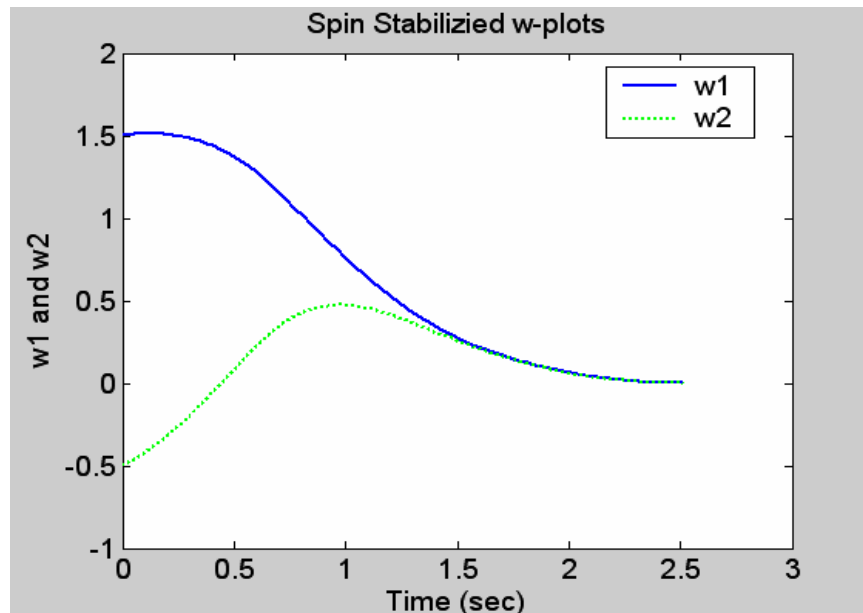


**Figure 31** *Time Histories of  $w_1$  and  $w_2$  for Spinning Spacecraft Time-optimal Maneuver*

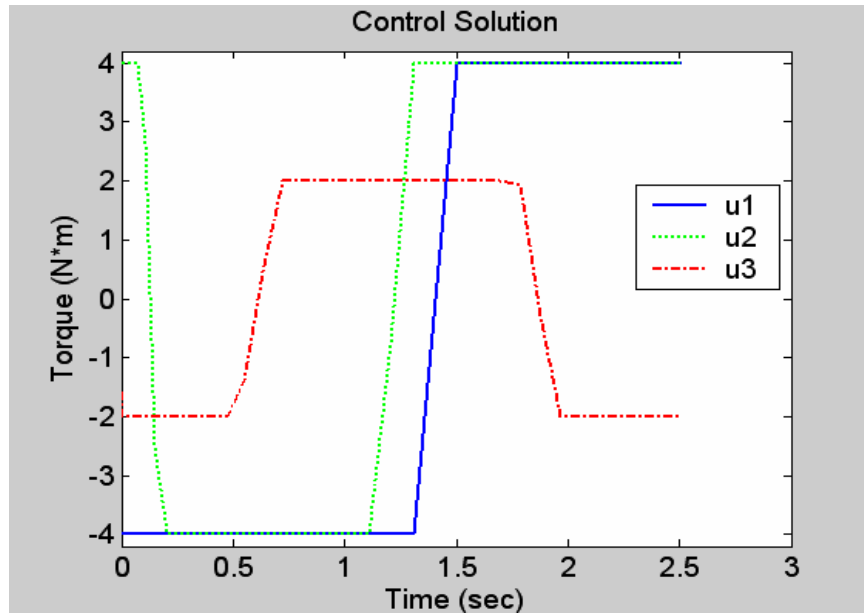


**Figure 32** *Spinning Axisymmetric Spacecraft Time-optimal Control Solution*

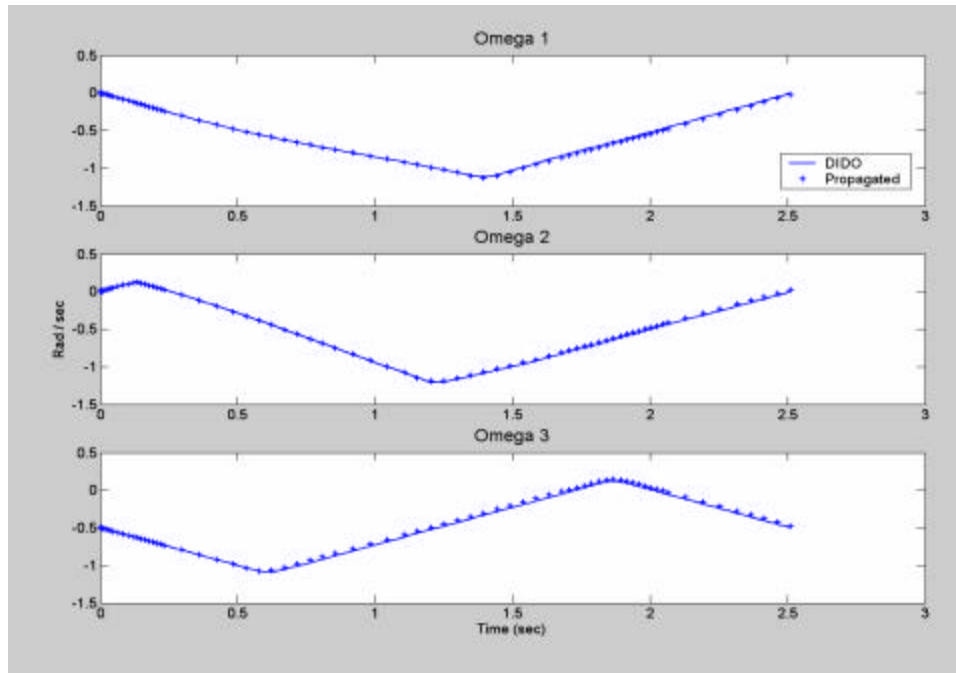


**Figure 33** *Spinning Axisymmetric Spacecraft Angular Rate Solution Validation by Propagation*

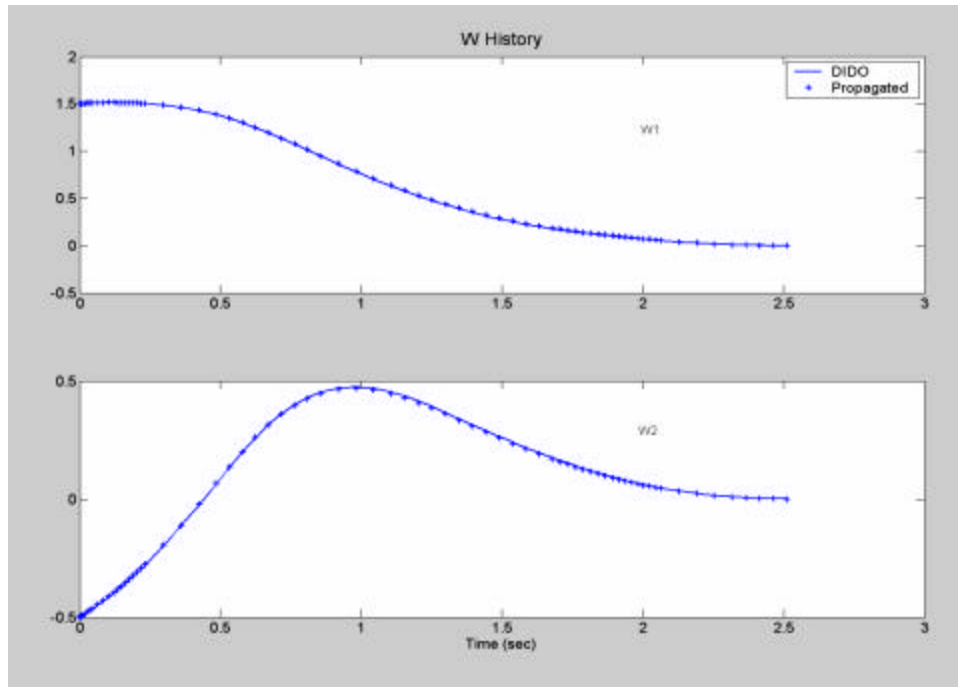


**Figure 34** *Spinning Axisymmetric Spacecraft W History Solution Validation by Propagation*

Minimization of the Hamiltonian with respect to the control vector allows us to establish the switching functions. These are shown, overlaid with the unity scaled control solution (Figure 35, Figure 36, and Figure 37).

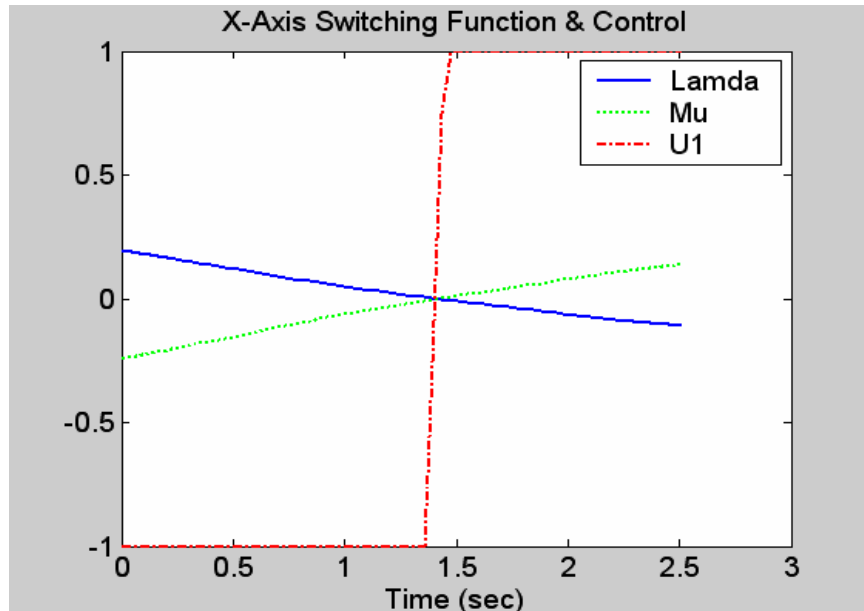


**Figure 35** *Spinning Axisymmetric Spacecraft X-axis Switching Function and Normalized Control*

Finally, we evaluate the Hamiltonian and observe it is constant over time and numerically equal to -1. This is expected for the Mayer formulation of the cost function when the Hamiltonian has no direct time dependence.

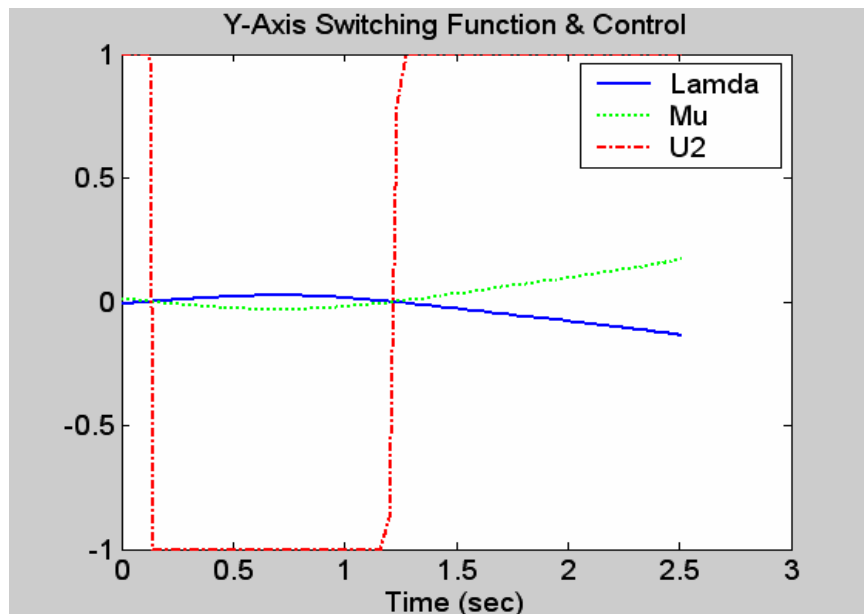


**Figure 36** *Spinning Axisymmetric Spacecraft Y-axis Switching Function and Normalized Control*

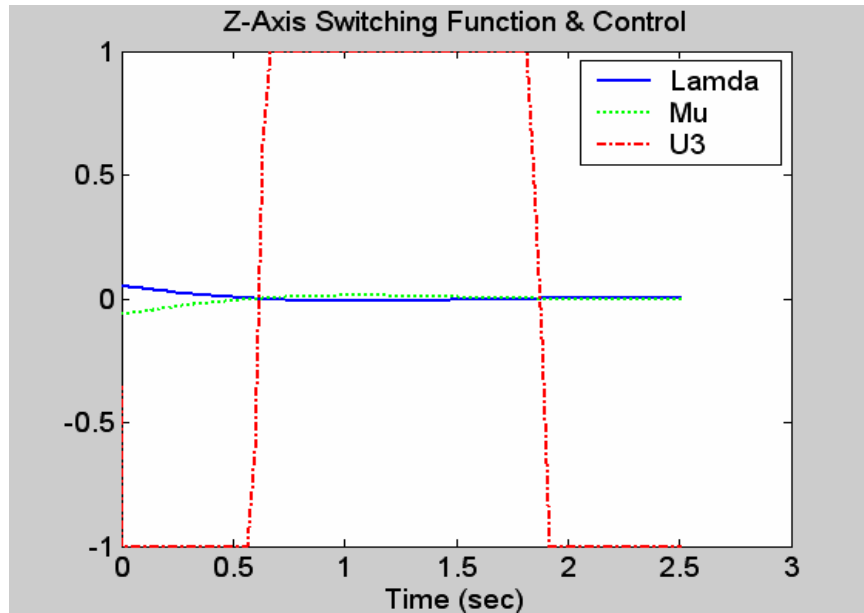


**Figure 37** *Spinning Axisymmetric Spacecraft Z-axis Switching Function and Normalized Control*

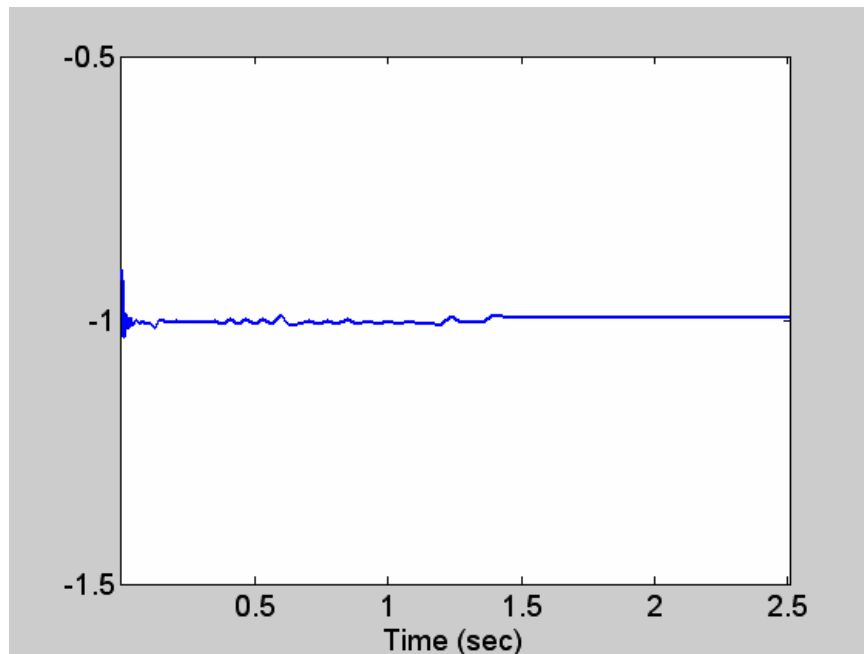


**Figure 38** *Spinning Axisymmetric Spacecraft Time-optimal Solution Hamiltonian*

### **3. Numerical Considerations and Notes**

Operationally, it is often preferable to maintain a constant satellite spin rate about the axis of symmetry. However, we have shown that if a third torque is available about the axis of symmetry then the time-optimal solution will involve a change in the spacecraft spin rate. This change in spin rate is appreciable and results in a measurable time savings over the two control torque solution.

### **4. Conclusions**

In this section we examined the time-optimal maneuver for an axisymmetric spacecraft with three independent control torques. We saw that for maneuvers about the axis of symmetry the relative moment of inertias have significant effects on the maneuvers. As the moment of inertia about the symmetry axis increased the maneuver approached the eigenaxis maneuver in both time required and spacecraft response. Additionally, we demonstrated that while reorientation of the spin axis is possible with two control torques spanning the plane perpendicular to the spin axis, the addition of a third control torque about the axis of symmetry further reduces the objective function and is the true time-optimal solution. This third control torque is in general assumed to be available as it was required to generate the spinning motion.

### **D. ASYMMETRIC SPACECRAFT REORIENTATION MANEUVERS**

In this section we will numerically investigate the time-optimal reorientation of a rigid asymmetric body. Livenh and Wie<sup>21</sup> presented an extensive analytical analysis of the asymmetric reorientation problem under constant body-fixed torques. Additionally, the work of Proulx and Ross<sup>22</sup> determined an admissible switching structure which was elegantly illustrated by the traversal of a unit cube. Using this to limit the search space a combination of a genetic algorithm and pseudospectral method was used to obtain the optimal solution. Additionally, they suggested a method of evaluating the “optimality” of a solution by evaluating the Hamiltonian derived from the costates obtained through the Covector

Mapping Theorem. This method of evaluating compliance with the Minimum Principle is employed throughout this work.

## 1. Problem Formulation

In order to facilitate future work and extension to other control actuators the orientation of the asymmetric spacecraft will be represented with respect to an Earth centered inertial reference frame. This will require the incorporation of orbital velocity and reference frame transformations to properly represent the dynamic constraints.

As before, for a rigid body the applied torque about the center of mass is equal to the time rate of change of the angular momentum.<sup>23</sup>

$$\vec{M} = \frac{d}{dt}(\vec{H})$$

From the transportation theorem we have,

$$\frac{d}{dt}(\vec{H}) \equiv \left\{ \frac{d\vec{H}}{dt} \right\}_N = \left\{ \frac{d\vec{H}}{dt} \right\}_B + {}^N\vec{\omega}^b \times \vec{H}$$

Following the previous development we obtain Euler's equations:

$$\begin{aligned} M_1 &= I_x \dot{w}_x + (I_z - I_y) w_y w_z \\ M_2 &= I_y \dot{w}_y + (I_x - I_z) w_x w_z \\ M_3 &= I_z \dot{w}_z + (I_y - I_x) w_x w_y \end{aligned} \quad (3.32)$$

The quaternion kinematics equations are unchanged from previous (equation (3.13)) except that emphasis is placed on the notation.

$$\begin{aligned} \dot{q}_1 &= \frac{1}{2} [w_1 q_4 - w_2 q_3 + w_3 q_2] \\ \dot{q}_2 &= \frac{1}{2} [w_1 q_3 + w_2 q_4 - w_3 q_1] \\ \dot{q}_3 &= \frac{1}{2} [-w_1 q_2 + w_2 q_1 + w_3 q_4] \\ \dot{q}_4 &= \frac{1}{2} [-w_1 q_1 - w_2 q_2 - w_3 q_3] \end{aligned} \quad (3.33)$$

As shown above the angular rates ( $w_1, w_2, w_3$ ) are of the body with respect to the orbit frame. For convenience we choose to define the state of the spacecraft in terms of the quaternion vector and the angular rates with respect to the Newtonian frame. Thus the state vector is given by:

$$\underline{x} = \begin{bmatrix} \underline{q} \\ {}^N \underline{w}_B^b \end{bmatrix} \in \mathbb{R}^7$$

## 2. Time Optimal Maneuvers

The formal statement of the optimal control problem is as follows:

$$\text{Minimize } J(\underline{x}(\cdot), u(\cdot), t_f) = t_f - t_0$$

$$\begin{aligned} \text{s.t.} \quad & \dot{\underline{q}} = \frac{1}{2} \Omega \underline{q} \\ & \dot{w}_x = \frac{u_1}{I_x} - \left( \frac{I_z - I_y}{I_x} \right) w_y w_z \\ & \dot{w}_y = \frac{u_2}{I_y} - \left( \frac{I_x - I_z}{I_y} \right) w_x w_z \\ & \dot{w}_z = \frac{u_3}{I_z} - \left( \frac{I_x - I_y}{I_z} \right) w_1 w_3 \\ & |u_i| \leq 1 \end{aligned}$$

The maneuver under consideration will be rest-to-rest in the orbit frame; however, the final angular velocity in the inertial frame will depend on the final attitude. This is clear from equation (3.8). The maneuver under consideration is an x-axis rotation typically 135 degrees. This maneuver magnitude was selected based on the anticipated orbital parameters of NPAST1, the potential test bed for later algorithms. The initial condition was chosen somewhat arbitrarily as nadir pointing. Then the problem initial and final conditions may be presented in standard form as follows:

$$\begin{aligned}\underline{x} &= [q_1 \quad q_2 \quad q_3 \quad q_4 \quad \mathbf{w}_x \quad \mathbf{w}_y \quad \mathbf{w}_z]^T \\ \underline{x}_0 &= [0 \quad 0 \quad 0 \quad 1 \quad 0 \quad -\mathbf{w}_o \quad 0]^T \\ \underline{x}_f &= \left[ \sin\left(\frac{135^\circ}{2}\right) \quad 0 \quad 0 \quad \cos\left(\frac{135^\circ}{2}\right) \quad \mathbf{w}_x(t_f) \quad \mathbf{w}_y(t_f) \quad \mathbf{w}_z(t_f) \right]^T\end{aligned}$$

Additionally, spacecraft moment of inertias for subsequent examples have been selected to match the planned NPSAT1 moment of inertias and are given as follows:

$$\begin{aligned}I_x &= 5 \text{ kg}\cdot\text{m}^2 \\ I_y &= 5.1 \text{ kg}\cdot\text{m}^2 \\ I_z &= 2 \text{ kg}\cdot\text{m}^2\end{aligned}$$

As before, the first step in our approach is to form and minimize the Hamiltonian. Recall that the Hamiltonian is a function of the state, control and Lagrange multipliers.

$$H(\mathbf{I}, \mathbf{x}, u, t) = \mathbf{I}^T f(\mathbf{x}, u)$$

Since quaternion kinematics are typically written in terms of the body angular rates with respect to the orbit frame, a lengthy algebraic process of coordinate transformations is required to properly write the Hamiltonian. Once completed the Hamiltonian takes the following form:

$$\begin{aligned}H &= \frac{I_{q_1}}{2} (\mathbf{w}_x q_4 - \mathbf{w}_y q_3 + \mathbf{w}_z q_2 + \mathbf{w}_o q_3) + \frac{I_{q_2}}{2} (\mathbf{w}_x q_3 + \mathbf{w}_y q_4 - \mathbf{w}_z q_1 + \mathbf{w}_o q_4) \\ &+ \frac{I_{q_3}}{2} (-\mathbf{w}_x q_2 + \mathbf{w}_y q_1 + \mathbf{w}_z q_z - \mathbf{w}_o q_1) + \frac{I_{q_4}}{2} (-\mathbf{w}_x q_1 - \mathbf{w}_y q_2 - \mathbf{w}_z q_3 - \mathbf{w}_o q_2) \\ &+ I_{w_x} \left( \frac{u_1}{I_x} - \left( \frac{I_z - I_y}{I_x} \right) \mathbf{w}_y \mathbf{w}_z \right) + I_{w_y} \left( \frac{u_2}{I_y} - \left( \frac{I_x - I_z}{I_y} \right) \mathbf{w}_x \mathbf{w}_z \right) + I_{w_z} \left( \frac{u_3}{I_z} - \left( \frac{I_x - I_y}{I_z} \right) \mathbf{w}_x \mathbf{w}_y \right)\end{aligned}\tag{3.34}$$

In accordance with the Minimum Principle the Lagrangian of the Hamiltonian is formed and partial derivatives with respect to the control vector are formed which establish the control switching functions.

$$\begin{aligned}
 \frac{\partial \bar{H}}{\partial u_1} &= \frac{I_{w_1}}{I_x} + \mathbf{m}_1 = 0 \\
 \frac{\partial \bar{H}}{\partial u_2} &= \frac{I_{w_2}}{I_y} + \mathbf{m}_2 = 0 \\
 \frac{\partial \bar{H}}{\partial u_3} &= \frac{I_{w_3}}{I_z} + \mathbf{m}_3 = 0
 \end{aligned} \tag{3.35}$$

The reader should note that the switching functions of the asymmetric case are no different than those of the axisymmetric case given in equation(3.31). This would correctly lead us to surmise that as the moment of inertias approach those previously studied the results would closely match those previously obtained.

The control solution for the asymmetric body under consideration is shown in Figure 39. It clearly exhibits the structure we have come to expect. In general, the control is bang-bang in all three axes. There are five switches in all, characteristic of a large angle slew with a single-switch in the primary axis of rotation.

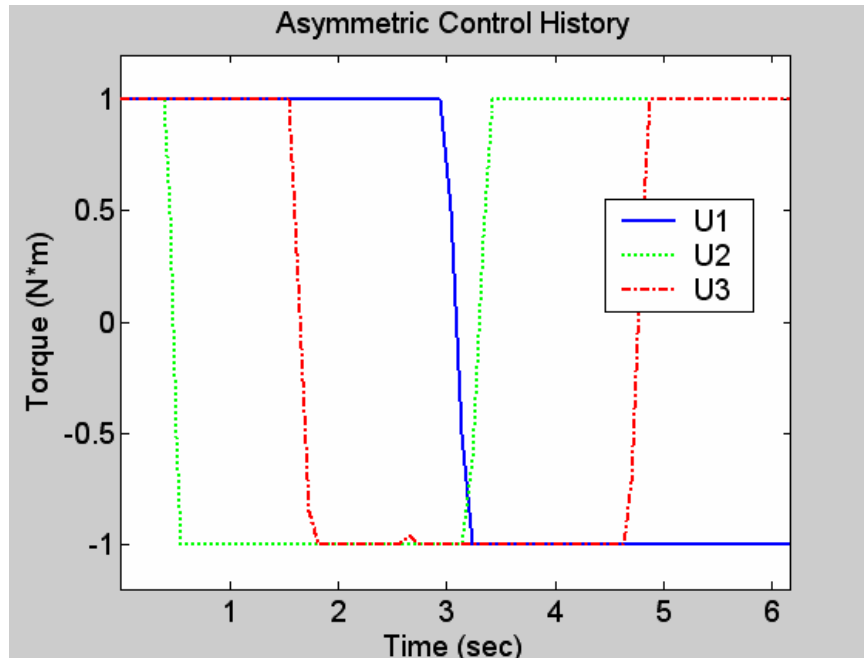


**Figure 39 Asymmetric Spacecraft Time-optimal Maneuver Control Solution**

The process of solution validation begins with propagating the candidate solution through the state dynamics. A feasible solution must drive the spacecraft from its known initial state to the desired end state. The calculated state histories are shown (Figure 40 & Figure 41) with the propagation results (Figure 42 & Figure 43). The original solution obtained is shown in solid lines overlaid with the propagated states shown as '+' marks below.

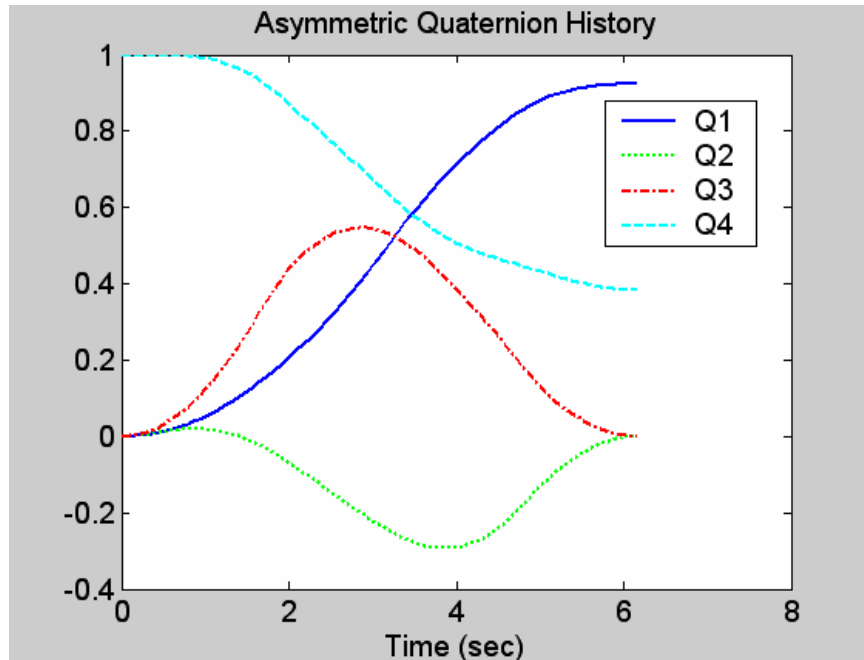


**Figure 40** *Asymmetric Spacecraft Time-optimal Maneuver Quaternion History*

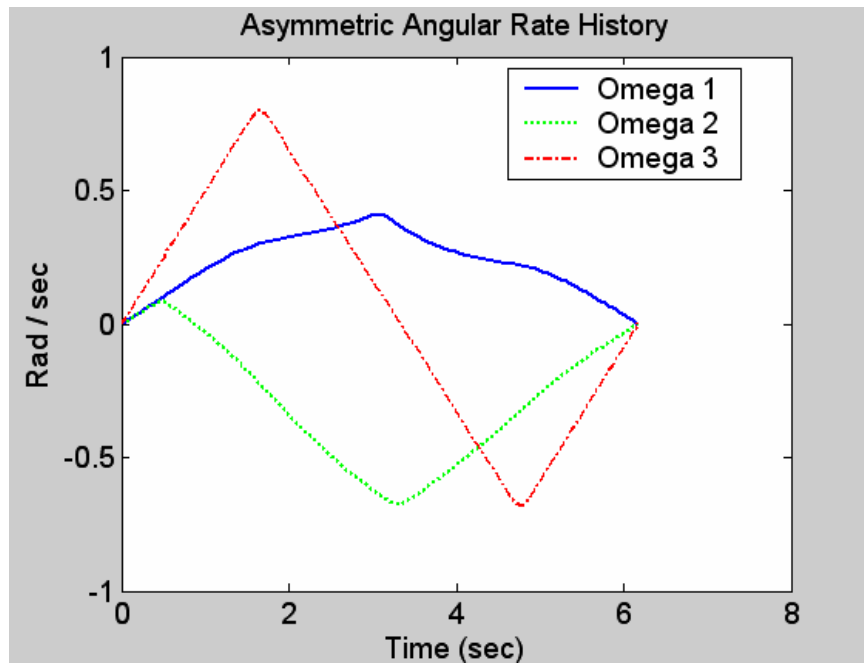


**Figure 41** *Asymmetric Spacecraft Time-optimal Maneuver Angular Rate History*

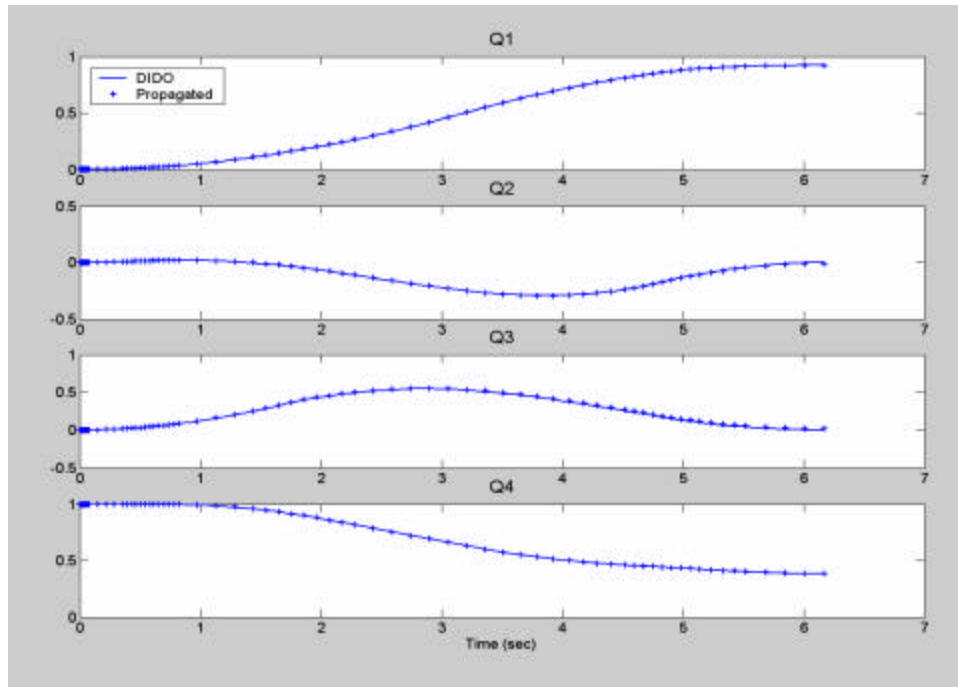


**Figure 42** *Asymmetric Spacecraft Quaternion Solution Validation by Propagation.*

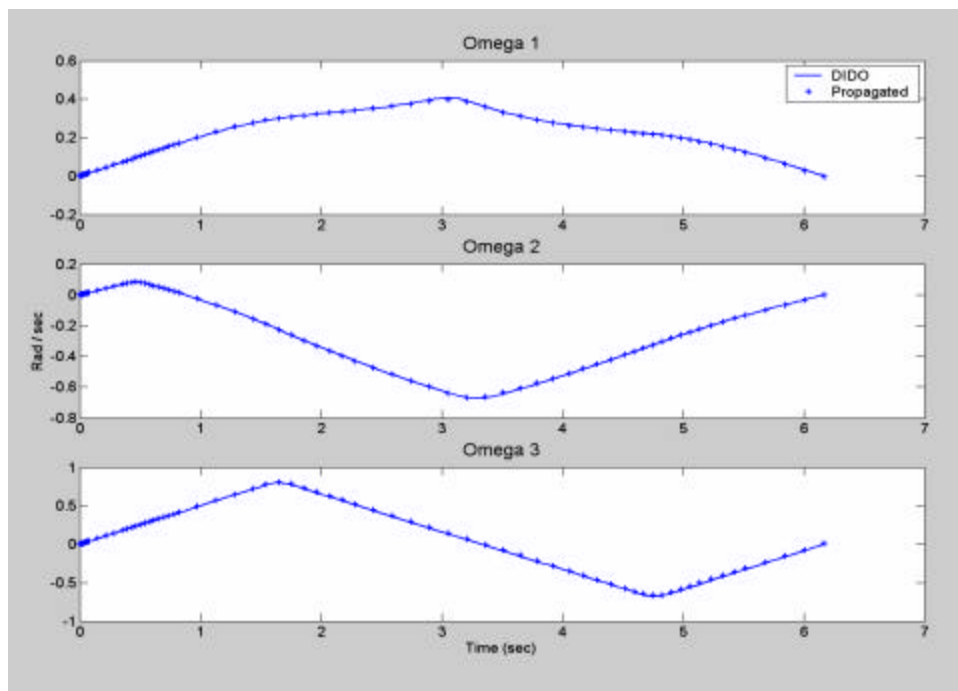


**Figure 43** *Asymmetric Spacecraft Angular Rate Solution Validation by Propagation.*

The solution, confirmed feasible, is evaluated for optimality by observing the switching functions and Hamiltonian evolution. The switching functions, equations (3.35) are shown graphically with the overlaid control solution.

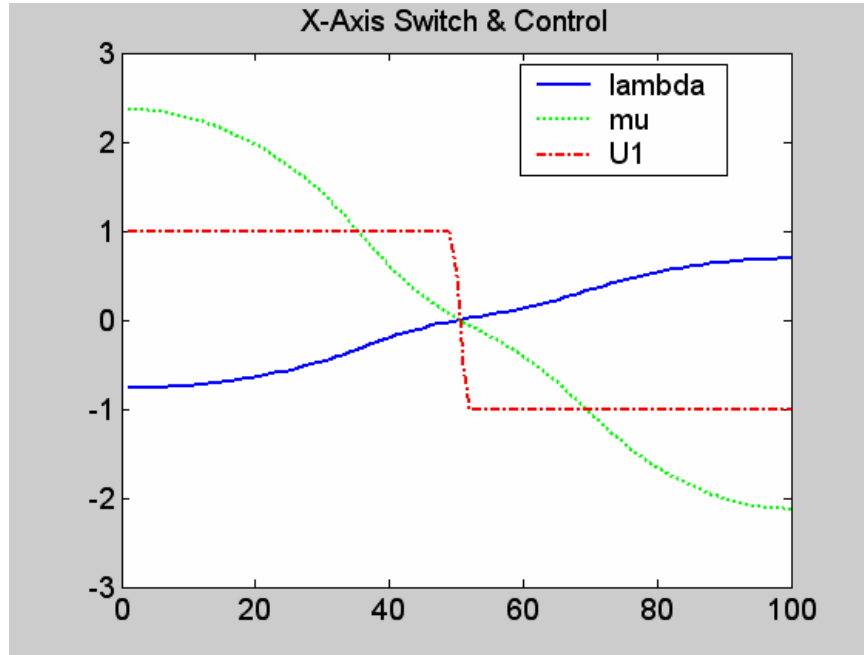


**Figure 44** *Asymmetric Spacecraft X-axis Switching Function and Control Solution*

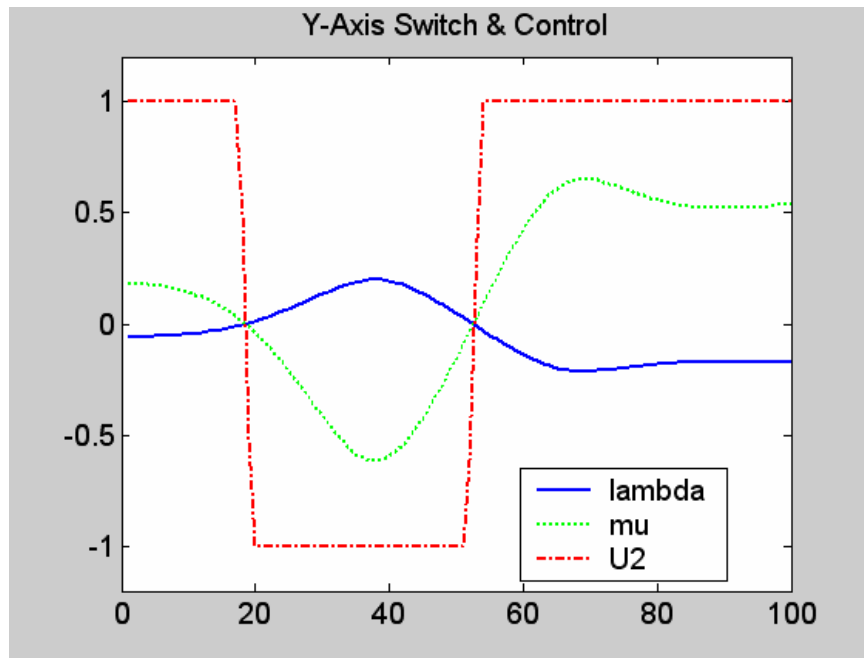


**Figure 45** *Asymmetric Spacecraft Y-axis Switching Function and Control Solution*

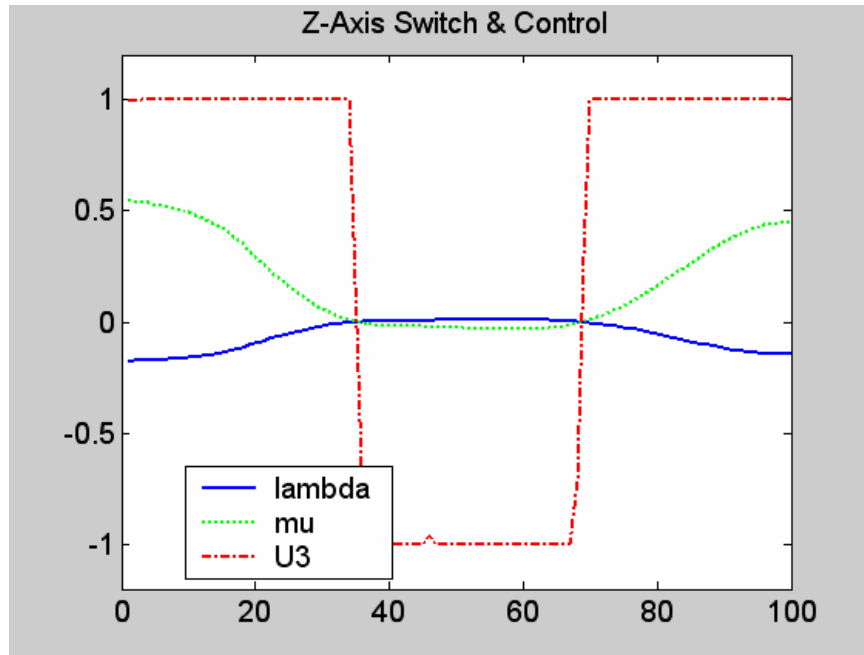


**Figure 46** *Asymmetric Spacecraft Z-axis Switching Function and Control Solution.*

These figures illustrate both the Hamiltonian minimization and the system's compliance with the KKT conditions.

Inspection of the Hamiltonian reveals no direct dependence on time. Thus we expect a constant value Hamiltonian. The final value of the Hamiltonian is given by the transversality condition, equation(3.25). Taken together we expect a constant Hamiltonian of -1. Figure 47 shows the Hamiltonian with the optimality characteristics predicted.

Finally, we compare the time-optimal solution with the eigenaxis maneuver once theorized as nearly time-optimal. The results, (Table 4) show a significant reduction in maneuver time.

<b><i>Asymmetric Maneuver Comparison</i></b>	
<b>Eigenaxis</b>	<b>6.8742 seconds</b>
<b>Time-optimal</b>	<b>6.1737 seconds</b>
<b>Reduction</b>	<b>10.19 %</b>

Table 4 ***Asymmetric Maneuver Comparison***

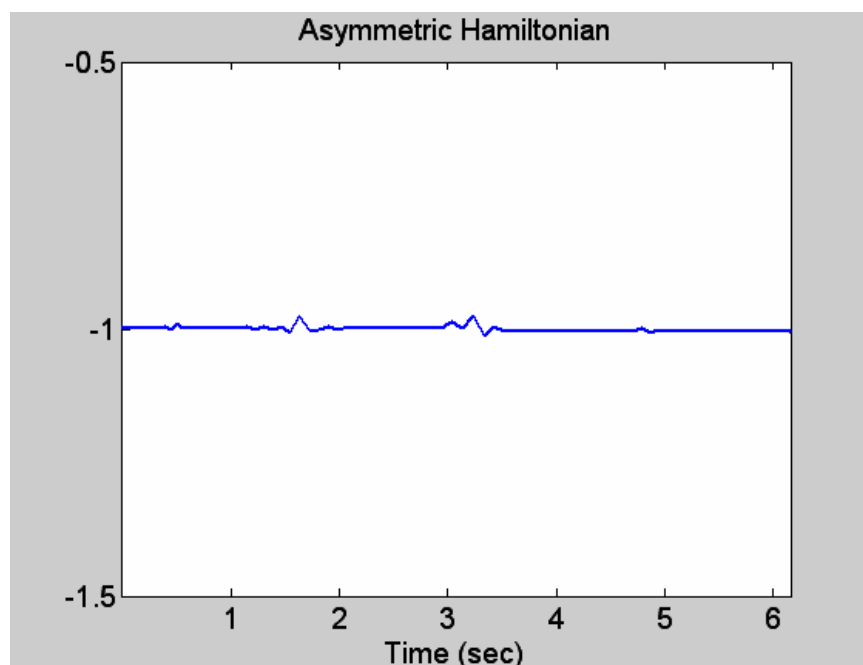


***Figure 47 Asymmetric Spacecraft Time-optimal Hamiltonian Evolution and Transversality***

### **3. Numerical Considerations and Notes**

The problem was transformed into the orbital frame as a stepping stone to the magnetic torque problem. Orbital position and velocity will be necessary for magnetic field computations. Additionally, this problem formulation incorporated linear scaling factors. While not strictly necessary for the problem formulation under consideration, incorporating scaling factors in the independent torque

problem allowed validation of the scaling algorithm prior to the incorporation of the more complicated magnetic field calculations.

For evaluation, the torque available was reduced from 1 Newton-meter to 0.01 Newton-meters. Without scaling, it was noted that costate estimates increased by 4 orders of magnitude. In this work we have found that large costate estimates have generally been an indication of a numerically poor problem formulation. Results in these cases have generally displayed poor accuracy and long computational times. Numerical scaling was implemented in the following form:

$$\begin{aligned}\bar{u} &= k_m u \\ \bar{w} &= k_w w \\ \bar{t} &= k_t t \\ \frac{d\bar{w}}{d\bar{t}} &= \frac{dw}{dt} \left( \frac{k_w}{k_t} \right)\end{aligned}$$

where the overbar indicates a scaled variable.

#### 4. Conclusions

In this section we have shown that the asymmetric problem displays many of the characteristics previously noted in symmetric and axisymmetric configurations. The time-optimal solution, as we might have predicted, is not an eigenaxis maneuver but instead is bang-bang in all control axes. The sequential switching structure theorized and observed by Proulx and Ross<sup>24</sup> was observed for the problem. The number of possible configurations for asymmetric spacecraft combined with the possible slew maneuvers limits the extent to which numerical analysis can be used to form general conclusions. However, the method employed allows us to generate the time-optimal solution to the asymmetric configuration, validate the feasibility of the candidate solution, and evaluate its compliance with the Minimum Principle.

---

## ENDNOTES

- <sup>1</sup> Bilimoria & Wie. (1993). "Time-Optimal Three-Axis Reorientation of a Rigid Spacecraft," *Journal of Guidance, Control, and Dynamics*. Vol. 16, No. 3. American Institute of Aeronautics and Astronautics, Reston, VA.
- <sup>2</sup> Shen & Tsiotras. (1999). "Time-Optimal Control of Axisymmetric Rigid Spacecraft Using Two Controls," *Journal of Guidance, Control, and Dynamics*. Vol. 22, No. 5. American Institute of Aeronautics and Astronautics, Reston, VA.
- <sup>3</sup> Proulx & Ross. "Time-Optimal Reorientation of Asymmetric Rigid Bodies," *Astrodynamics 2001, Part II, Advances in the Astronautical Sciences*, Vol. 109. *Proceedings of the AAS/AIAA Astrodynamics Conference of July 30 to August 2, 2001* (AAS 01-384). Univelt Incorporated. San Diego, CA.
- <sup>4</sup> Bilimoria & Wie. "Time-Optimal Three-Axis Reorientation of a Rigid Spacecraft," *Journal of Guidance, Control, and Dynamics*. Vol. 16, No. 3. American Institute of Aeronautics and Astronautics, Reston, VA.
- <sup>5</sup> Kane, T.R., et al. (1983). *Spacecraft Dynamics*. McGraw-Hill Book Co. New York, NY.
- <sup>6</sup> Sidi, M.J. (1997). *Spacecraft Dynamics and Control*. Cambridge University Press. New York, NY.
- <sup>7</sup> Wie, B. (1998). *Space Vehicle Dynamics and Control*. AIAA Education Series. Reston, VA.
- <sup>8</sup> Ibid.
- <sup>9</sup> Ibid.
- <sup>10</sup> Sidi, M.J. (1997). *Spacecraft Dynamics and Control*. Cambridge University Press. New York, NY.
- <sup>11</sup> Bryson, Arthur, E. & Ho, Y. (1975). *Applied Optimal Control*. Taylor & Francis Publishing. New York, NY.
- <sup>12</sup> Bilimoria & Wie. (1993). "Time-Optimal Three-Axis Reorientation of a Rigid Spacecraft," *Journal of Guidance, Control, and Dynamics*. Vol. 16, No. 3. American Institute of Aeronautics and Astronautics, Reston, VA.
- <sup>13</sup> Hanselman, Duane & Littlefield, Bruce. (2001). *Mastering MATLAB® 6*. Prentice Hall. Upper Saddle River, NJ.
- <sup>14</sup> Bilimoria & Wie. (1993). "Time-Optimal Three-Axis Reorientation of a Rigid Spacecraft," *Journal of Guidance, Control, and Dynamics*. Vol. 16, No. 3. American Institute of Aeronautics and Astronautics, Reston, VA.
- <sup>15</sup> Shen & Tsiotras. (1999). *Time-Optimal Control of Axisymmetric Rigid Spacecraft Using Two Controls*. *Journal of Guidance, Control, and Dynamics*. Vol. 22, No. 5. American Institute of Aeronautics and Astronautics, Reston, VA
- <sup>16</sup> Ibid.
- <sup>17</sup> Bilimoria & Wie. (1993). "Time-Optimal Three-Axis Reorientation of a Rigid Spacecraft," *Journal of Guidance, Control, and Dynamics*. Vol. 16, No. 3. American Institute of Aeronautics and Astronautics, Reston, VA.
- <sup>18</sup> Shen & Tsiotras. (1999). "Time-Optimal Control of Axisymmetric Rigid Spacecraft Using Two Controls," *Journal of Guidance, Control, and Dynamics*. Vol. 22, No. 5. American Institute of Aeronautics and Astronautics, Reston, VA.
- <sup>19</sup> Tsiotras & Longuski. (1995). A New Parameterization of the Attitude Kinematics. *The Journal of the Astronautical Sciences*, Vol. 43, No. 3. American Astronautical Society. Springfield, VA.
- <sup>20</sup> Shen & Tsiotras. (1999). "Time-Optimal Control of Axisymmetric Rigid Spacecraft Using Two Controls," *Journal of Guidance, Control, and Dynamics*. Vol. 22, No. 5. American Institute of Aeronautics and Astronautics, Reston, VA.

---

<sup>21</sup> Livneh & Wie. (1997). *New Results for an Asymmetric Rigid Body with Constant Body-Fixed Torques*. Journal of Guidance, Control, and Dynamics. Vol. 20, No. 5. American Institute of Aeronautics and Astronautics, Reston, VA.

<sup>22</sup> Proulx & Ross. (2001). *Time-Optimal Reorientation of Asymmetric Rigid Bodies*. Astrodynamics 2001, Part II, Advances in the Astronautical Sciences, Vol. 109. Proceedings of the AAS/AIAA Astrodynamics Conference of July 30 to August 2, 2001 (AAS 01-384). Univelt Incorporated. San Diego, CA.

<sup>23</sup> Wie, B. (1998). *Space Vehicle Dynamics and Control*. AIAA Education Series. Reston, VA.

<sup>24</sup> Proulx & Ross(2001). "Time-Optimal Reorientation of Asymmetric Rigid Bodies," *Astrodynamics 2001, Part II, Advances in the Astronautical Sciences*, Vol. 109. *Proceedings of the AAS/AIAA Astrodynamics Conference of July 30 to August 2, 2001* (AAS 01-384). Univelt Incorporated. San Diego, CA.

THIS PAGE INTENTIONALLY LEFT BLANK

## IV. MAGNETIC TORQUE CONTROL

### A. INTRODUCTION

Magnetic torque control has been effectively used for momentum management in zero-momentum systems on many spacecraft systems. The methods are well known and flight tested. The use of magnetic torque control for spacecraft three-axis stabilization is less well known but the body of research is growing. Magnetic torque control represents a low cost method to control small spacecraft in reasonably low earth orbit. In this section we examine the basics of magnetic torque control and the solution to the time-optimal slew of spacecraft using magnetic torque generating devices. This problem is significantly more complicated than the idealized actuator problem of Chapter III. This is due to the resultant cross-product torque generation and varying magnetic field. It is well known that there are body-frame orientations where no torque can be generated in specific directions.

Junkins and Turner, reference [1], discuss the magnetic time-optimal control of spin-stabilized spacecraft. They were able to solve the open loop problem for spin-axis reorientation and implement their solution on the NOVA-1 spacecraft in 1981.<sup>1</sup>

### B. BASIC MAGNETIC TORQUE ATTITUDE CONTROL

The magnetic moment generated within the spacecraft, whether generated intentionally or inadvertently, interacts with the Earth's magnetic field to produce a torque according to:

$$\vec{T}_B = \vec{m} \times \vec{B}$$

where  $\vec{m}$  is the magnetic dipole moment generated inside the spacecraft body\* and  $\vec{B}$  is the Earth's magnetic field intensity.<sup>2</sup>

---

\* Magnetic dipole moment is represented as a lower case m in order to distinguish it from an applied torque which is commonly represented as an upper case M.

The Earth's magnetic field intensity as approximated by McElvain (1962) is:

$$\begin{bmatrix} B_x(t) \\ B_y(t) \\ B_z(t) \end{bmatrix} = \frac{\mathbf{m}_t}{R^3} \begin{bmatrix} \cos(\omega_o t) \sin(i_m) \\ -\cos(i_m) \\ 2\sin(\omega_o t) \sin(i_m) \end{bmatrix} \quad (4.1)$$

where,  $i_m$  is the inclination of the satellite orbit with respect to the magnetic equator,  $R$  is the semi-major axis of the orbit,  $\omega_o$  is the orbital angular velocity,  $t$  is zero at the point in the satellite orbit where the ascending node crosses the equator, and  $\mathbf{m}_t$  is the magnetic dipole strength of the Earth (circa 1975) given as:

$$\mathbf{m}_t = 7.96 \times 10^{15} \text{ Wb} \cdot \text{m}$$

So we see that magnetic field intensity decreases rapidly with orbital altitude. A typical magnetic field approximation is shown for a satellite in a circular orbit with inclination of 35.4 degrees at altitude of 560 Km. As expected the behavior in the x-z planes is harmonic (Figure 48) at the orbital frequency.

The magnetic model used for this problem differs from equation (4.1). The above model is reasonably accurate as a first-order approximation but does not take into account the rotation of the earth. For this reason, a model with slightly higher fidelity was adopted. Shown below, as equation (4.2), is a model adopted from Wertz, Spacecraft Attitude Determination and Control.<sup>3</sup> This model assumes no orbit precession but does allow for the Earth's rotation.

$$\begin{bmatrix} B_{x_0} \\ B_{y_0} \\ B_{z_0} \end{bmatrix} = \frac{K}{R^3} \begin{bmatrix} \cos(a) [\cos(e)\sin(i) - \sin(e)\cos(i)\cos(u)] - \sin(a)\sin(e)\sin(u) \\ -\cos(e)\cos(i) - \sin(e)\sin(i)\sin(u) \\ 2\sin(a) [\cos(e)\sin(i) - \sin(e)\cos(i)\cos(u)] + 2\cos(a)\sin(e)\sin(u) \end{bmatrix}$$

where,

$$K = 7.943 \times 10^{15} \frac{N \cdot m^2}{amp} \quad (4.2)$$

$R$  = radius from Earth c.m. to s/c c.m. (m)

$$a = \omega_0 t$$

$u = \omega_e t$ ,  $\omega_e \equiv$  Earth rotational frequency (rad/sec)

$e = 11.7^\circ$  magnetic dipole tilt

$i =$  orbit inclination

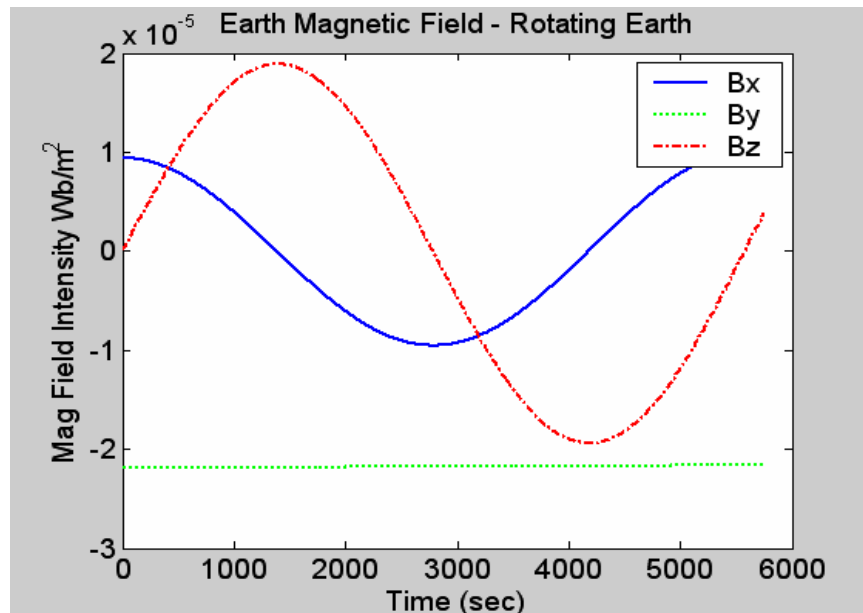


**Figure 48 Earth Magnetic Field**

Recall Euler's equations (repeated from previous for the convenience of the reader).

$$\begin{aligned} M_1 &= I_x \dot{w}_x + (I_z - I_y) w_y w_z \\ M_2 &= I_y \dot{w}_y + (I_x - I_z) w_x w_z \\ M_3 &= I_z \dot{w}_z + (I_y - I_x) w_x w_y \end{aligned}$$

The external torque can now be replaced by the torque generated by the interaction of the Earth's magnetic field and the satellite magnetic dipole moment. The rotational dynamics equation of motion in vector form then becomes,

$$I\dot{\mathbf{w}} + \mathbf{w} \times I\mathbf{w} = \mathbf{m} \times \mathbf{B} \quad (4.3)$$

where angular velocities are by necessity referenced to the Newtonian frame and,

$$\vec{m} \times \vec{B} = \begin{bmatrix} m_2 B_z - m_3 B_y \\ m_3 B_x - m_1 B_z \\ m_1 B_y - m_2 B_x \end{bmatrix} \quad (4.4)$$

As written, the cross-product of equation (4.4) is meaningless since the dipole moments ( $m_i$ ) are in the body frame and the magnetic field components are represented in the orbit frame. Therefore, the components of the magnetic field which are in the orbit frame must be rotated into the spacecraft frame by:

$$\vec{B}_B = {}^B\bar{C}^o \vec{B}_o \quad (4.5)$$

where the DCM was previously defined in equation (3.5). Then the magnetic field in the body frame in expanded form is given by:

$$\begin{aligned} B_1 &= B_{x_o} (q_1^2 - q_2^2 - q_3^2 + q_4^2) + 2B_{y_o} (q_1 q_2 + q_3 q_4) + 2B_{z_o} (q_1 q_3 + q_2 q_4) \\ B_2 &= 2B_{x_o} (q_1 q_2 - q_3 q_4) + B_{y_o} (q_1^2 - q_2^2 - q_3^2 + q_4^2) + 2B_{z_o} (q_2 q_3 + q_1 q_4) \\ B_3 &= 2B_{x_o} (q_1 q_3 + q_2 q_4) + 2B_{y_o} (q_2 q_3 - q_1 q_4) + B_{z_o} (q_3^2 - q_1^2 - q_2^2 + q_4^2) \end{aligned} \quad (4.6)$$

Finally, by substituting equation (4.6) into equation (4.3) we can form the dynamic constraint equations as follows,

$$\begin{aligned}\dot{w}_x &= \frac{1}{I_x}(m_2 B_3 - m_3 B_2) + k_1 w_y w_z, & k_1 &= \frac{I_y - I_z}{I_x} \\ \dot{w}_y &= \frac{1}{I_y}(m_3 B_1 - m_1 B_3) + k_2 w_x w_z, & k_2 &= \frac{I_z - I_x}{I_y} \\ \dot{w}_z &= \frac{1}{I_z}(m_1 B_2 - m_2 B_1) + k_3 w_x w_y, & k_3 &= \frac{I_x - I_y}{I_z}\end{aligned}$$

These represent the rotational dynamical equations of motion for our spacecraft, Earth magnetic field system.

### C. TIME-OPTIMAL MAGNETIC TORQUE CONTROLLED SLEW

In this section we consider the time-optimal reorientation of a spacecraft with magnetic torque control. The maneuver is defined as rest-to-rest in the orbit frame where the initial and final states are given.

#### 1. Problem Formulation

The spacecraft state is defined by its position and angular velocity.

$$\underline{x} = \begin{bmatrix} q \\ \underline{w} \end{bmatrix}$$

The position is represented by a four-element quaternion vector, we have previously adopted the convention that the fourth element of the quaternion vector is the scalar quantity. The angular velocity is in body coordinates with respect to the Newtonian frame.

We choose our control parameter as the magnetic dipole moment of the torque rods. Dipole moment is controlled by current flow however the response of dipole moment to changes in current can be considered instantaneous. Since

the actual torque generated is limited by the maximum dipole moment of the torque rod, we impose a bound on the control dipole moment.

$$\underline{u} = \begin{bmatrix} m_1 \\ m_2 \\ m_3 \end{bmatrix} \rightarrow |m_i| \leq 30A \cdot m^2 \quad (4.7)$$

The minimum time, rest-to-rest, reorientation problem may then be stated as follows:

Determine the controls  $[u_1^*, u_2^*, u_3^*]$  that drive the spacecraft from its initial rest position, given by  $[\underline{x}_0]$  to its final rest position given by  $[\underline{x}_f]$  while minimizing the cost function:

$$J(\underline{x}(\cdot), \underline{u}(\cdot), t_f) = t_f - t_0$$

where we have used the Mayer form of the cost function, subject to the following constraints:

Control Constraint: The control constraint is defined in the standard form,

$$h^L(t) \leq h(u, t) \leq h^U(t)$$

then our control constraint can be written,

$$-30 \leq u_i \leq 30$$

Dynamic Constraints:

$$\begin{aligned}
 \dot{q}_1 &= \frac{1}{2} [\mathbf{w}_1 q_4 - \mathbf{w}_2 q_3 + \mathbf{w}_3 q_2] \\
 \dot{q}_2 &= \frac{1}{2} [\mathbf{w}_1 q_3 + \mathbf{w}_2 q_4 - \mathbf{w}_3 q_1] \\
 \dot{q}_3 &= \frac{1}{2} [-\mathbf{w}_1 q_2 + \mathbf{w}_2 q_1 + \mathbf{w}_3 q_4] \\
 \dot{q}_4 &= \frac{1}{2} [-\mathbf{w}_1 q_1 - \mathbf{w}_2 q_2 - \mathbf{w}_3 q_3] \\
 \dot{w}_x &= \frac{1}{I_x} (m_2 B_3 - m_3 B_2) + k_1 w_y w_z, & k_1 &= \frac{I_y - I_z}{I_x} \\
 \dot{w}_y &= \frac{1}{I_y} (m_3 B_1 - m_1 B_3) + k_2 w_x w_z, & k_2 &= \frac{I_z - I_x}{I_y} \\
 \dot{w}_z &= \frac{1}{I_z} (m_1 B_2 - m_2 B_1) + k_3 w_x w_y, & k_3 &= \frac{I_x - I_y}{I_z}
 \end{aligned} \tag{4.8}$$

## 2. Solving the Optimal Control Problem

The first step in solving the optimal control problem is to form the Hamiltonian. Basic format of the Hamiltonian is repeated here<sup>†</sup>,

$$H(\mathbf{I}, \mathbf{x}, u, t) = F(\mathbf{x}, u, t) + \mathbf{I}^T f(\mathbf{x}, u, t)$$

Since the cost functional was formulated without a Lagrange cost term the Hamiltonian reduces to the following.

$$H(\mathbf{I}, \mathbf{x}, u, t) = \mathbf{I}^T f(\mathbf{x}, u, t)$$

Again, since the quaternion kinematics are written in terms of angular velocity of the body with respect to the orbit frame, equation (4.8), a lengthy algebraic rotation sequence is required to write the Hamiltonian in standard form:

---

<sup>†</sup> Recall that in this notation F is the Lagrange (running) cost and f are the state dynamics.

$$\begin{aligned}
H = & \frac{I_{q_1}}{2} (\mathbf{w}_x q_4 - \mathbf{w}_y q_3 + \mathbf{w}_z q_2 + \mathbf{w}_o q_3) + \frac{I_{q_2}}{2} (\mathbf{w}_x q_3 + \mathbf{w}_y q_4 - \mathbf{w}_z q_1 + \mathbf{w}_o q_4) \\
& + \frac{I_{q_3}}{2} (-\mathbf{w}_x q_2 + \mathbf{w}_y q_1 + \mathbf{w}_z q_2 - \mathbf{w}_o q_1) + \frac{I_{q_4}}{2} (-\mathbf{w}_x q_1 - \mathbf{w}_y q_2 - \mathbf{w}_z q_3 - \mathbf{w}_o q_2) + \\
& I_{w_x} \left\{ \frac{1}{I_x} (u_2 B_3 - u_3 B_2) + k_1 \mathbf{w}_y \mathbf{w}_z \right\} + I_{w_y} \left\{ \frac{1}{I_y} (u_3 B_1 - u_1 B_3) + k_2 \mathbf{w}_x \mathbf{w}_z \right\} + \\
& I_{w_z} \left\{ \frac{1}{I_z} (u_1 B_2 - u_2 B_1) + k_3 \mathbf{w}_x \mathbf{w}_y \right\}
\end{aligned} \tag{4.9}$$

The subscripts on the Lagrange multipliers have been chosen for bookkeeping purposes. The control vector is defined in equation (4.7).

Now, according to Pontryagin's principle the control which minimizes the cost functional must meet the conditions we established earlier. It is however, important to note that not all of these conditions reveal usable information about the nature of the problem.

#### **a. Hamiltonian Minimization**

We know from previous work that a necessary condition for the Hamiltonian to be a minimum with respect to the control variable is that the partial derivative of the Lagrangian with respect to the control equals zero. In this case the control that satisfies this condition must also lie within the control constraint set. We apply Lagrange multipliers in the form,

$$\bar{H}(\mathbf{I}, \mathbf{x}, u, t, \mathbf{m}) \doteq H(\mathbf{I}, \mathbf{x}, u, t) + \mathbf{m}^T h(u, t) \tag{4.10}$$

Then, by inspection of equations (4.9) and (4.10), we can write the necessary conditions for the Hamiltonian minimization as follows.

$$\begin{aligned}
\frac{I_{w_z}}{I_z} B_2 - \frac{I_{w_y}}{I_y} B_3 + \mathbf{m}_1 &= 0 \\
\frac{I_{w_x}}{I_x} B_3 - \frac{I_{w_z}}{I_z} B_1 + \mathbf{m}_2 &= 0 \\
\underbrace{\frac{I_{w_y}}{I_y} B_1 - \frac{I_{w_x}}{I_x} B_2}_{S_i} + \underbrace{\mathbf{m}_3}_{m_{u_i}} &= 0
\end{aligned} \tag{4.11}$$

These represent useful information that can be evaluated to validate the candidate solution.

**b. Hamiltonian Evolution and Final Value**

The Hamiltonian evolves in accordance with the simple equation,

$$\dot{H} = \frac{\partial H}{\partial t} \tag{4.12}$$

Previously, we dealt only with Hamiltonian equations that had no specific dependence on time and therefore the time-rate of change was zero. In this case the magnetic field of the Earth introduces a time-dependence into the Hamiltonian. That is  $\partial H / \partial t \neq 0$ . Therefore, the Hamiltonian is *not* a constant in the interval under consideration.

The final value of the Hamiltonian is given by,

$$H[t_f] + \frac{\partial E}{\partial t_f} + \mathbf{u}^t \frac{\partial e}{\partial t_f} = 0$$

where the end manifold ( e ) is written in the standard form,

$$e(\underline{x}_f, t_f) = \begin{bmatrix} q_{1_f} - \sin\left(\frac{f}{2}\right) \\ q_{2_f} \\ q_{3_f} \\ q_{4_f} - \cos\left(\frac{f}{2}\right) \\ w_{x_f} \\ w_{y_f} + w_o \cos(f) \\ w_{z_f} - w_o \sin(f) \end{bmatrix} = 0$$

Then by inspection we can see that the final value of the Hamiltonian is negative one.

$$H[t_f] + 1 = 0 \rightarrow H[t_f] = -1$$

Although the Hamiltonian is not a constant for the interval under consideration its final value represents a second numerical figure of merit to validate the optimality of the solution.

### 3. Numerical Results

The numerical example for this work was taken from the Naval Postgraduate School's current small satellite program, "NPSAT 1." Designed primarily to allow a hands-on learning experience this satellite, still in the design phase, will provide three-axis magnetic torque control with a pitch wheel for increased stabilization. The moment of inertias and orbital parameters used in the numerical examples were taken from NPSAT 1 preliminary designs. The contribution of the pitch bias wheel will be addressed in a later chapter. The NPSAT 1 data includes:

<b>NPSAT 1 Parameters</b>	
<b>lx</b>	<b>5 kg·m<sup>2</sup></b>
<b>ly</b>	<b>5.1 kg·m<sup>2</sup></b>
<b>lz</b>	<b>2 kg·m<sup>2</sup></b>
<b>Max Dipole Moment</b>	<b>30 Amp·m<sup>2</sup></b>
<b>Orbital Altitude</b>	<b>560 km (Circular)</b>
<b>Inclination</b>	<b>35.4 degrees</b>

Table 5 *NPSAT 1 Parameters for Numerical Simulations*

The maneuver selected for simulation is a 135 degree roll (x-axis slew).

The time-optimal control solution for this maneuver demonstrates a surprisingly clean bang-bang structure. The solution, shown in Figure 49, has 10 control switches distributed among the three axes.

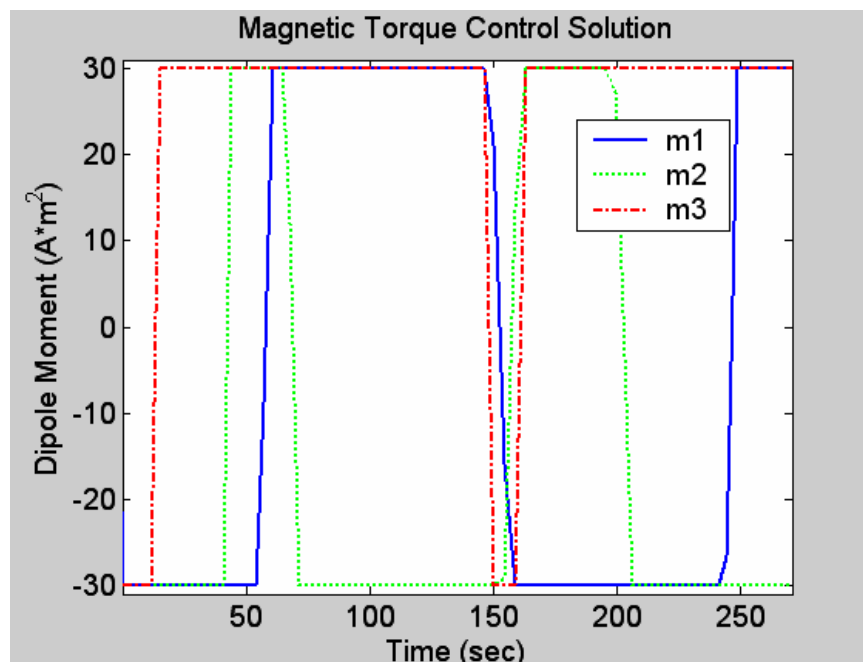
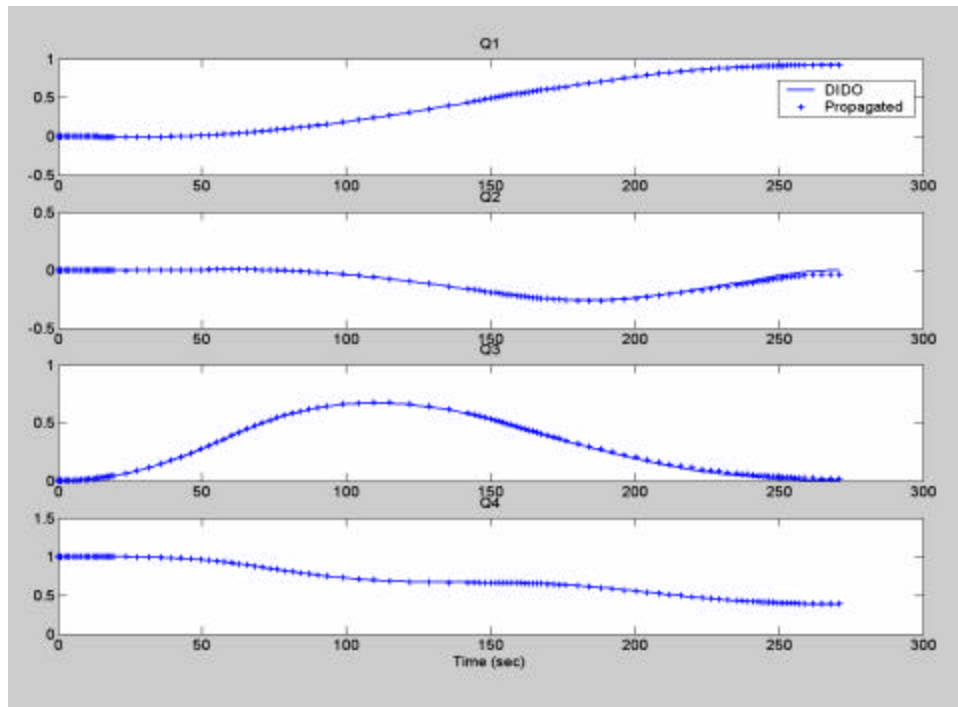
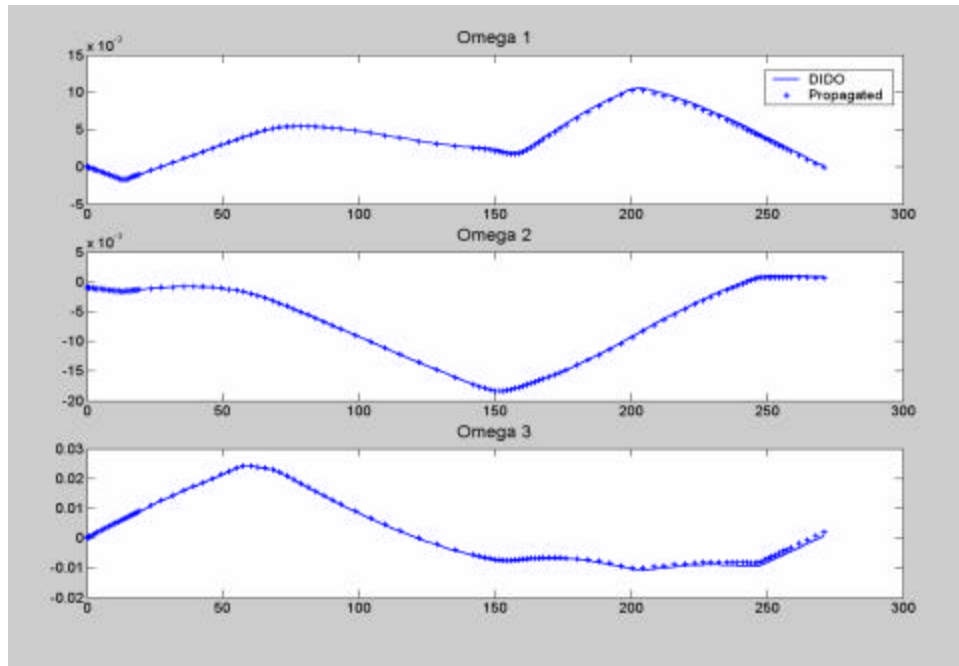


Figure 49 *Time-optimal Control Solution for Magnetic Torque Problem*

Before evaluating the optimality of the candidate solution the feasibility is evaluated. The control solution is propagated through a separate ODE 45 dynamics simulator to verify that the candidate solution drives the dynamic system from the initial state to the final state. The propagation results (Figure 50 & Figure 51) show that the control solution does meet the end point constraints and that the estimated states closely match those obtained during propagation. The original solution obtained is shown in solid lines overlaid with the propagated states shown as '+' marks below.



**Figure 50** *Quaternion Solution and Validation by Propagation*



**Figure 51 Angular Rate Solution and Validation by Propagation**

The quaternion and angular rate histories are shown (Figure 52 & Figure 53). The maneuver is clearly not an eigenaxis slew. This is evident from both the variation in the quaternions  $q_2$  &  $q_3$  and the non-zero angular rates of  $w_2$  &  $w_3$ .

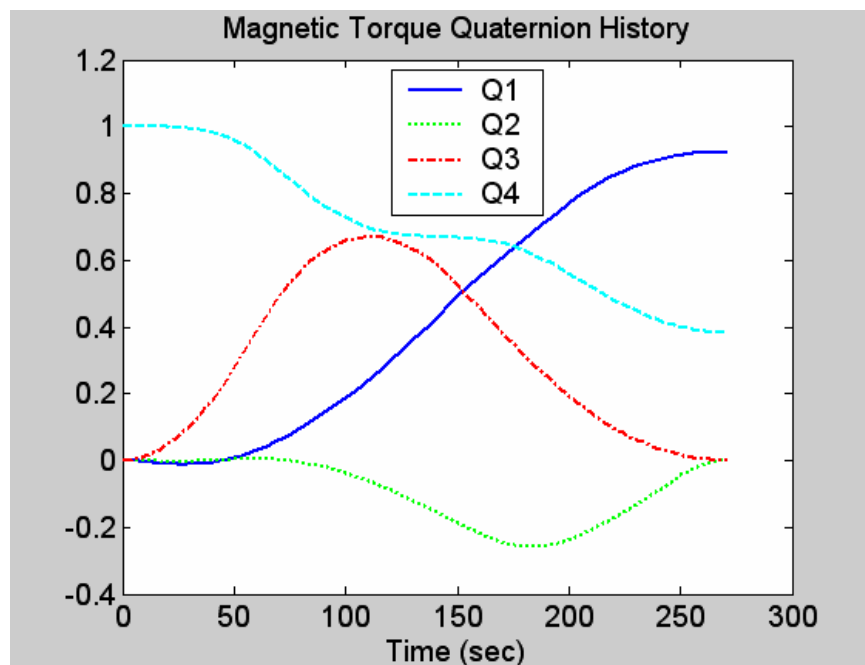


**Figure 52 Magnetic Torque Slew Time-optimal Quaternion History**

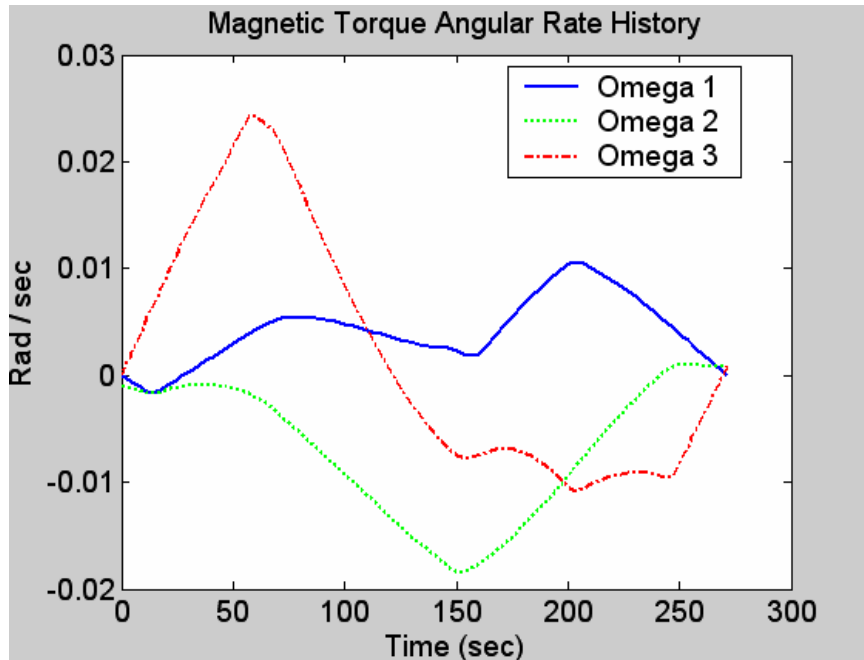


**Figure 53** *Magnetic Torque Slew Time-optimal Angular Rate History*

Next we evaluate the optimality of the feasible, candidate solution. The switching functions are given in equations (4.11). These are plotted overlaid with the scaled control solution (Figure 54, Figure 55, & Figure 56).

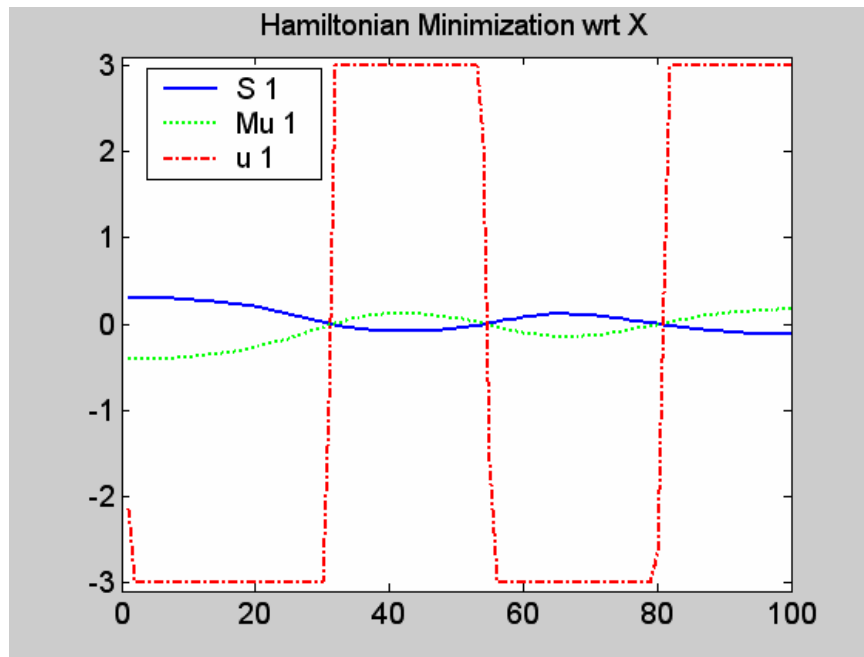


**Figure 54** *Magnetic Torque Control X-axis Switching Function and Control Solution*

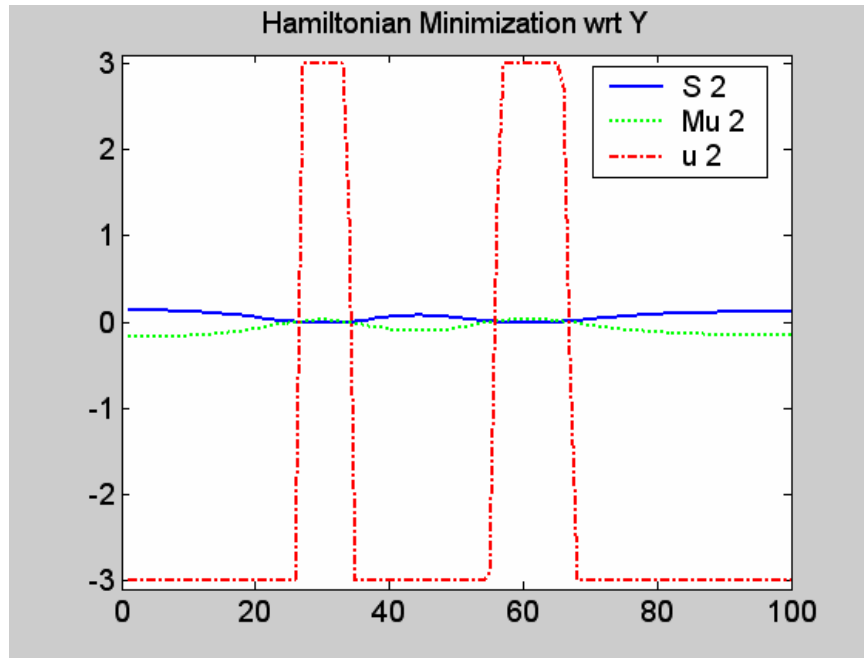


**Figure 55** *Magnetic Torque Control Y-axis Switching Function and Control Solution*

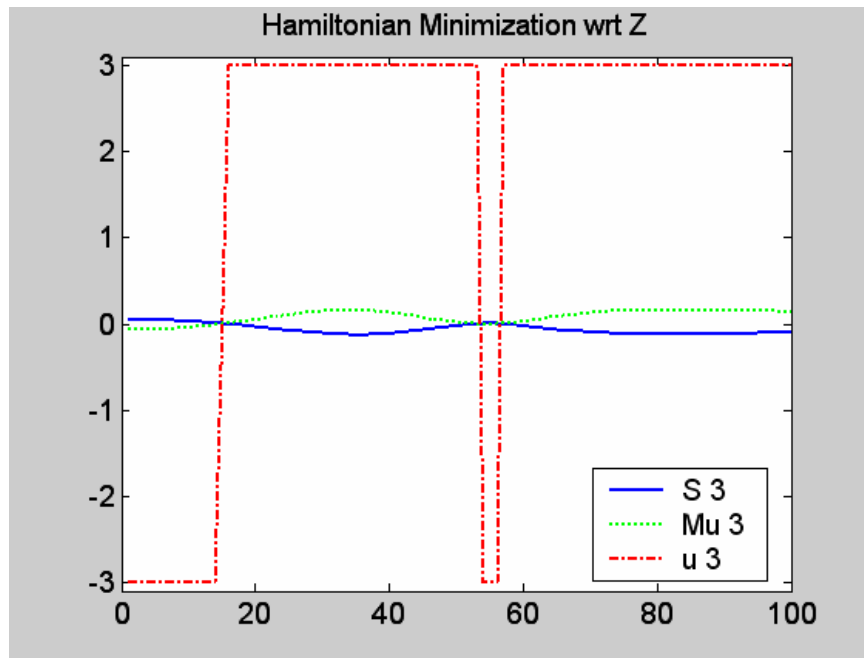


**Figure 56** *Magnetic Torque Control Z-axis Switching Function and Control Solution*

Shown are the switching functions ( $S_i$ ) previously defined as the partial derivative of the Hamiltonian with respect to the control vector. The KKT multiplier ( $\mu$ ) is also shown plotted separately from the switching function. The sum of the switching function and the KKT multiplier is the definition of the minimization of the Hamiltonian, equation (4.11), and should be numerically equal to zero. Additionally, as before the switching function and control are related by the KKT conditions:

$$u_i^* = \begin{cases} \text{maximum} & S_i < 0 \\ \text{minimum} & S_i > 0 \\ \text{singular} & S_i \equiv 0 \end{cases}$$

These figures clearly illustrate that the control solution meets optimality criteria established by the Hamiltonian minimization.

The Hamiltonian transversality and evolution conditions are complicated by the varying magnetic field. The Hamiltonian and the predicted final value are shown (Figure 57). The numerical final value of the Hamiltonian and the theoretical final value differ by only 0.0646. Therefore we conclude that the candidate solution has met the necessary conditions for optimality.

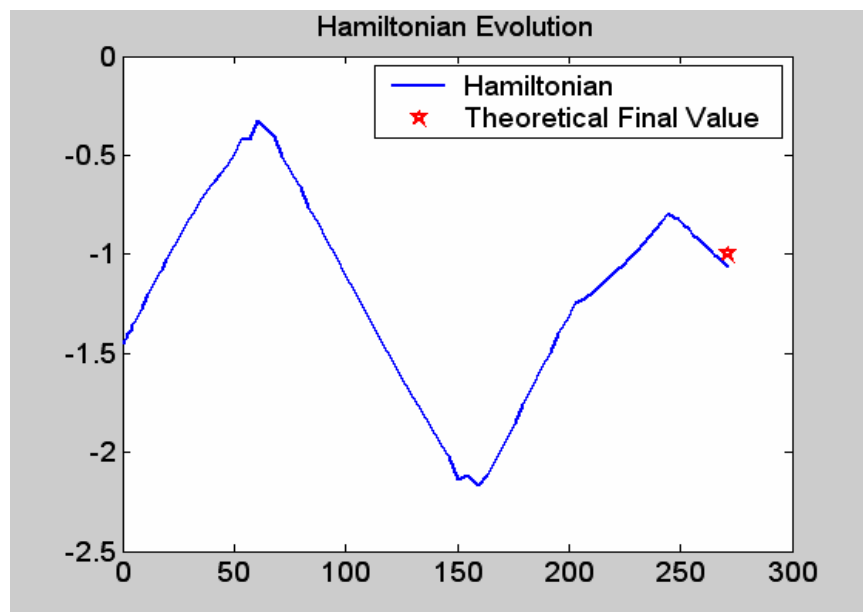


**Figure 57** *Magnetic Torque Solution Hamiltonian and Final Value*

Additionally, to validate our hypothesis that the time-dependence of the Hamiltonian was due to the varying magnetic field the problem was evaluated with a constant magnetic field approximation. The Hamiltonian for the case of a constant magnetic field is shown in Figure 58. The Hamiltonian for this case has lost its apparent dependence on time and settled to a value that is numerically close to the value of -1 that was predicted.

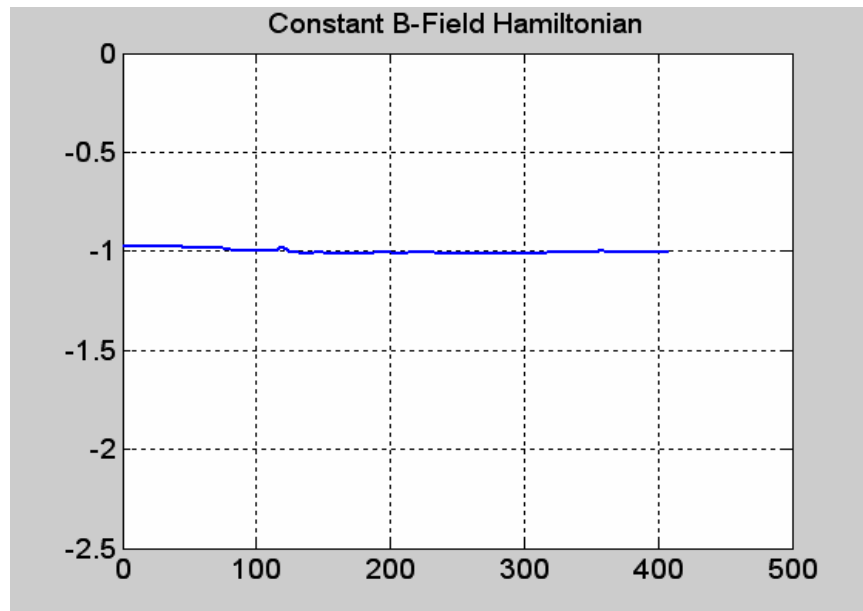


**Figure 58** *Constant Magnetic Field Approximation Hamiltonian Solution*

#### 4. Numerical Considerations and Scaling

The linear scaling used throughout these algorithms was introduced in the previous section. In this section scaling was also added for the Earth’s magnetic field in the form:

$$\bar{B}_i = k_B B_i$$

The goal of the scaling is to bring all numerical values seen by the optimization solver into the same order of magnitude. Scaling values were adjusted from an unscaled solution to improve the quality of the solution and then readjusted as necessary. Proper scaling reduced computation time and improved the accuracy of the solution. Additionally, the switching functions of properly scaled problems

behaved more closely to theoretical predictions indicating that results were improved by proper scaling.

<b>Scaling Effects</b>	
<b>Maneuver Time (before scaling)</b>	<b>230.0845 seconds</b>
<b>Maneuver Time (after scaling)</b>	<b>271.1564 seconds</b>
<b>Error</b>	<b>15.15 %</b>

Table 6 *Effects of Scaling on Solution Fidelity*

## 5. Conclusions

In this section the open loop time-optimal control for a magnetic torque controlled asymmetric spacecraft was determined. The candidate solution was determined by propagation to be a feasible solution to the problem. The optimality of the solution was validated through an analysis of the Hamiltonian minimization, switching functions and the behavior of the Hamiltonian. The hitherto unseen variation of the Hamiltonian over time was theorized to be caused by the time dependence of the Earth's magnetic field. When this dependence was eliminated the Hamiltonian returned to the constant values we have seen previously. Therefore, we conclude that the solution is feasible and meets the necessary conditions for optimality.

---

## ENDNOTES

<sup>1</sup> Junkins, J.L. & Turner, J.D. (1986). *Optimal Spacecraft Rotational Maneuvers*. Elsevier. Amsterdam, The Netherlands.

<sup>2</sup> Sidi, M.J. (1997). *Spacecraft Dynamics and Control*. Cambridge University Press. New York, NY..

<sup>3</sup> Presented in the class notes of Professor B. Leonard AA-3818 / Fall '04. *Spacecraft Dynamics and Control*. US Naval Postgraduate School, Monterey, CA.

THIS PAGE INTENTIONALLY LEFT BLANK

## V. NPSAT 1 CONTROL SYSTEM

### A. INTRODUCTION

NPSAT 1 is a small satellite design project currently in work at the U.S. Naval Postgraduate School (Figure 59). It was conceived as a three-axis stabilized magnetic torque controlled satellite. Later in the design process, a pitch bias wheel was added to improve stability and reliability. In this section we explore the time-optimal reorientation of this small asymmetric satellite where both the three torque rods and the pitch wheel are available as torque generating devices.

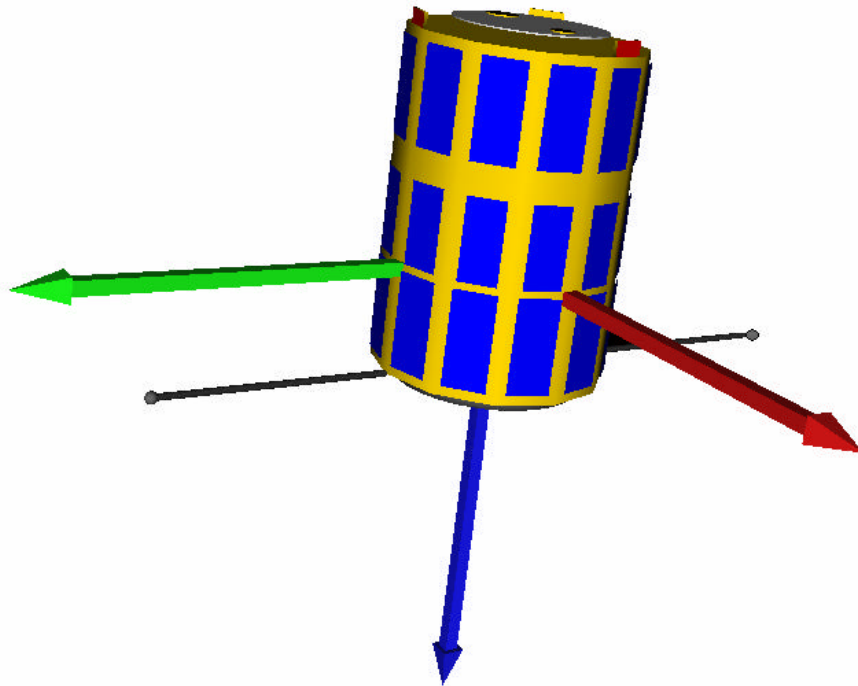


*Figure 59 NPSAT1 Conceptual Image courtesy of Dan Sakoda*

## B. PROBLEM FORMULATION

In this case the spacecraft state is defined by its position, angular velocity and the angular momentum of the pitch wheel.

$$\underline{x} = \begin{bmatrix} \underline{q} \\ \underline{w} \\ h_w \end{bmatrix} \in \mathbb{R}^8$$

The position is represented by a four-element quaternion vector; we have previously adopted the convention that the fourth element of the quaternion vector is the scalar quantity. The angular velocity is in body coordinates with respect to the Newtonian frame. The pitch wheel is assumed to be aligned with the spacecraft #2 principal axis. This assumption simplifies the formulation of the rotational dynamics equations. The orbital parameters are as given in Table 5.

The quaternion kinematics equations are well known and shown in equation (3.33). These equations are unchanged by the addition of the pitch bias wheel. The rotational dynamics however, are now the result of the external torque generated by the interaction of the magnetic field and the torque rods in addition to the pitch wheel angular momentum and torque.

The time rate of change of angular momentum can be expressed as<sup>1</sup>,

$$\bar{M}_{ext} = \left[ \frac{d}{dt} \bar{H}_S \right]_N = \left[ \frac{d}{dt} \bar{H}_S \right]_b + {}^N \bar{w}^b \times \bar{H}_S \quad (5.1)$$

where  $\bar{H}_S$  is the total angular momentum of the spacecraft-wheel system and is expressed in the body frame. Then by assuming that the wheel's center of mass is collocated with the spacecraft center of mass we can express the system angular momentum as,

$$\bar{H} = I_B {}^N \bar{w}^b + I_W {}^N \bar{w}^W \quad (5.2)$$

where  $I_B$  &  $I_W$  are the body and wheel moments of inertia respectively, and the angular velocity of the wheel with respect to the Newtonian frame is given by,

$${}^N \bar{w}^W = {}^N \bar{w}^b + {}^b \bar{w}^W$$

Then the angular momentum of the system can be written as,

$$\vec{H}_S = I_B {}^N \vec{\omega}^b + I_W {}^N \vec{\omega}^b + I_W {}^b \vec{\omega}^W$$

By defining,

$$\mathbf{J} \doteq I_B + I_W$$

we have,

$$\vec{H}_S = \mathbf{J} {}^N \vec{\omega}^b + I_W {}^b \vec{\omega}^W \quad (5.3)$$

This result is easily derived under the assumptions stated. Kane<sup>2</sup> provides a detailed derivation to show that this result holds for any configuration.

Then, referring to equation (5.1) we have,

$$M_{\text{ext}} = \mathbf{J} {}^N \dot{\vec{\omega}}^b + I_W {}^b \dot{\vec{\omega}}^W + {}^N \vec{\omega}^b \times (\mathbf{J} {}^N \vec{\omega}^b + I_W {}^b \vec{\omega}^W)$$

By defining,

$$\left[ \frac{d}{dt} \vec{h} \right]_B = I_W {}^b \dot{\vec{\omega}}^W \doteq \dot{\vec{h}}_W$$

we can write,

$$M_{\text{ext}} = \mathbf{J} {}^N \dot{\vec{\omega}}^b + \dot{\vec{h}}_W + {}^N \vec{\omega}^b \times \mathbf{J} {}^N \vec{\omega}^b + \vec{h}_W$$

If we allow  $M_{\text{ext}}$  to be the sum of disturbance torques and the torque generated by the interaction of the Earth's magnetic field and the magnetic torque rods, setting the disturbance torque to zero we can write,

$$\mathbf{J} \dot{\vec{\omega}} + \vec{\omega} \times \mathbf{J} \vec{\omega} = \vec{m} \times \vec{B} - \dot{\vec{h}}_W - \vec{\omega} \times \vec{h}_W$$

where,

$$\dot{\vec{h}}_W \doteq \begin{bmatrix} 0 \\ \dot{h}_W \\ 0 \end{bmatrix}, \quad \vec{h}_W = \begin{bmatrix} 0 \\ h_W \\ 0 \end{bmatrix} \quad \text{and} \quad \vec{\omega} \doteq {}^N \vec{\omega}^b$$

Carrying out the cross products and rotational transformations previously defined gives the following result:

$$\begin{aligned}
J_1 \dot{w}_x - (J_2 - J_3) w_y w_z &= m_2 B_3 - m_3 B_2 + w_z h_w \\
J_2 \dot{w}_y - (J_3 - J_1) w_x w_z &= m_3 B_1 - m_1 B_3 - \dot{h}_w \\
J_3 \dot{w}_z - (J_1 - J_2) w_x w_y &= m_1 B_2 - m_2 B_1 - w_x h_w
\end{aligned}$$

where the Earth's Magnetic Field  $(B_1, B_2, B_3)$  is in the spacecraft body frame and was previously defined by equation (4.6). The four-element control vector is chosen as:

$$\underline{u} = \begin{bmatrix} m_1 \\ m_2 \\ m_3 \\ u_w \end{bmatrix} \tag{5.4}$$

Box constraints are imposed on the control elements based on the physical limitations of the control elements selected. The components under consideration in this model have the physical characteristics shown (Table 7).

<b>Component Characteristics</b>		
<b>Torque Rods</b>	<b>Maximum Magnetic Dipole Moment</b>	<b>30 Amp*m<sup>2</sup></b>
<b>Pitch Wheel</b>	<b>Maximum Angular Momentum</b>	<b>18 N*m*sec</b>
<b>Pitch Wheel</b>	<b>Maximum Torque</b>	<b>30 mN*m</b>

Table 7 *NPSAT 1 Simulation Component Characteristics*

Pitch wheel angular momentum limits are imposed as a state constraint. Other values are imposed as control constraints.

### C. TIME-OPTIMAL NPSAT 1 SLEW

In this section we consider the time-optimal reorientation of an asymmetric spacecraft controlled by a combination of magnetic torque rods and a pitch

momentum wheel. The maneuver is defined as rest-to-rest in the orbit frame where the initial attitude and attitude rates are known. The final attitude and attitude rates are determined by the eigenaxis of rotation and the rotation angle. The angular momentum of the wheel is the final state variable. For this variable and control combination there are four possible options. First, the initial wheel angular momentum may be left unspecified as an optimization variable to be determined. Then, if wheel torque does not equal zero, the algorithm selects the initial wheel speed and control history for the minimum time maneuver. This is the case that is numerically evaluated below. The wheel speed can also be fixed at the end points. In this case a non-zero torque limit will achieve the time optimal solution within the constraints provided. Under the condition of zero torque, wheel speed free, the algorithm will determine the optimal, constant wheel speed for the desired maneuver. Finally, if wheel speed and torque are set to zero the results match those previously obtained for the magnetic torque control section. It is important to note that these changes in boundary conditions do not affect our ability to minimize the objective function and obtain valid solutions.

### 1. Problem Statement

Determine the controls  $[u_1^*, u_2^*, u_3^*, u_4^*]$  that drive the spacecraft from its initial rest position, given by  $[\underline{x}_0]$  to its final rest position given by  $[\underline{x}_f]$  while minimizing the cost function:

$$J(\underline{x}(\cdot), \underline{u}(\cdot), t_f) = t_f - t_0$$

where we have used the Mayer form of the cost function, subject to the following constraints:

Control / State Constraint: The control and state constraints are defined in the standard form,

$$h^L(t) \leq h(u, t) \leq h^U(t)$$

then our control constraints are written,

$$\begin{aligned}
-30 \leq u_i \leq 30 \text{ (Amp} \cdot \text{m}^2) \quad i = 1, 2, 3 \\
-30 \times 10^{-3} \leq u_4 \leq 30 \times 10^{-3} \text{ (N} \cdot \text{m)}
\end{aligned}$$

and the state constraint is given by:

$$-0.18 \leq x_8 \leq 0.18 \text{ (N} \cdot \text{m} \cdot \text{sec)}$$

Dynamic Constraints:

$$\begin{aligned}
\dot{q}_1 &= \frac{1}{2} [\mathbf{w}_1 q_4 - \mathbf{w}_2 q_3 + \mathbf{w}_3 q_2] \\
\dot{q}_2 &= \frac{1}{2} [\mathbf{w}_1 q_3 + \mathbf{w}_2 q_4 - \mathbf{w}_3 q_1] \\
\dot{q}_3 &= \frac{1}{2} [-\mathbf{w}_1 q_2 + \mathbf{w}_2 q_1 + \mathbf{w}_3 q_4] \\
\dot{q}_4 &= \frac{1}{2} [-\mathbf{w}_1 q_1 - \mathbf{w}_2 q_2 - \mathbf{w}_3 q_3] \\
\dot{\mathbf{w}}_x &= \frac{1}{J_x} (m_2 B_3 - m_3 B_2 - \mathbf{w}_z h_w) + k_1 \mathbf{w}_y \mathbf{w}_z, \quad k_1 = \frac{J_y - J_z}{J_x} \\
\dot{\mathbf{w}}_y &= \frac{1}{J_y} (m_3 B_1 - m_1 B_3 + \dot{h}_w) + k_2 \mathbf{w}_x \mathbf{w}_y, \quad k_2 = \frac{J_z - J_x}{J_y} \\
\dot{\mathbf{w}}_z &= \frac{1}{J_z} (m_1 B_2 - m_2 B_1 + \mathbf{w}_x h_w) + k_3 \mathbf{w}_x \mathbf{w}_y, \quad k_3 = \frac{J_x - J_y}{J_z} \\
\dot{h}_w &= u_w
\end{aligned} \tag{5.5}$$

## 2. Solving the Optimal Control Problem

The Hamiltonian is given by,

$$\begin{aligned}
 H = & \frac{I_{q_1}}{2} (\mathbf{w}_x q_4 - \mathbf{w}_y q_3 + \mathbf{w}_z q_2 + \mathbf{w}_o q_3) + \frac{I_{q_2}}{2} (\mathbf{w}_x q_3 + \mathbf{w}_y q_4 - \mathbf{w}_z q_1 + \mathbf{w}_o q_4) + \\
 & \frac{I_{q_3}}{2} (-\mathbf{w}_x q_2 + \mathbf{w}_y q_1 + \mathbf{w}_z q_z - \mathbf{w}_o q_1) + \frac{I_{q_4}}{2} (-\mathbf{w}_x q_1 - \mathbf{w}_y q_2 - \mathbf{w}_z q_3 - \mathbf{w}_o q_2) + \\
 & I_{w_x} \left\{ \frac{1}{J_x} (u_2 B_3 - u_3 B_2 - \mathbf{w}_z h_w) + k_1 \mathbf{w}_y \mathbf{w}_z \right\} + I_{w_y} \left\{ \frac{1}{J_y} (u_3 B_1 - u_1 B_3 + u_4) + k_2 \mathbf{w}_x \mathbf{w}_z \right\} + \\
 & I_{w_z} \left\{ \frac{1}{J_z} (u_1 B_2 - u_2 B_1 + \mathbf{w}_x h_w) + k_3 \mathbf{w}_x \mathbf{w}_y \right\} + I_{h_w} u_4
 \end{aligned}$$

The subscripts on the Lagrange multipliers have been chosen for bookkeeping purposes. The control vector is defined in equation (5.4).

Following the solution method previously established we begin by minimizing the Hamiltonian subject to the control constraint set. Then the necessary conditions for the Hamiltonian minimization are as follows:

$$\begin{aligned}
 \frac{I_{w_z}}{J_z} B_2 - \frac{I_{w_y}}{J_y} B_3 + \mathbf{m}_1 &= 0 \\
 \frac{I_{w_x}}{J_x} B_3 - \frac{I_{w_z}}{J_z} B_1 + \mathbf{m}_2 &= 0 \\
 \frac{I_{w_y}}{J_y} B_1 - \frac{I_{w_x}}{J_x} B_2 + \mathbf{m}_3 &= 0 \\
 \underbrace{\frac{I_{w_y}}{J_y}}_{S_i} + I_{h_w} + \underbrace{\mathbf{m}_4}_{m u_i} &= 0
 \end{aligned} \tag{5.6}$$

These relationships will be evaluated to validate the candidate solution.

We saw that in the case of the magnetic torque problem the magnetic field of the Earth introduced a time-dependence into the Hamiltonian. Therefore, the Hamiltonian was *not* a constant in the interval under consideration. For the

current problem the Earth's magnetic field is still a factor in the Hamiltonian. However, in this case, we will see that the effect of the magnetic field is reduced by the introduction of the pitch wheel, and the time rate of change of the Hamiltonian is reduced significantly.

The final value of the Hamiltonian is again given by,

$$H[t_f] + \frac{\partial E}{\partial t_f} + \mathbf{u}^t \frac{\partial e}{\partial t_f} = 0$$

where the end manifold (  $e$  ) is written in the standard form previously established,

$$e(\underline{x}_f, t_f) = 0$$

Then by inspection we can see that the final value of the Hamiltonian is negative one.

$$H[t_f] + 1 = 0 \rightarrow H[t_f] = -1$$

### 3. Numerical Results

The numerical example for this work was again taken from the Naval Postgraduate School's current small satellite program, "NPSAT 1." The moment of inertias and orbital parameters were previously established in Table 5 and are assumed to be the system moments of inertia. The control parameters are given in Table 7.

The maneuver selected for simulation is a 135 degree roll (x-axis slew) and is a rest-to-rest maneuver in the orbit frame. The initial and final pitch wheel angular momentums are free within the state bounds as an optimization parameter. The time-optimal control solution is shown in Figure 60 and Figure 61.

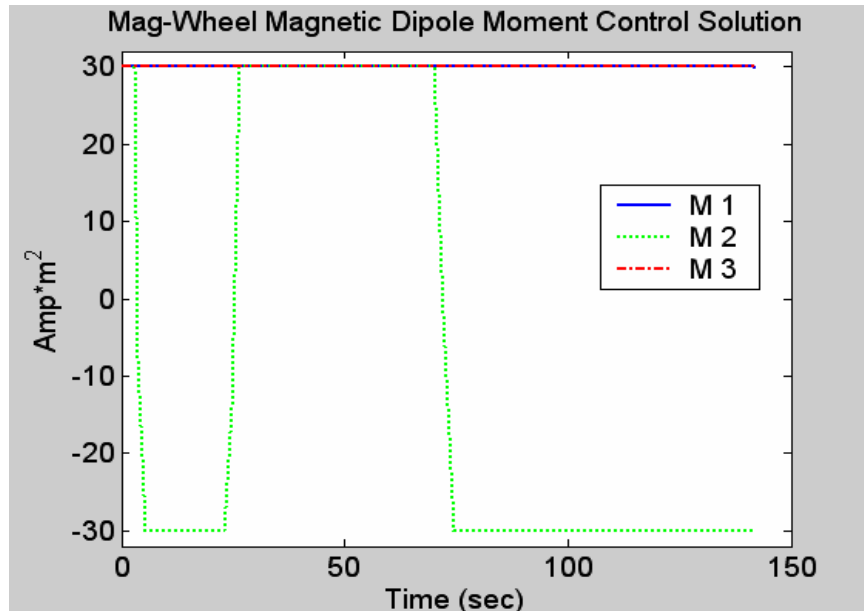


**Figure 60** *NPSAT 1 Torque Rod & Wheel Time-optimal Control Solution (1)*

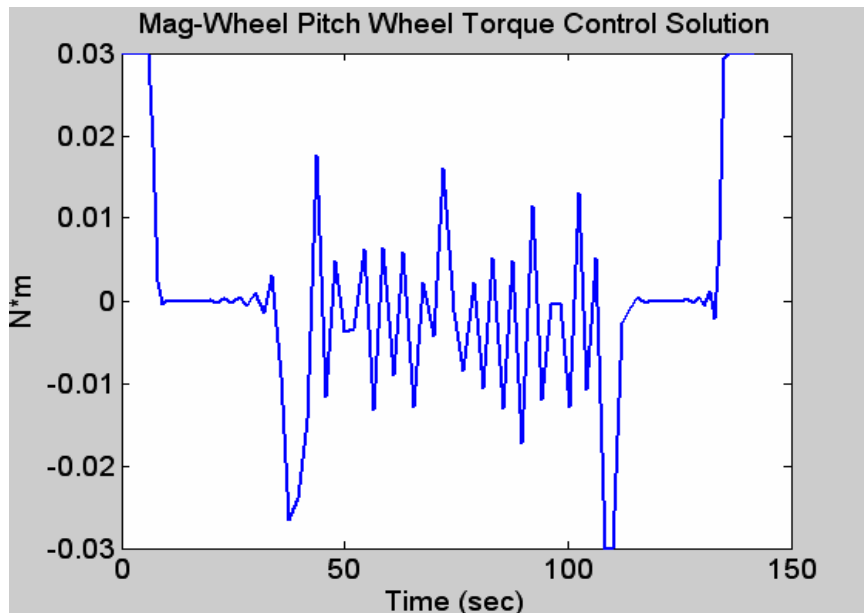


**Figure 61** *NPSAT 1 Pitch Wheel Torque Time-optimal Control Solution (2)*

There are several interesting characteristics to this solution not the least of which is an apparent singular arc in the switching structure for the pitch wheel torque ( $u_4$ ). Before evaluating the optimality of the candidate solution the feasibility is evaluated. The control solution is again propagated through a

separate ODE 45 dynamics simulator to verify that the candidate solution drives the dynamic system from the initial state to the final state. Previous control solutions were propagated using a linear interpolation. In this case a piecewise cubic hermite interpolating polynomial (pchip) produced more accurate results. The propagation results (Figure 62, Figure 63, and Figure 64) show that the control solution does meet the end point constraints and that the estimated states closely match those obtained during propagation. The original solution obtained is shown in solid lines overlaid with the propagated states shown as '+' marks below. Therefore we conclude that the control solution is feasible.

The state histories are shown (Figure 65, Figure 66, and Figure 67). It comes as no surprise that the time-optimal maneuver is not an eigenaxis maneuver. This is evident from both the variation in the quaternions  $q_2$  &  $q_3$  and the non-zero angular rates of  $w_2$  &  $w_3$ .

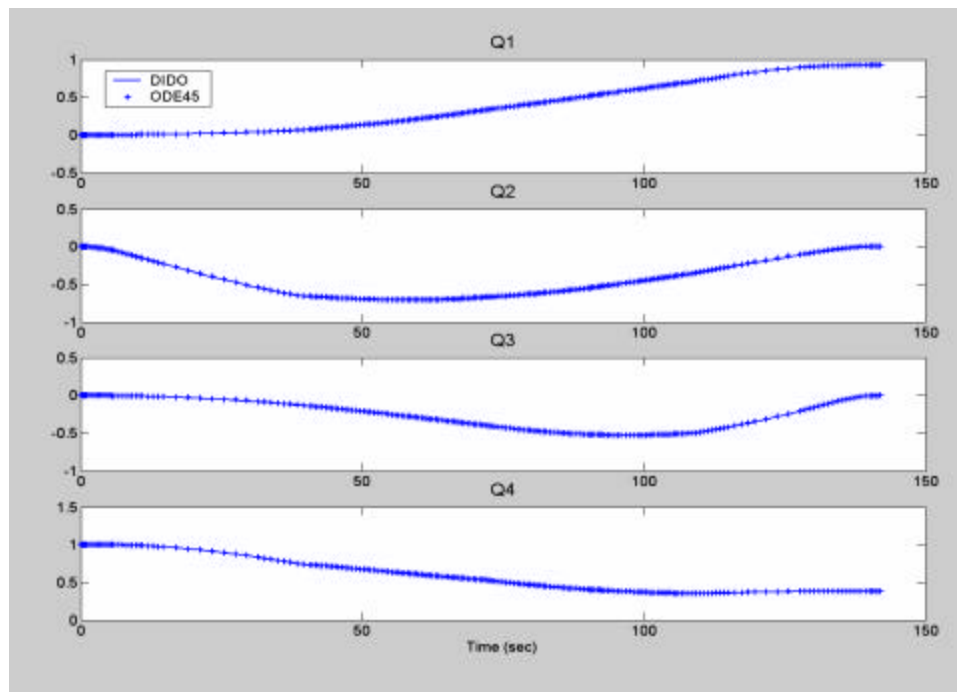


**Figure 62** Quaternion Solution and Validation by Propagation

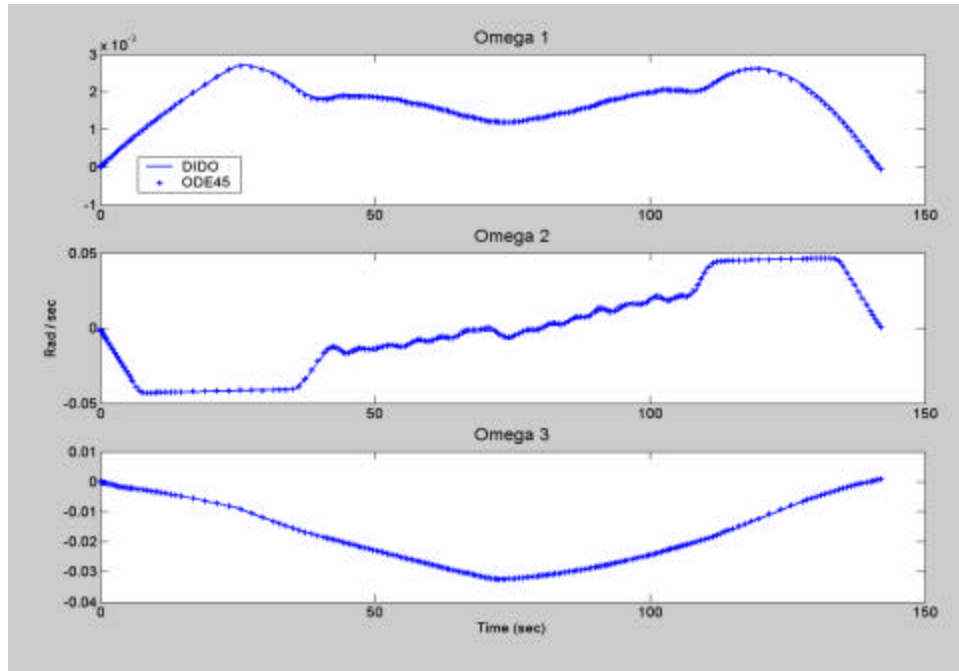


**Figure 63** Angular Rate Solution and Validation by Propagation

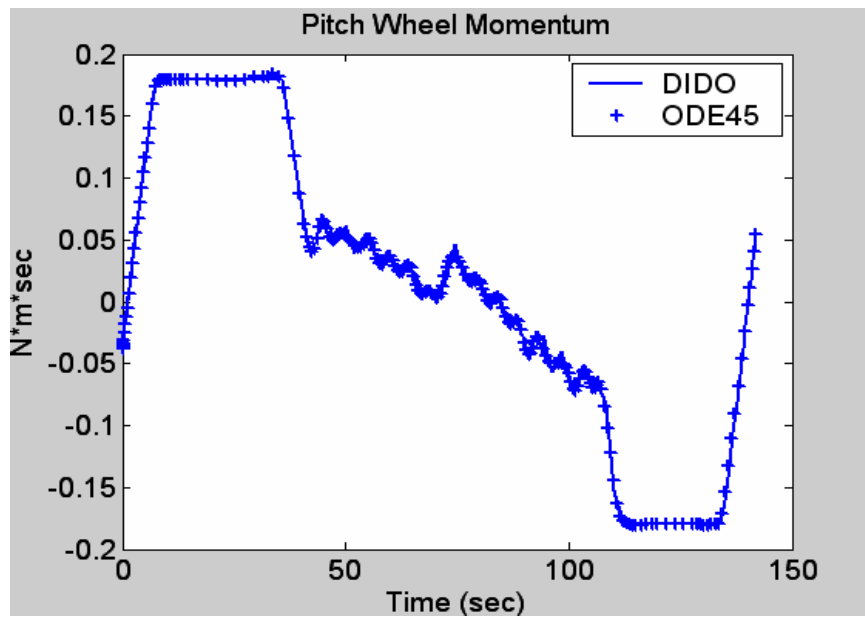


**Figure 64** Pitch Wheel Momentum Solution and Validation by Propagation

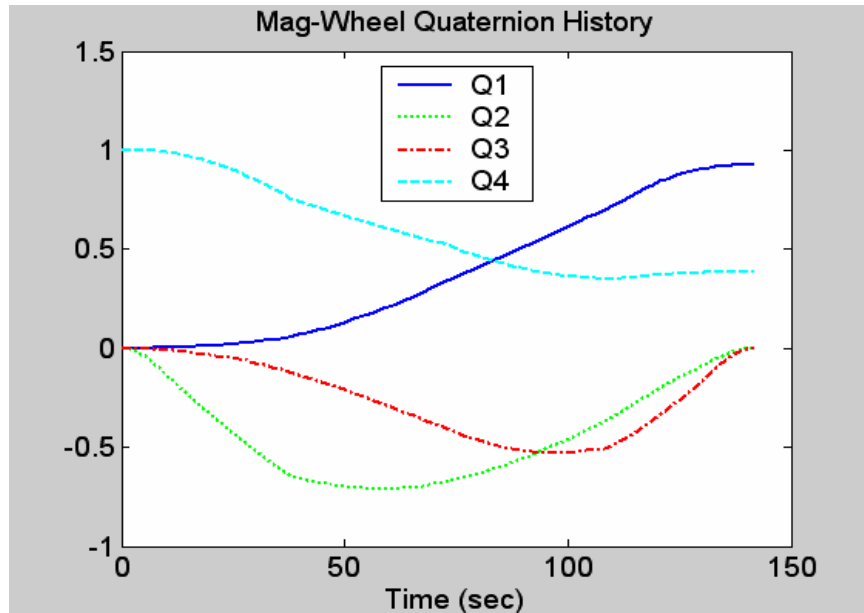


**Figure 65** *NPSAT 1 Slew Time-optimal Quaternion History*

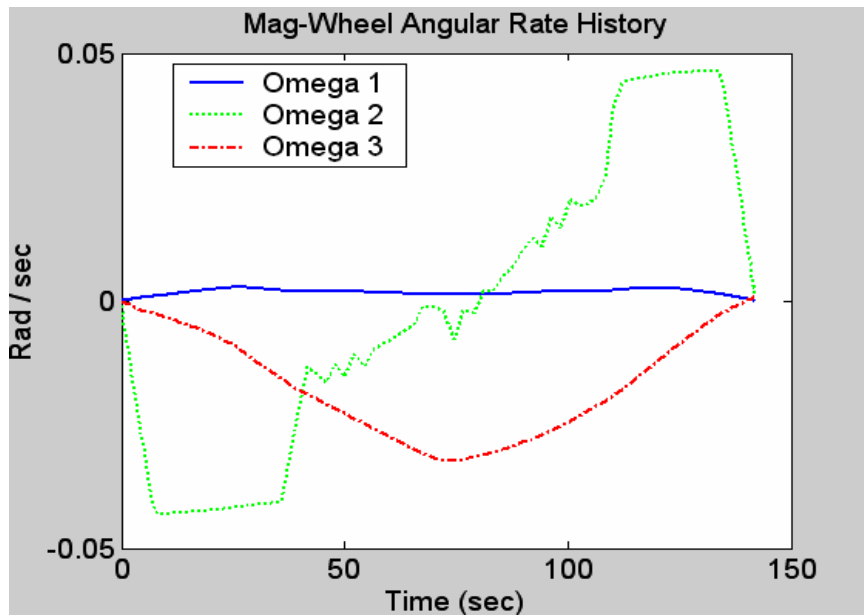


**Figure 66** *NPSAT 1 Slew Time-optimal Angular Rate History*

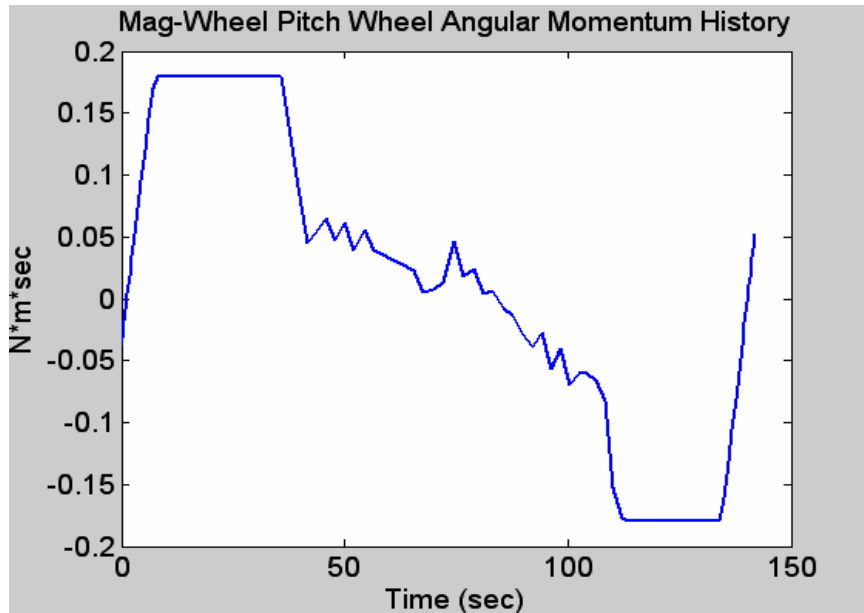


**Figure 67** *NPSAT 1 Slew Time-optimal Pitch Wheel Angular Momentum History*

Next we evaluate the optimality of the feasible, candidate solution. The switching functions are given in equations (4.11). These are plotted overlaid with the scaled control solution (Figure 68, Figure 69, Figure 70, and Figure 71).

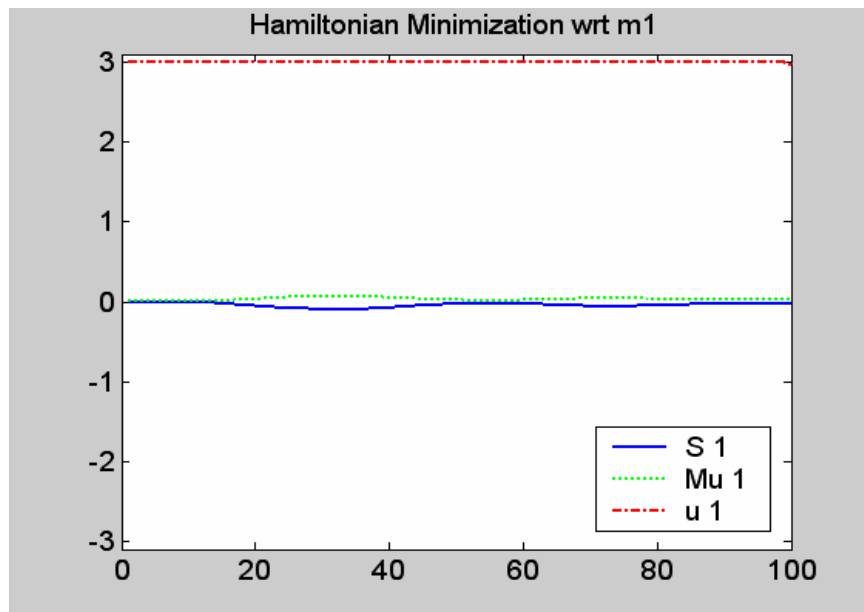


**Figure 68** *NPSAT 1 Control Switching Function and Control Solution (1)*

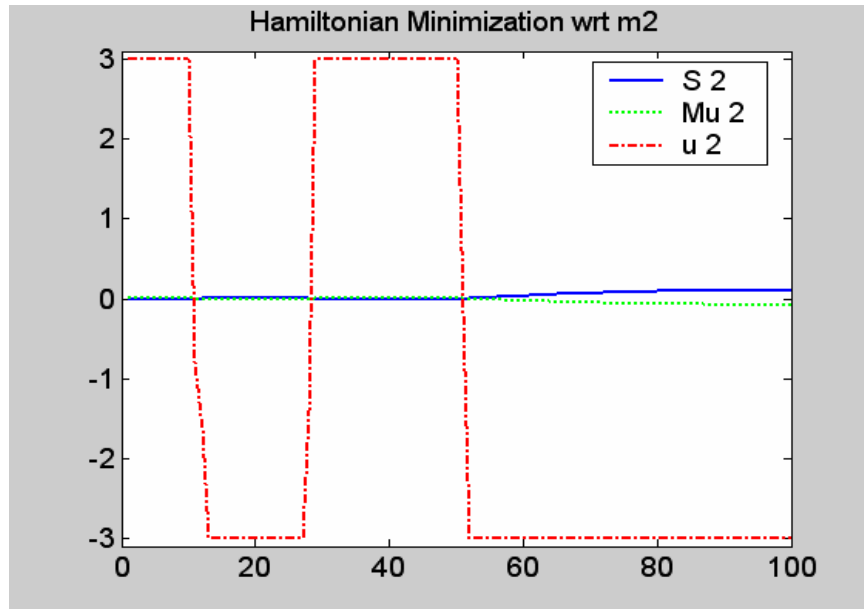


**Figure 69** NPSAT 1 Control Switching Function and Control Solution (2)

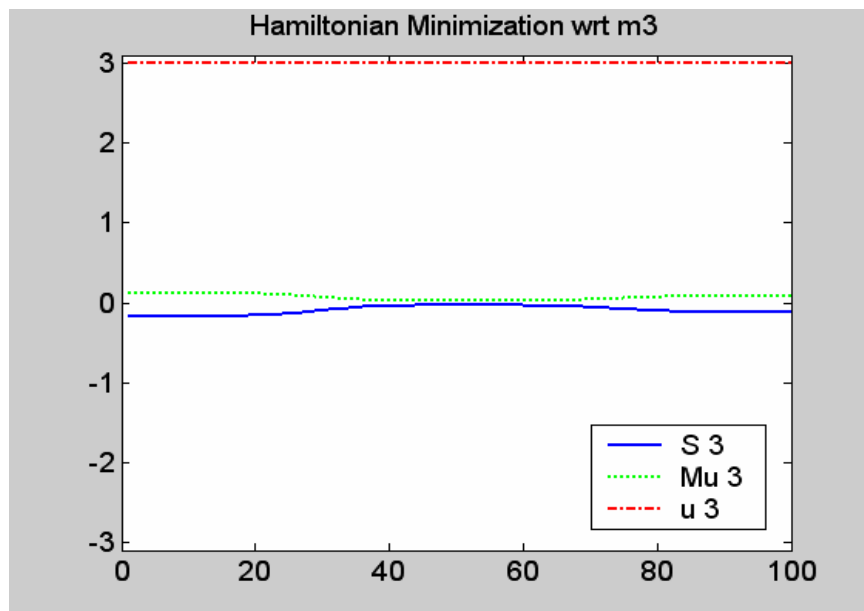


**Figure 70** NPSAT 1 Control Switching Function and Control Solution (3)

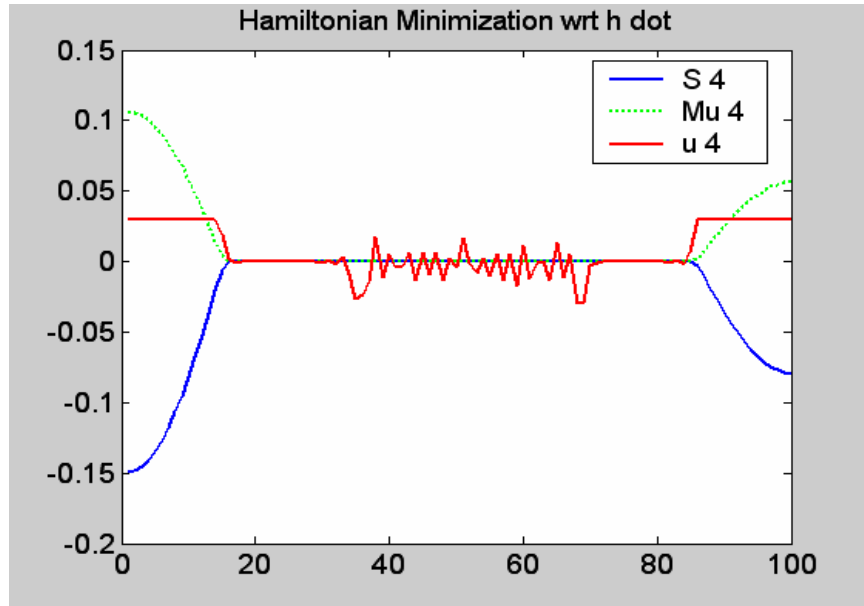


**Figure 71 NPSAT 1 Control Switching Function and Control Solution (4)**

Shown are the switching functions ( $S_i$ ) previously defined as the partial derivative of the Hamiltonian with respect to the control vector. The KKT multiplier ( $Mu$ ) is also shown plotted separately from the switching function. The sum of the switching function and the KKT multiplier is the definition of the minimization of the Hamiltonian, equation (4.11), and should be numerically equal to zero. As before the switching function and control are related by the KKT conditions:

$$u_i^* = \begin{cases} \text{maximum} & S_i < 0 \\ \text{minimum} & S_i > 0 \\ \text{singular} & S_i \equiv 0 \end{cases}$$

The Hamiltonian for this problem is shown in Figure 72. As we alluded to earlier the time dependence observed in the magnetic torque control problem appears to have been eliminated. In fact, it has been reduced to the extent that it is no longer visible. By constraining the pitch wheel to zero torque and zero angular momentum the previous magnetic torque results are obtained.

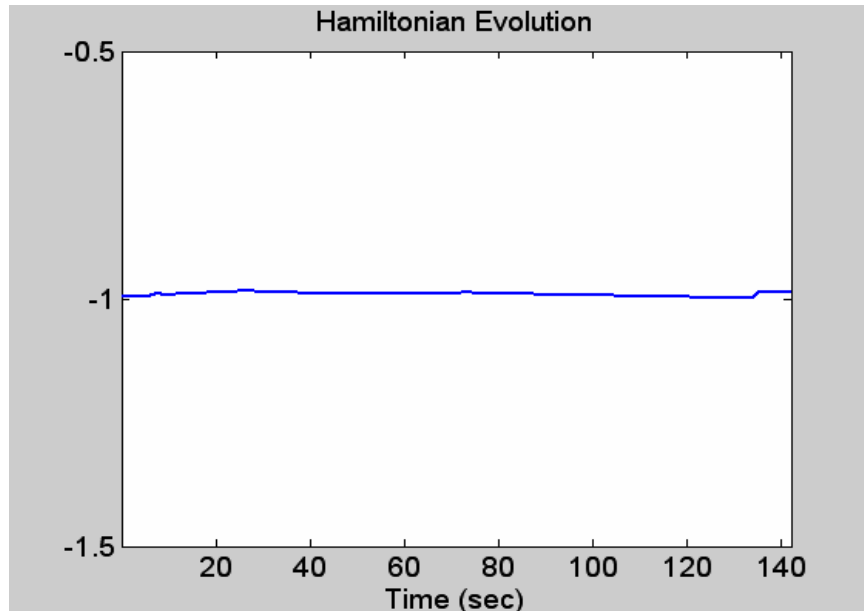


**Figure 72 NPSAT 1 Torque Rod & Wheel Problem Hamiltonian Evolution**

These figures clearly illustrate that the control solution meets optimality criteria established by the Hamiltonian minimization. A closer look at the Hamiltonian minimization with respect to the pitch wheel torque is given in Figure 73. The switching function appears singular during the period in which the pitch wheel torque is zero.

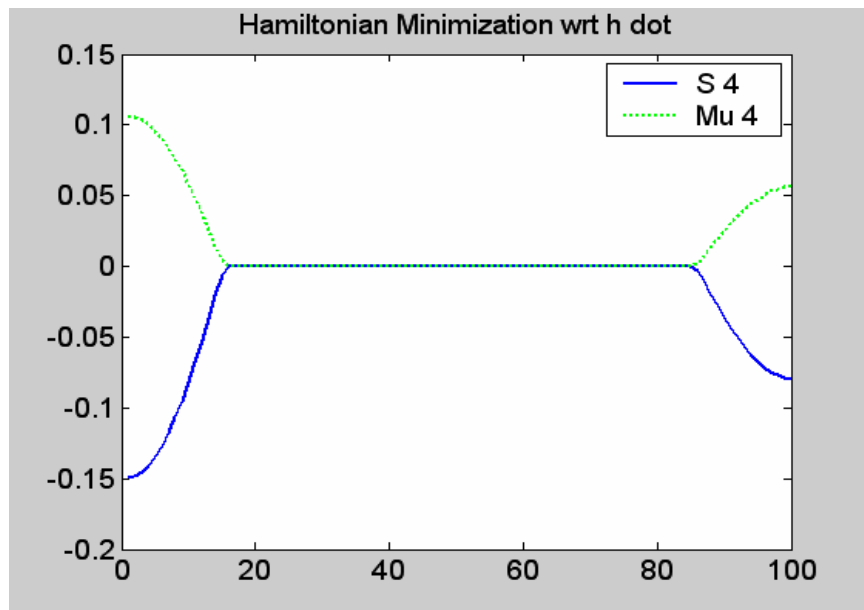


**Figure 73 NPSAT 1 Control Switching Function for Wheel Torque (Close up)**

#### 4. Numerical Considerations and Scaling

We continue with the linear scaling established previously. In this section scaling was also added for the pitch wheel parameters in the form:

$$\bar{h} = k_h h$$
$$\bar{\dot{h}} = \frac{k_h}{k_t} \dot{h}$$

As before the goal of the scaling is to bring all numerical values seen by the optimization solver into the same order of magnitude. Scaling values were adjusted from an unscaled solution to improve the quality of the solution and then readjusted as necessary.

#### 5. Conclusions

In this section the open loop time-optimal control for an asymmetric spacecraft equipped with three magnetic torque rods and a pitch wheel was determined. The candidate solution was determined by propagation to be a feasible solution to the problem. The optimality of the solution was validated through an analysis of the Hamiltonian minimization, switching functions and the behavior of the Hamiltonian. Therefore, we conclude that the solution is feasible and meets the necessary conditions for optimality.

By allowing the use of the pitch wheel as a spacecraft control, the time required for the reorientation maneuver was significantly reduced. In the original configuration, with only magnetic torque control available, the time required for the optimal maneuver was 271.1564 seconds. In the new configuration the same maneuver required only 141.9933 seconds. This represents a 47.6 percent reduction in time required for the same maneuver.

---

## ENDNOTES

- <sup>1</sup> Wie, B. (1998). *Space Vehicle Dynamics and Control*. AIAA Education Series, American Institute of Aeronautics and Astronautics, Inc. Reston, VA.
- <sup>2</sup> Kane, T. (1983). *Spacecraft Dynamics*. McGraw-Hill Inc. New York, NY.

## VI. CONTROL MOMENT GYRO CONTROL SYSTEMS

### A. INTRODUCTION

Control moment gyros (CMGs) are well known for their large torque generating capability. However, in the past, because of their mechanical complexity, cost and weight they have been restricted to large satellites with high agility requirements. Recent research in the design of smaller, less expensive CMGs has created a renewed interest in CMG spacecraft control. However, the primary focus of this large body of work has been singularity avoidance<sup>1,2,3,4</sup>. In this section we calculate the time-optimal solution for an asymmetric spacecraft using the much studied four-CMG pyramid configuration. In addition to completing a time-optimal maneuver we will show that the problem formulation generates a singularity free solution.

### B. CONTROL MOMENT GYRO BASICS

A control moment gyro contains a flywheel which spins at a constant rate. The spin axis of the flywheel is connected to a gimbal which allows reorientation of the spin axis. Therefore, the direction of the angular momentum vector can be changed with respect to the spacecraft body frame by gimbaling (Figure 74).

#### Single-gimbal Control Moment Gyro

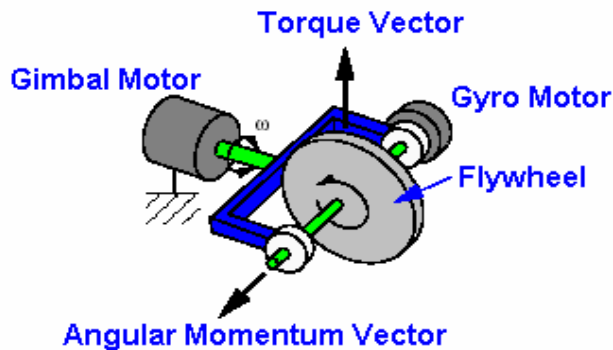


Figure 74 Single-Gimbal Control Moment Gyro (After Ref.[5])

For single-gimbal control moment gyros (SGCMG), the spin axis reorientation is restricted to a plane perpendicular to the gimbal axis. The advantage of CMGs is that small gimbaling results in a large control torque on the spacecraft. This resultant torque is orthogonal to both the gimbal and spin axes.<sup>6</sup> The torque from the CMG is given by:

$$\vec{M}_{CMG} = \vec{h} \times \dot{\vec{d}} \quad (6.1)$$

where  $\vec{h}$  is the angular momentum vector and has units of Newton-meter-seconds,  $\dot{\vec{d}}$  is the gimbal angle rate with units of radians per second. This torque amplification property makes CMGs desirable for applications that require spacecraft agility.

### C. PROBLEM FORMULATION

Following a similar development to that used in Chapter V, recall that the time rate of change of angular momentum can be expressed as,

$$\vec{M}_{ext} = \left[ \frac{d}{dt} \vec{H}_S \right]_N = \left[ \frac{d}{dt} \vec{H}_S \right]_b + {}^N\vec{\omega}^b \times \vec{H}_S \quad (6.2)$$

where  $\vec{H}_S$  is the total angular momentum of the spacecraft-CMG system and is expressed in the spacecraft body frame. Assuming that the CMG center of mass is collocated with the spacecraft center of mass we can express the system angular momentum as:

$$\vec{H} = I_B {}^N\vec{\omega}^b + I_{CMG} {}^N\vec{\omega}^{CMG}$$

where  $I_B$  and  $I_{CMG}$  are the spacecraft and CMG system moment of inertias respectively and the angular velocity of the CMG with respect to the Newtonian frame is given by,

$${}^N\vec{\omega}^{CMG} = {}^N\vec{\omega}^b + {}^b\vec{\omega}^{CMG}$$

Then the angular momentum of the system can be written as,

$$\vec{H}_S = I_B {}^N \vec{\omega}^b + I_{CMG} {}^N \vec{\omega}^b + I_{CMG} {}^b \vec{\omega}^{CMG}$$

Once again, by defining,

$$\mathbf{J} \doteq I_B + I_{CMG}$$

we have,

$$\vec{H}_S = \mathbf{J} {}^N \vec{\omega}^b + I_{CMG} {}^b \vec{\omega}^{CMG}$$

Then referring to equation (6.2) we have,

$$M_{ext} = \mathbf{J} {}^N \dot{\vec{\omega}}^b + I_{CMG} {}^b \dot{\vec{\omega}}^{CMG} + {}^N \vec{\omega}^b \times (\mathbf{J} {}^N \vec{\omega}^b + I_{CMG} {}^b \vec{\omega}^{CMG})$$

Finally, by defining,

$$\left[ \frac{d}{dt} \vec{h}_{CMG} \right]_B = I_{CMG} {}^b \dot{\vec{\omega}}^{CMG} \doteq \dot{\vec{h}}_{CMG}$$

we obtain the following:

$$M_{ext} = \mathbf{J} {}^N \dot{\vec{\omega}}^b + \dot{\vec{h}}_{CMG} + {}^N \vec{\omega}^b \times \mathbf{J} {}^N \vec{\omega}^b + \vec{h}_{CMG}$$

If we allow  ${}^N \vec{\omega}^b = \mathbf{w}$  and  $M_{ext}$  to be all disturbance torque, then setting disturbance torque equal to zero we write,

$$\mathbf{J} \dot{\vec{\omega}} + \vec{\omega} \times \mathbf{J} \vec{\omega} = -\dot{\vec{h}}_{CMG} - \vec{\omega} \times \vec{h}_{CMG} \quad (6.3)$$

The CMG angular momentum vector ( $h$ )\* is a function of the gimbal angles ( $\mathbf{d}$ ) in the body frame and for multiple CMG configurations, a function of the configuration. Here we consider the four-CMG pyramid configuration (Figure 75). Each face of the pyramid is inclined from the horizontal by a skew angle ( $\mathbf{b}$ ). The four CMGs have gimbal axes orthogonal to the pyramid faces and so are constrained to gimbal on the faces of the pyramid. We have selected a skew angle,  $\mathbf{b} = 54.73$  degrees. For CMGs with equal angular momentum about the

---

\* We have adopted the notation lower case 'h' as CMG angular momentum and subsequently dropped the subscript.

spin axis this configuration results in a nearly spherical momentum envelope. Additionally, this configuration has been extensively studied in the literature.<sup>7</sup>

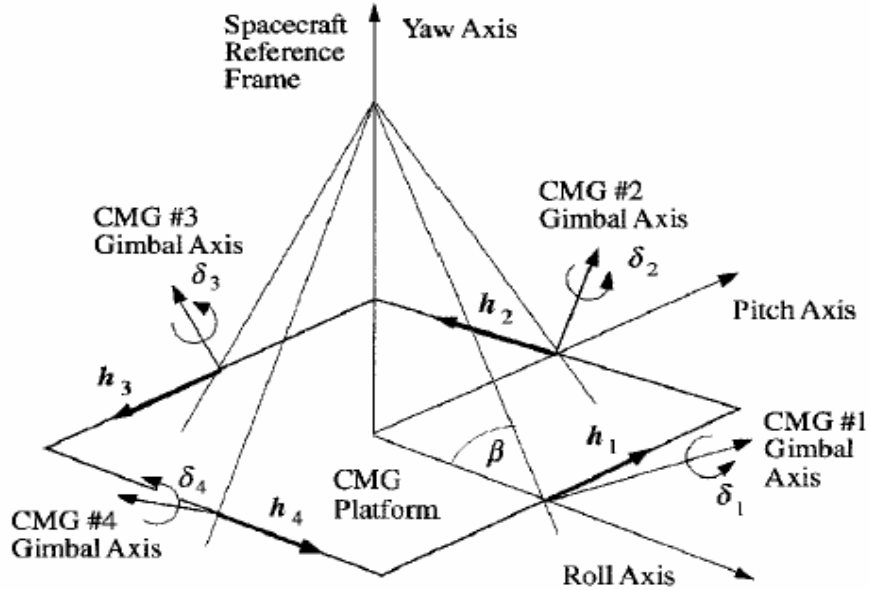


**Figure 75 Pyramid Mounting Arrangement of Four Single Gimbal CMGs (from Ref.[8])**

Then referencing Figure 75, we can write the total CMG angular momentum expressed in the body frame as:

$$\vec{h} = \begin{bmatrix} -cb \sin d_1 \\ \cos d_1 \\ sb \sin d_1 \end{bmatrix} + \begin{bmatrix} -\cos d_2 \\ -cb \sin d_2 \\ sb \sin d_2 \end{bmatrix} + \begin{bmatrix} cb \sin d_3 \\ -\cos d_3 \\ sb \sin d_3 \end{bmatrix} + \begin{bmatrix} \cos d_4 \\ cb \sin d_4 \\ sb \sin d_4 \end{bmatrix} \quad (6.4)$$

where  $cb \equiv \cos b$  and  $sb \equiv \sin b$ . The angular momentum magnitude is set to unity without loss of generality ( $h_0 = 1$ ). Then the time of rate of change of angular momentum may be written as:

$$\frac{d\vec{h}}{dt} = \underbrace{\begin{bmatrix} -cb \cos d_1 & \sin d_2 & cb \cos d_3 & -\sin d_4 \\ -\sin d_1 & -cb \cos d_2 & \sin d_3 & cb \cos d_4 \\ sb \cos d_1 & sb \cos d_2 & sb \cos d_3 & sb \cos d_4 \end{bmatrix}}_A \begin{bmatrix} \dot{d}_1 \\ \dot{d}_2 \\ \dot{d}_3 \\ \dot{d}_4 \end{bmatrix} \quad (6.5)$$

The matrix  $A$  is defined from equation (6.4) as,

$$A = \frac{\partial h_i}{\partial \mathbf{d}_j}$$

and is a  $3 \times n$  Jacobian matrix where  $n$  is the number of CMGs in the configuration. Expanding equation (6.3) shows<sup>†</sup>,

$$\begin{aligned} J_x \dot{\mathbf{w}}_x - (J_y - J_z) \mathbf{w}_y \mathbf{w}_z &= -\dot{h}_1 - \mathbf{w}_2 h_3 + \mathbf{w}_3 h_2 \\ J_y \dot{\mathbf{w}}_y - (J_z - J_x) \mathbf{w}_x \mathbf{w}_z &= -\dot{h}_2 - \mathbf{w}_3 h_1 + \mathbf{w}_1 h_3 \\ J_z \dot{\mathbf{w}}_z - (J_x - J_y) \mathbf{w}_x \mathbf{w}_y &= -\dot{h}_3 - \mathbf{w}_1 h_2 + \mathbf{w}_2 h_1 \end{aligned}$$

where the values of  $h_i$  are established in equation (6.4) and the values of  $\dot{h}_i$  are established in equation (6.5). A lengthy direct substitution allows us to write the time rate of change of angular velocity in the standard form:

$$\dot{\mathbf{w}}_i = f(\mathbf{x}_i, \mathbf{u}_i)$$

where the state vector and control vector are defined as:

$$\begin{aligned} \text{state: } [\underline{q}, \underline{\mathbf{w}}, \underline{\mathbf{d}}]^T &\in \mathbb{R}^{11} \\ \text{control: } [\underline{\mathbf{u}}]^T &\in \mathbb{R}^4 \end{aligned}$$

#### D. CMG TIME-OPTIMAL SLEW MANEUVERS

In this section we consider the time-optimal reorientation of an asymmetric spacecraft controlled by control moment gyros. In order to simplify the formulation the spacecraft is assumed to be in inertial space. The maneuver is defined as rest-to-rest in the inertial frame where the initial attitude and attitude rates are known. The final attitude and attitude rates are specified. The gimbal angle of the CMG, the final state variable is left free as an optimization variable.

---

<sup>†</sup> This derivation is also found in reference [6] where it is used in the development of a feedback control law.

## 1. Problem Statement

Determine the controls  $[u_1^*, u_2^*, u_3^*, u_4^*]$  that drive the spacecraft from its initial rest position, given by  $[\underline{x}_0]$  to its final rest position given by  $[\underline{x}_f]$  while minimizing the cost function:

$$J(\underline{x}(\cdot), \underline{u}(\cdot), t_f) = t_f - t_0$$

where we have used the Mayer form of the cost function, subject to the following constraints:

Control / State Constraint: The control and state constraints are defined in the standard form,

$$h^l(t) \leq h(u, t) \leq h^u(t)$$

then our control constraints are written,

$$-1 \leq u_i \leq 1 \text{ rad/sec} \quad i = 1, 2, 3, 4$$

and the state constraint is given by:

$$-p \leq d_i \leq p \text{ rad} \quad i = 1, 2, 3, 4$$

Physically, these equate to a CMG that is capable of full 360 degree rotation about its gimbal axis at a rate of 1 radian per second. With a unit angular momentum then from equation (6.1) the maximum torque output from the CMG is 1 Newton-meter.

Dynamic Constraints:

$$\begin{aligned}
 \underline{\dot{q}} &= \frac{1}{2} \underline{\underline{\Omega q}} \\
 \dot{w}_x &= \frac{J_y - J_z}{J_x} w_y w_z - \frac{\dot{h}_1}{J_x} - \frac{1}{J_x} (w_y h_3 - w_z h_2) \\
 \dot{w}_y &= \frac{J_z - J_x}{J_y} w_x w_z - \frac{\dot{h}_2}{J_y} - \frac{1}{J_y} (w_z h_1 - w_x h_3) \\
 \dot{w}_z &= \frac{J_x - J_y}{J_z} w_x w_y - \frac{\dot{h}_3}{J_z} - \frac{1}{J_z} (w_x h_2 - w_y h_1) \\
 \dot{d}_i &= u_i \quad i = 1, \dots, 4
 \end{aligned} \tag{6.6}$$

where the quaternion kinematics equations shown have been previously defined. The quantity  $\dot{h}_i$  is defined in equation (6.5) in terms of the state  $\mathbf{d}$  and the control and the quantity  $h_i$  is defined in equation (6.4) in terms of the state  $\mathbf{d}$ .

## 2. Solving the Optimal Control Problem

As before, the first step in solving the optimal control problem is to form the Hamiltonian. Basic format of the Hamiltonian is repeated here<sup>‡</sup>,

$$H(\mathbf{I}, \mathbf{x}, \mathbf{u}, t) = F(\mathbf{x}, \mathbf{u}, t) + \mathbf{I}^T f(\mathbf{x}, \mathbf{u}, t)$$

Since the cost functional was formulated without a Lagrange cost term the Hamiltonian reduces to the following.

$$H(\mathbf{I}, \mathbf{x}, \mathbf{u}, t) = \mathbf{I}^T f(\mathbf{x}, \mathbf{u}, t) \tag{6.7}$$

Substituting equation (6.6) into equation (6.7) gives the Hamiltonian for the CMG spacecraft system.

---

<sup>‡</sup> Recall that in this notation F is the Lagrange (running) cost and f are the state dynamics.

$$\begin{aligned}
H = & \underline{\mathbf{I}}_q^T \left( \frac{1}{2} \underline{\underline{\Omega}} \underline{\underline{q}} \right) + \underline{\mathbf{I}}_{w_x} \left( \frac{J_y - J_z}{J_x} \mathbf{w}_y \mathbf{w}_z - \frac{\dot{h}_1}{J_x} - \frac{1}{J_x} (\mathbf{w}_y h_3 - \mathbf{w}_z h_2) \right) + \\
& \underline{\mathbf{I}}_{w_y} \left( \frac{J_z - J_x}{J_y} \mathbf{w}_x \mathbf{w}_z - \frac{\dot{h}_2}{J_y} - \frac{1}{J_y} (\mathbf{w}_z h_1 - \mathbf{w}_x h_3) \right) + \\
& \underline{\mathbf{I}}_{w_z} \left( \frac{J_x - J_y}{J_z} \mathbf{w}_x \mathbf{w}_y - \frac{\dot{h}_3}{J_z} - \frac{1}{J_z} (\mathbf{w}_x h_2 - \mathbf{w}_y h_1) \right) + \\
& \underline{\mathbf{I}}_d^T \underline{\underline{u}}
\end{aligned} \tag{6.8}$$

Recall from equation (6.7) that the Hamiltonian is written in terms of the Lagrange multipliers, state vector, control vector and time. In order for equation (6.8) to be rigorously correct substitutions from equation (6.4) and equation (6.5) are required. However, this lengthy substitution is omitted.

Since the control is constrained, Hamiltonian minimization is accomplished by adjoining the control constraint equations to the Hamiltonian as,

$$\bar{H}(\mathbf{I}, \mathbf{x}, \mathbf{u}, t, \mathbf{m}) \doteq H(\mathbf{I}, \mathbf{x}, \mathbf{u}, t) + \mathbf{m}^T h(\mathbf{u}, t) \tag{6.9}$$

Then, by differentiation of equation (6.8), with respect to the control vector and substituting from equation (6.4) and (6.5), we can write the necessary conditions for the Hamiltonian minimization as follows.

$$\begin{aligned}
\frac{\partial \bar{H}}{\partial u_1} &= \frac{\underline{\mathbf{I}}_{w_x}}{J_x} \cos \mathbf{b} \cos \mathbf{d}_1 + \frac{\underline{\mathbf{I}}_{w_y}}{J_y} \sin \mathbf{d}_1 - \frac{\underline{\mathbf{I}}_{w_z}}{J_z} \sin \mathbf{b} \cos \mathbf{d}_1 + \underline{\mathbf{I}}_{d_1} + \underline{\mathbf{m}}_{d_1} = 0 \\
\frac{\partial \bar{H}}{\partial u_2} &= -\frac{\underline{\mathbf{I}}_{w_x}}{J_x} \sin \mathbf{d}_2 + \frac{\underline{\mathbf{I}}_{w_y}}{J_y} \cos \mathbf{b} \cos \mathbf{d}_2 - \frac{\underline{\mathbf{I}}_{w_z}}{J_z} \sin \mathbf{b} \cos \mathbf{d}_2 + \underline{\mathbf{I}}_{d_2} + \underline{\mathbf{m}}_{d_2} = 0 \\
\frac{\partial \bar{H}}{\partial u_3} &= -\frac{\underline{\mathbf{I}}_{w_x}}{J_x} \cos \mathbf{b} \cos \mathbf{d}_3 - \frac{\underline{\mathbf{I}}_{w_y}}{J_y} \sin \mathbf{d}_3 - \frac{\underline{\mathbf{I}}_{w_z}}{J_z} \sin \mathbf{b} \cos \mathbf{d}_3 + \underline{\mathbf{I}}_{d_3} + \underline{\mathbf{m}}_{d_3} = 0 \\
\frac{\partial \bar{H}}{\partial u_4} &= \underbrace{\frac{\underline{\mathbf{I}}_{w_x}}{J_x} \sin \mathbf{d}_4 - \frac{\underline{\mathbf{I}}_{w_y}}{J_y} \cos \mathbf{b} \cos \mathbf{d}_4 - \frac{\underline{\mathbf{I}}_{w_z}}{J_z} \sin \mathbf{b} \cos \mathbf{d}_4 + \underline{\mathbf{I}}_{d_4}}_{S_i} + \underbrace{\underline{\mathbf{m}}_{d_4}}_{\underline{\underline{M}}_i} = 0
\end{aligned} \tag{6.10}$$

These conditions will be evaluated to validate the candidate solution.

Inspection of the Hamiltonian equation reveals no direct dependence on time. Therefore the time rate of change of the Hamiltonian is zero and we expect a constant valued Hamiltonian for the interval under consideration.

The final value of the Hamiltonian is given by,

$$H[t_f] + \frac{\partial E}{\partial t_f} + \mathbf{u}^t \frac{\partial e}{\partial t_f} = 0$$

where the end manifold ( e ) is written in the standard form previously established,

$$e(\underline{x}_f, t_f) = 0$$

Then by inspection we can see that the final value of the Hamiltonian is negative one.

$$H[t_f] + 1 = 0 \rightarrow H[t_f] = -1 \tag{6.11}$$

Thus we expect a Hamiltonian with a constant value of -1 over the interval of the maneuver.

### 3. Numerical Results

For this numerical example we used the asymmetric moment of inertia of the NPSAT 1 small satellite design previously established (Table 5) and assumed to be the system moments of inertia. The orbital parameters were neglected since the model was assumed in inertial space. The physical parameters for the CMG are summarized in Table 8.

<b>NPSAT 1 SIMULATED CMG SYSTEM</b>	
Gimbal Rotation Range	<b>360 deg</b>
Maximum Gimbal Rotation Rate	<b>1 rad/sec</b>
Maximum Angular Momentum	<b>1 N-m-sec</b>
Maximum Output Torque	<b>1 N-m</b>

Table 8 ***Simulated CMG Characteristics***

The maneuver selected for simulation is a 135 degree roll (x-axis slew) and is a rest-to-rest maneuver in the inertial frame. The initial and final CMG gimbal angles are free within the state bounds. Therefore, we can write the end point conditions as follows:

$$\begin{aligned}
 x &= [q_1, q_2, q_3, q_4, w_1, w_2, w_3, d_1, d_2, d_3, d_4]^T \\
 x_0 &= [0, 0, 0, 1, 0, 0, 0, d_{1_0}, d_{2_0}, d_{3_0}, d_{4_0}]^T \\
 x_f &= \left[ \sin\left(\frac{135}{2}\right), 0, 0, \cos\left(\frac{135}{2}\right), 0, 0, 0, d_{1_f}, d_{2_f}, d_{3_f}, d_{4_f} \right]^T
 \end{aligned}$$

The time-optimal control solution is shown in Figure 76. Our engineering intuition would lead us to expect a bang-bang solution for a time-optimal maneuver. The control solution indicates that the solution is a bang-bang response from all four CMGs with 5 control switches. This is a surprisingly clean solution considering the complexity of the CMG dynamics derived above.

As we have seen previously, the feasibility of the candidate solution is evaluated propagating the control solution through a separate ODE 45 dynamics simulator to verify that the candidate solution drives the dynamic system from the initial state to the final state. A linear interpolation was used in the propagation sub-routine. The propagation results (Figure 77, Figure 78, and Figure 79) show that the control solution does meet the end point constraints and that the estimated states closely match those obtained during propagation. The original solution obtained is shown in solid lines overlaid with the propagated states shown as '+' marks below. Therefore we conclude that the control solution is feasible.

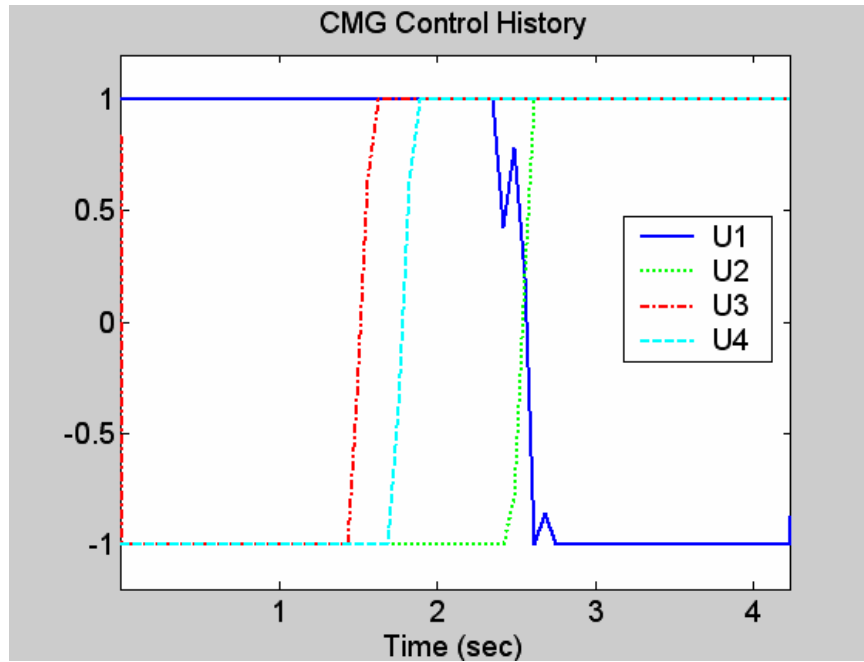


**Figure 76** *CMG Time-optimal Control Solution*

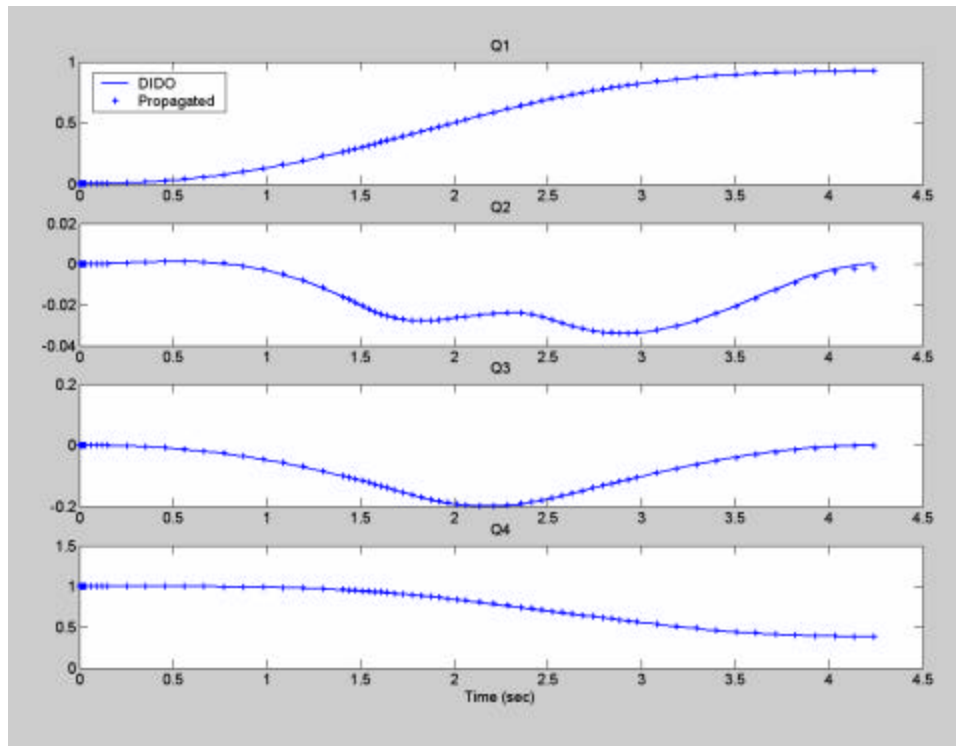


**Figure 77** *CMG Solution Quaternion History Validation by Propagation*

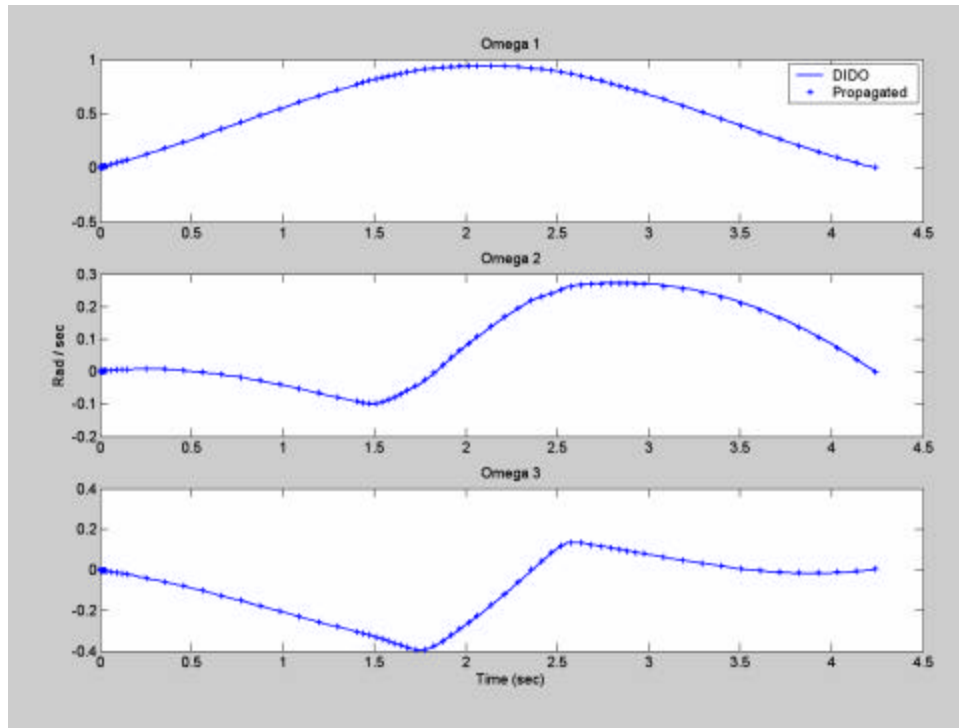


**Figure 78** CMG Solution Angular Rate History Validation by Propagation

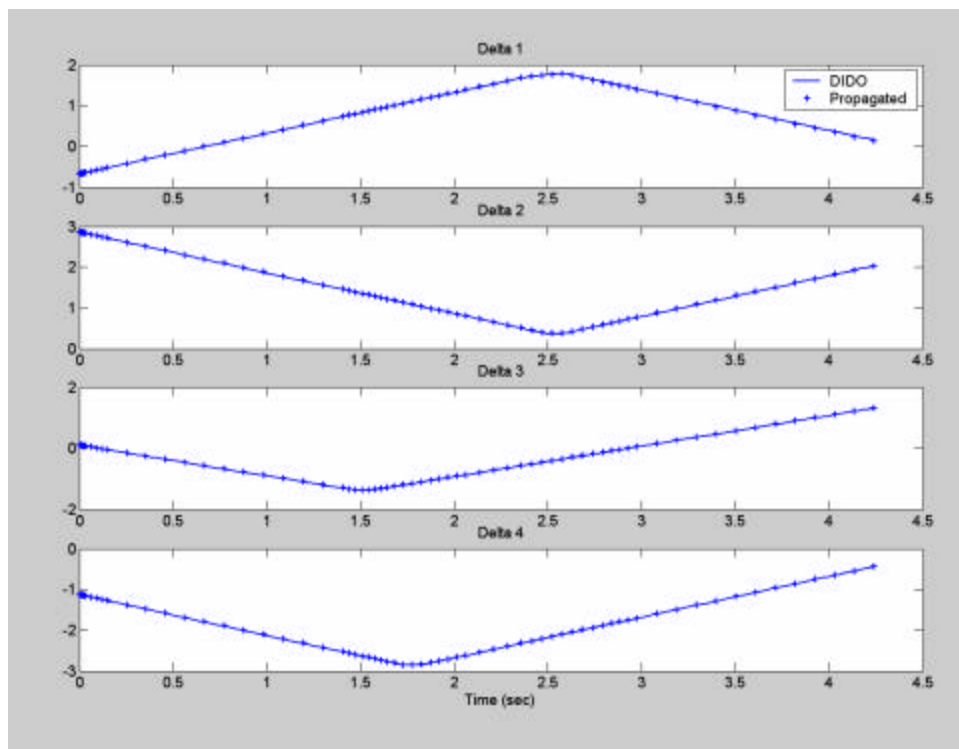


**Figure 79** CMG Solution Gimbal Angle History Validation by Propagation

The state histories are shown (Figure 80, Figure 81, and Figure 82). Once again we see that the time-optimal maneuver is not an eigenaxis maneuver. This is evident from both the variation in the quaternions  $q_2$  &  $q_3$  and the non-zero angular rates of  $w_2$  &  $w_3$ . Additionally, the gimbal angle history demonstrates

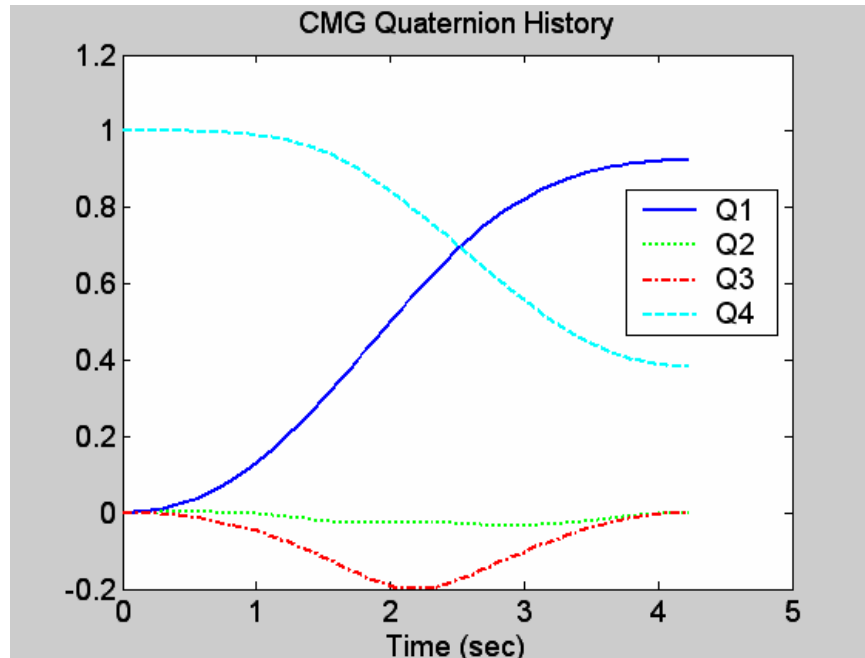


**Figure 80** *CMG Slew Time-optimal Quaternion History*

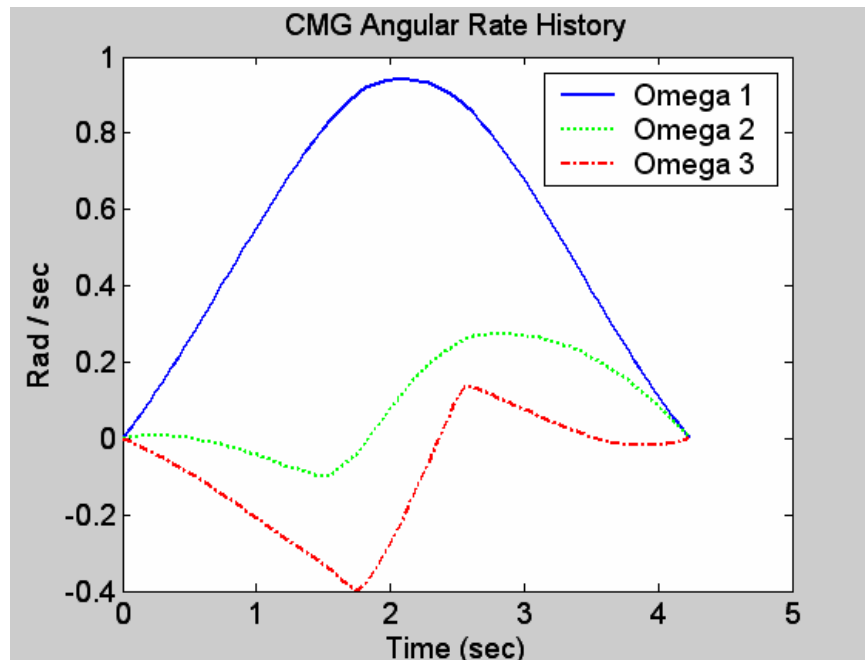


**Figure 81** *CMG Slew Time-optimal Angular Rate History*

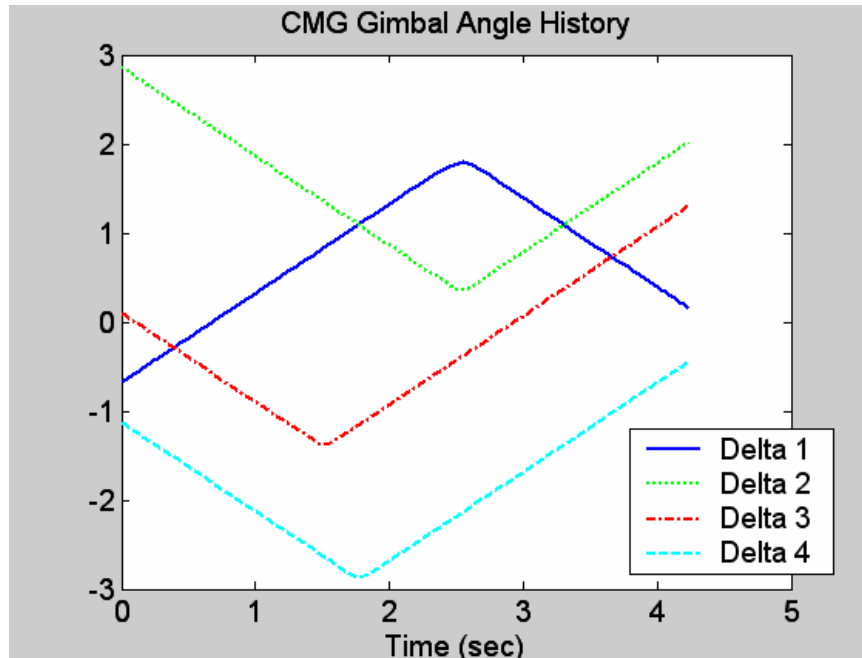


**Figure 82** *CMG Slew Time-optimal Gimbal Angle History*

the state is reasonably well behaved and within the state constraints  $[-p,p]$  imposed in the problem formulation. The time required to complete the maneuver is 4.24 seconds. This, as expected, is faster than the previous idealized actuator solution for this moment of inertia configuration (see Chapter III). The torque available from the four actuators is higher than the previous idealized actuator torque numerical example and therefore we expect faster maneuvering. So our engineering judgment leads us to believe that the solution is correct.

Next we evaluate the optimality of the feasible, candidate solution. The switching functions are given in equations (6.10). These are plotted overlaid with the control solution (Figure 83 through Figure 86). Shown are the switching functions ( $S_i$ ) previously defined as the partial derivative of the Hamiltonian with respect to the control vector. The KKT multiplier ( $\mu$ ) is also shown plotted separately from the switching function. The sum of the switching function and the KKT multiplier is the definition of the minimization of the Hamiltonian, equation(4.10), and should be numerically equal to zero.

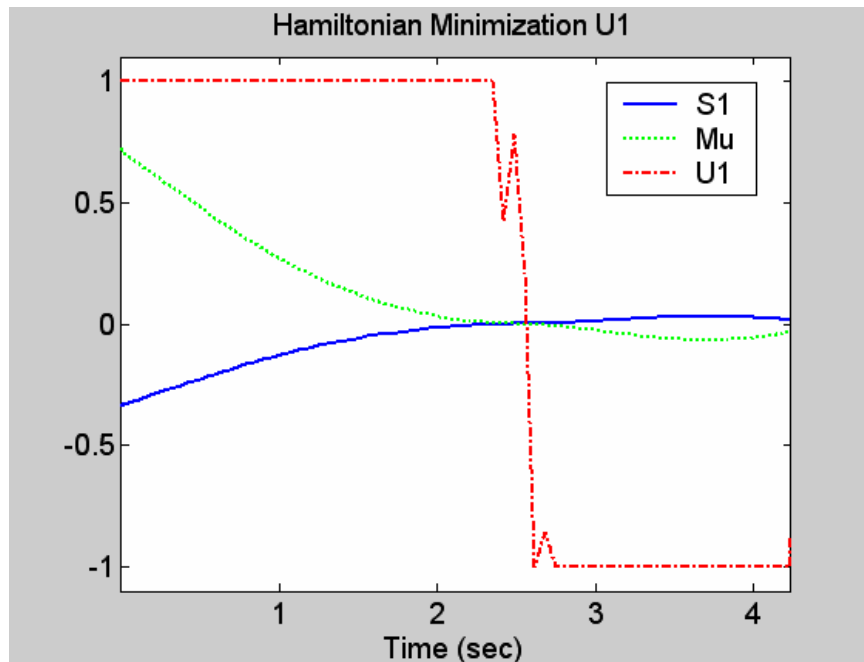


**Figure 83** CMG Control Switching Function and Control Solution

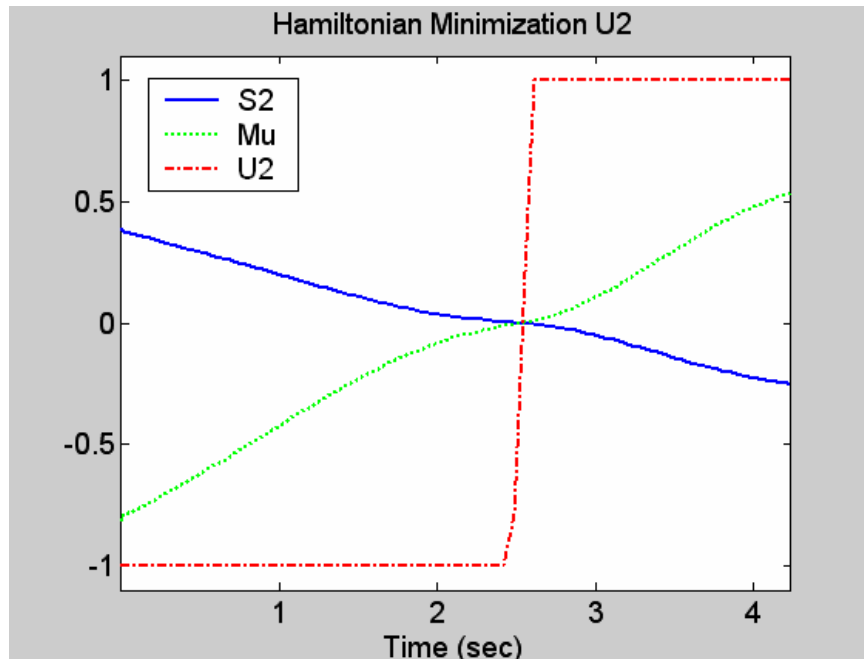


**Figure 84** CMG Control Switching Function and Control Solution (2)

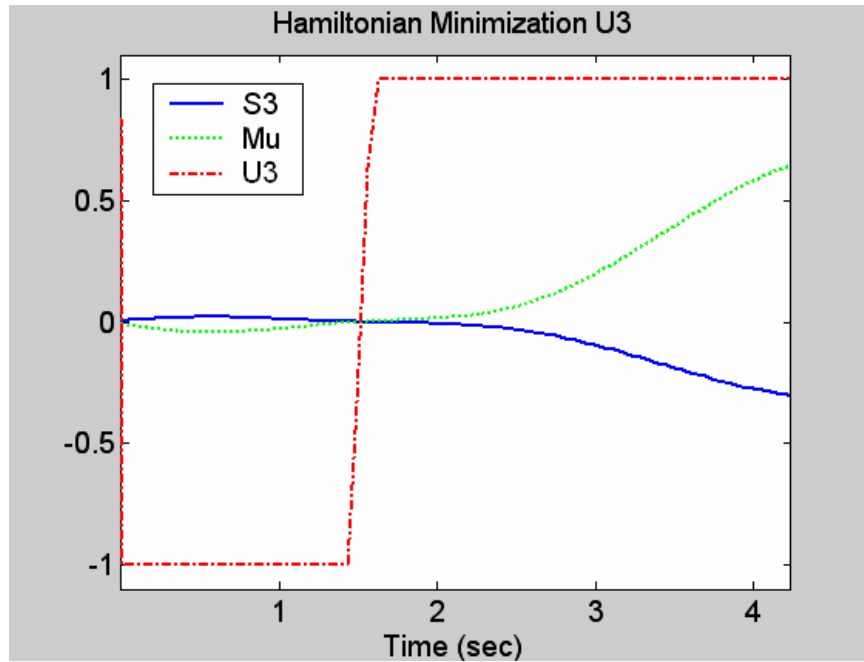


**Figure 85** CMG Control Switching Function and Control Solution (3)

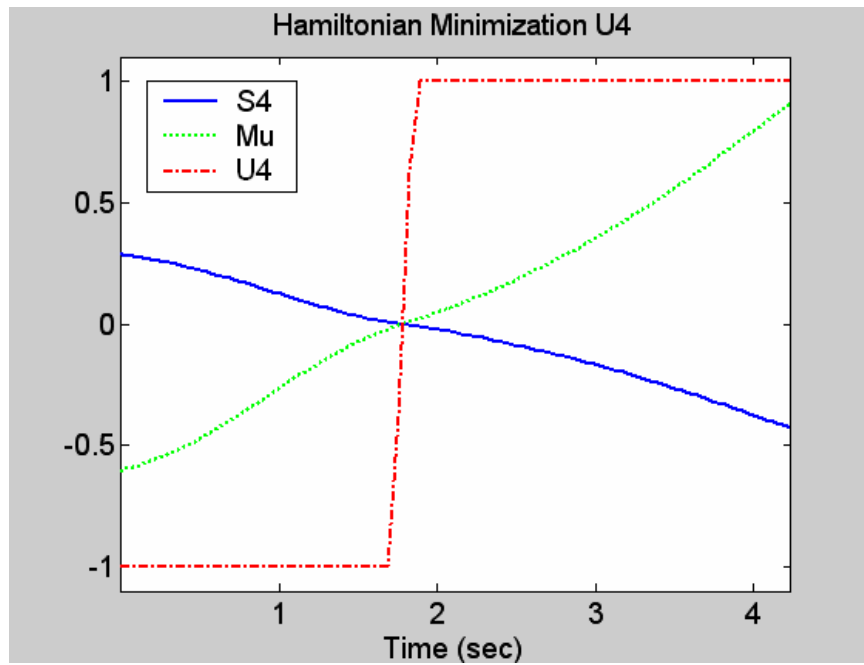


**Figure 86** CMG Control Switching Function and Control Solution (4)

As before the switching function and control are related by the KKT conditions:

$$u_i^* = \begin{cases} \text{maximum} & S_i < 0 \\ \text{minimum} & S_i > 0 \\ \text{singular} & S_i \equiv 0 \end{cases}$$

These figures clearly illustrate that the control solution meets the necessary conditions for optimality established by the Hamiltonian minimization.

The Hamiltonian transversality and evolution conditions were defined in equations (4.12) and (6.11). The computed Hamiltonian is shown in Figure 87. It is clear that the Hamiltonian is numerically well behaved and meets the necessary conditions for optimality.

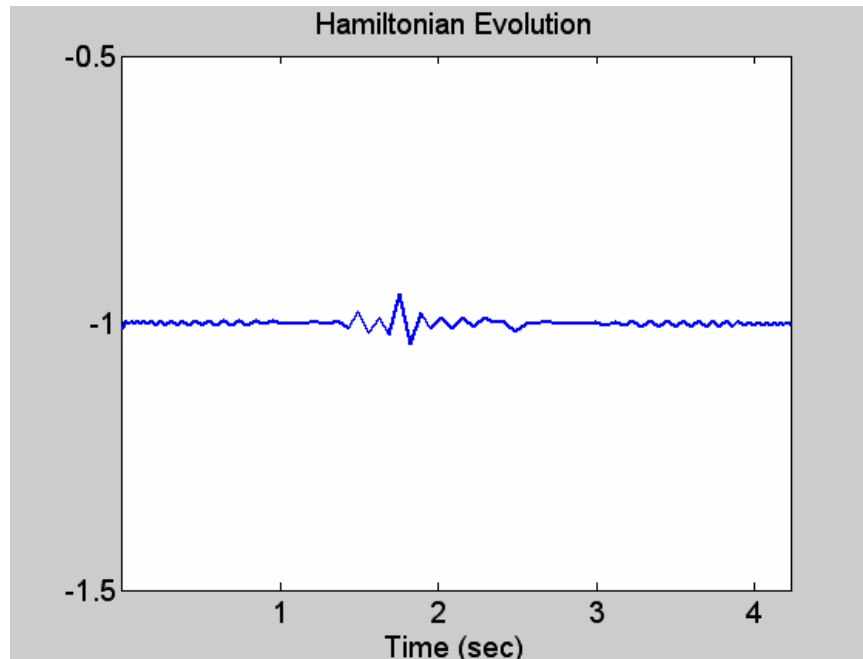


**Figure 87** *CMG Time-optimal Slew Solution Hamiltonian*

Based on an analysis of the necessary conditions and engineering judgment the solution obtained appears optimal for the system under consideration.

#### 4. Numerical Considerations

The principal problem associated with CMG systems for spacecraft attitude control is the well known geometric singularity condition.<sup>9</sup> This refers to a condition in which no torque is generated for a commanded control torque in a certain “singular” direction. Mathematically, this occurs when the  $A$  matrix defined in equation (6.5) is singular or rank deficient. By solving for the optimal control vector  $\underline{u}^*$  to minimize an objective function we have required that the control solution satisfy equation (6.5) as part of the constraints in the problem formulation. As a result the possibility of the matrix  $A$  being singular is eliminated. The condition number of  $A$  is an indication of how close this matrix is to being singular<sup>10</sup>. Condition number is defined as the ratio of the largest to the smallest singular value of the matrix. The condition number of an identity matrix is one and the condition number of a matrix approaches infinity as the matrix becomes singular. The condition number of the  $A$  matrix is shown in Figure 88. It is clear that the matrix is well behaved throughout the maneuver.

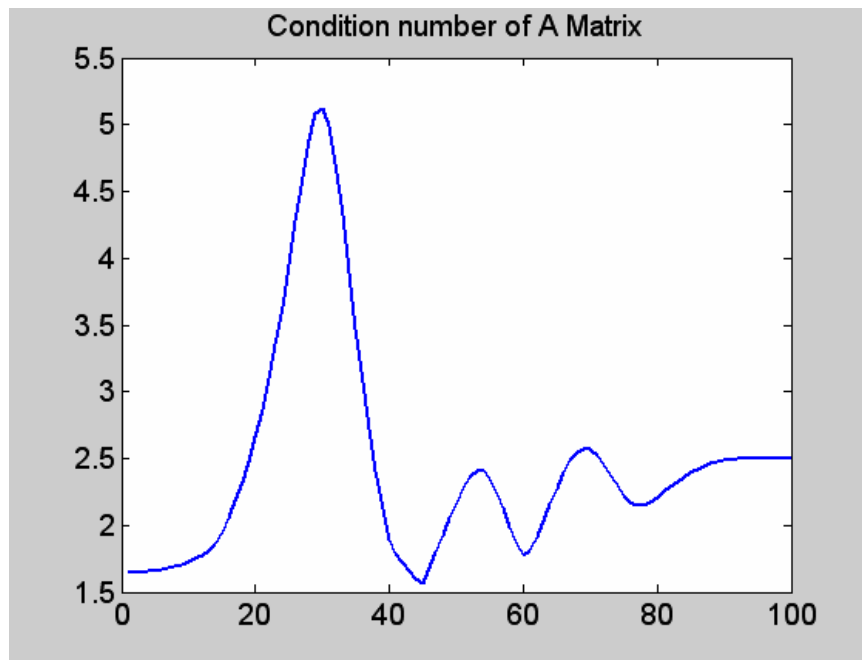


**Figure 88** Condition Number of CMG Control Solution Jacobian Matrix

The far-reaching effects of this singularity free solution will be discussed in the next chapter.

## **5. Conclusions**

In this section the open loop time-optimal control for an asymmetric spacecraft equipped with four CMGs arranged in a pyramid configuration was determined. The candidate solution was determined by propagation to be a feasible solution to the problem. The optimality of the solution was validated through an analysis of the Hamiltonian minimization, switching functions and the behavior of the Hamiltonian. Therefore, we conclude that the solution is feasible and meets the necessary conditions for optimality. Additionally, it was shown that the control solution is completely free of singularities. This leads us to conclude that if the control solution can be computed in real-time, then singularity avoidance in control moment gyro actuator based systems is unnecessary.

---

## ENDNOTES

<sup>1</sup> Ford, K.A. & Hall, C.D. (2000). "Singular Direction Avoidance Steering for Control-Moment Gyros." *Journal of Guidance, Control, and Dynamics*, Vol. 23, No. 4. American Institute of Aeronautics and Astronautics, Reston, VA.

<sup>2</sup> Heiberg, C.J. & Bailey, D. (2000). "Precision Spacecraft Pointing Using Single-Gimbal Control Moment Gyroscopes with Disturbance." *Journal of Guidance, Control, and Dynamics*, Vol. 23, No. 1. American Institute of Aeronautics and Astronautics, Reston, VA.

<sup>3</sup> Kurokawa, H. (1997). "Constrained Steering Law Pyramid-Type Control Moment Gyros and Ground Tests." *Journal of Guidance, Control, and Dynamics*, Vol. 20, No. 3. American Institute of Aeronautics and Astronautics, Reston, VA.

<sup>4</sup> Jung, D., and Tsiotras, P. (2004). "An Experimental Comparison of CMG Steering Control Laws," *Proceedings of the AIAA Astrodynamics Specialist Conference*, August 2004, Providence, RI.

<sup>5</sup> Kurokawa, H. (1998). "A Geometric Study of Single Gimbal Control Moment Gyros – Singularity Problems and Steering Laws," Doctoral Dissertation of the University of Tokyo.

<sup>6</sup> Wie, B. (1998). *Space Vehicle Dynamics and Control*. AIAA Education Series, American Institute of Aeronautics and Astronautics. Reston, VA.

<sup>7</sup> Ibid.

<sup>8</sup> Wie, B. et. al. (2002). "Rapid Multitarget Acquisition and Pointing Control of Agile Spacecraft." *Journal of Guidance, Control, and Dynamics*, Vol. 25, No. 1. American Institute of Aeronautics and Astronautics, Reston, VA.

<sup>9</sup> Wie, B. (2004). "Singularity Analysis and Visualization for Single-Gimbal Control Moment Gyro Systems," *Journal of Guidance, Control, and Dynamics*, Vol. 27, No. 2. American Institute of Aeronautics and Astronautics, Reston, VA.

<sup>10</sup> Lay, David, C. (2000). *Linear Algebra and Its Applications*. Addison-Wesley, Reading MA.

## VII. CLOSED LOOP CONTROL

### A. INTRODUCTION

Classical closed-loop control techniques are, in general, ill suited for slew maneuver time-optimal control. This is due in part to the nonlinear nature of the problem and the inability of classical control techniques to generate time-optimal solutions. Additionally, control solutions must be resolved into actuator input parameters to generate the desired torque. This method, which requires inverting the actuator dynamics equation, has led to singularity problems that continue to plague engineers as evidenced by ongoing research<sup>1,2,3,4,5</sup>.

This chapter addresses the computation of real-time optimal controls for spacecraft slew maneuvers. Prior research efforts were focused on minimizing deviations from a nominal optimal trajectory. These neighboring optimal control (NOC) laws, presented by Bryson and others<sup>6,7</sup> have been used in a variety of applications.

More recently a two degree-of-freedom, non-linear optimal control system architecture was suggested by Strizzi, Yan, et al.<sup>8,9</sup> This concept relied on the computational power of pseudospectral methods to develop optimal controls and NOC laws.

In this work optimal control solutions to the non-linear plant are generated to implement a sampled-data feedback control law.<sup>10</sup> Previous optimal solutions are used as guess for subsequent re-optimized trajectories and significant reductions in computation time are demonstrated.

### B. CLASSICAL CLOSED LOOP CONTROL

A basic diagram of a classical closed loop spacecraft attitude control system is shown in Figure 89. In this type of model sensors determine the attitude and attitude rates. These are in some way compared with desired

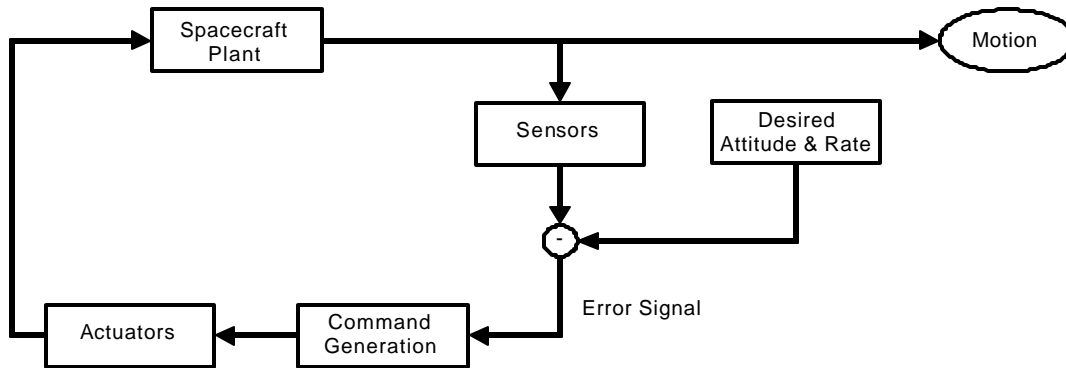


**Figure 89 Classic Closed Loop Spacecraft Attitude Control System**

attitude and rates and the difference or error signal is used to determine a desired control torque to reduce the error signal to zero. Typical approaches for control command generation involve using Euler angle errors for small rotations and either a direction cosine error matrix or a quaternion error vector for large angular rotations.<sup>11</sup> In either case proportional plus derivative gains are imposed in order to achieve desired performance. This type of command generation has two inherent problems. First, the command generation performs no better than an eigenaxis maneuver and in fact will seldom perform so well. Second, generating a desired control torque for use as an actuator input has led to numerous singularity problems of which the best known is the control moment gyro problem.

### 1. Error Signal Command Generation

In previous sections we have seen that the time-optimal solution is a function of the magnitude of the maneuver and the spacecraft moment of inertia. While error signal command generation is capable of generating the eigenaxis path the command signal is not the familiar bang-bang we have come to expect from time-optimal solutions. As the spacecraft approaches the desired attitude the command generated from the error signal approaches zero. Additionally, the command generation algorithm does not utilize spacecraft moment of inertia information in developing the command. Modern control system engineers have

made use of feedforward signals and other more imaginative techniques to improve slew performance however; these require an a priori knowledge of the maneuver and control solution. This is in effect a step back from the autonomy that we seek to achieve.

## 2. Singularity Issues

We have seen that the command generation algorithm outputs a desired torque output from the actuator based on the error signals without regard to the method of torque generation. This desired torque is sent to the actuator as a commanded torque signal to be accomplished. The question to consider is under what circumstance is the commanded torque actually output from the actuator and what are the effects on the desired maneuver when the commanded torque is not output from the actuator.

Consider an ideal, unlimited torque thruster which is mathematically modeled as:

$$\begin{bmatrix} 1 & 0 & 0 \\ 0 & 1 & 0 \\ 0 & 0 & 1 \end{bmatrix} \begin{bmatrix} T_{\text{signal}_1} \\ T_{\text{signal}_2} \\ T_{\text{signal}_3} \end{bmatrix} = \begin{bmatrix} T_{\text{out}_1} \\ T_{\text{out}_2} \\ T_{\text{out}_3} \end{bmatrix}$$

In this case the input signal ( $T_{\text{signal}}$ ), results in the corresponding output torque ( $T_{\text{out}}$ ). Therefore, given the desired actuator output torque ( $T_{\text{out}}$ ), from command generation, we can solve for the required input signal to the actuator ( $T_{\text{signal}}$ ) as,

$$\begin{bmatrix} T_{\text{signal}_1} \\ T_{\text{signal}_2} \\ T_{\text{signal}_3} \end{bmatrix} = \begin{bmatrix} 1 & 0 & 0 \\ 0 & 1 & 0 \\ 0 & 0 & 1 \end{bmatrix}^{-1} \begin{bmatrix} T_{\text{out}_1} \\ T_{\text{out}_2} \\ T_{\text{out}_3} \end{bmatrix}$$

The actuator dynamics, represented in matrix form, in this case as the identity matrix, must be inverted to resolve the desired output torque. In this case the commanded torque generates the output torque desired. Unfortunately, actuator dynamics are seldom this simple. As a result we define an actuator singularity as

a condition in which no control torque is generated for the commanded torque along a certain direction. Mathematically, this is a condition in which the actuator dynamics matrix is singular.

Consider the case of the asymmetric spacecraft subject to CMG control. This case was examined in detail in Chapter VI. Since we have determined that the error command generation algorithm is unsuited for generating bang-bang controls suppose that we elect to feed forward the bang-bang control structure shown in Figure 90. This control torque on the spacecraft would result in a 135 degree slew about the x-axis for NPSAT 1.

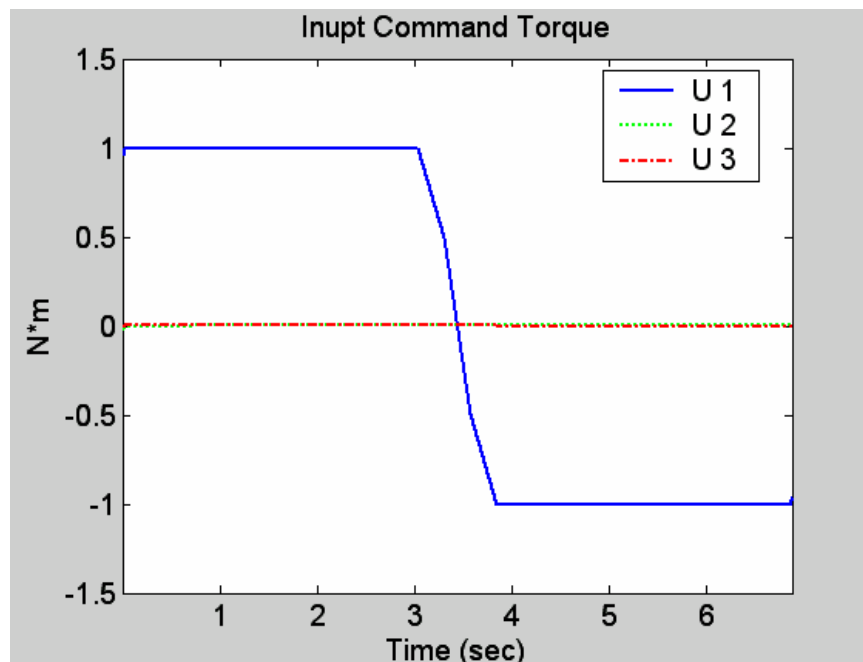


**Figure 90 Asymmetric Eigenaxis Rotation Torque Control Solution**

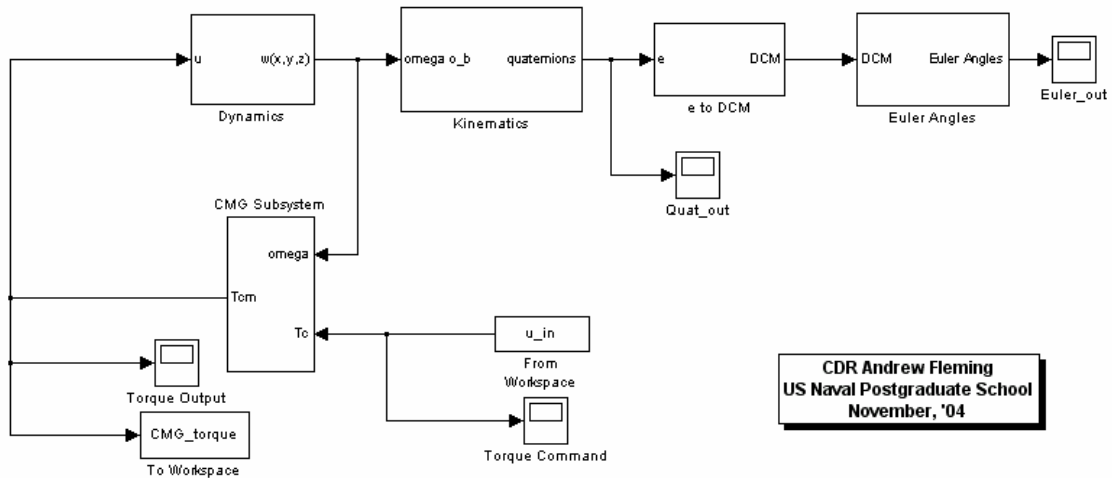
In this case the torque command signal becomes the input to the CMG actuator in our spacecraft model (Figure 91). The input or commanded torque signal must be resolved into a gimbal angle rate. This is generally accomplished in accordance with a command pseudoinverse steering logic<sup>12</sup>. In this steering logic for the commanded torque input ( $u$ ), the CMG momentum rate command ( $\dot{h}$ ) is defined as:

$$\dot{\underline{h}} = -\underline{u} - \underline{w} \times \underline{h}$$

and the gimbal rate command ( $\underline{d}$ ) is then obtained by:\*

$$\underline{d} = A^+ \dot{\underline{h}} = A^T (AA^T)^{-1} \dot{\underline{h}}$$

### CMG Open Loop Command Propagation



CDR Andrew Fleming  
US Naval Postgraduate School  
November, '04

**Figure 91** *Spacecraft Model with CMG Actuators*

where the matrix  $A$  is a function of the gimbal angles ( $\underline{d}$ ) and was previously defined in Chapter VI (Equation (6.5)). If the matrix  $A$  becomes rank deficient for certain sets of gimbal angles the pseudoinverse fails to exist and singular states are encountered. Previously, we showed that the time-optimal CMG solution resulted in well behaved condition numbers for the matrix  $A$  (See Figure 88). In this case the bang-bang control solution, when used as the desired torque on the spacecraft, produced the  $A$  matrix condition numbers shown in Figure 92. These results are four-orders of magnitude larger than those obtained in the

\*  $A^+$  is also called the *Moore-Penrose inverse* of  $A$  or the generalized inverse of  $A$ .

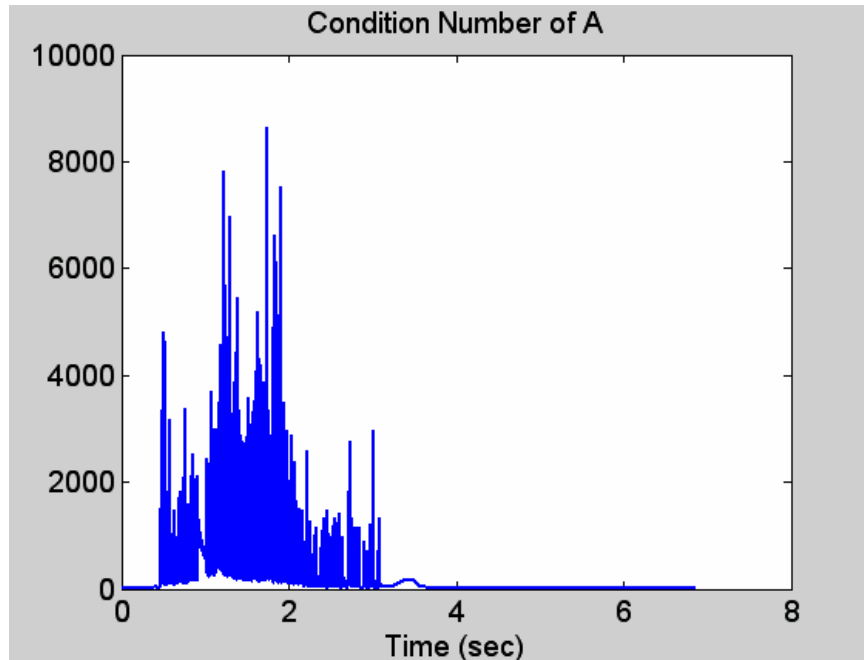


**Figure 92** *Condition Number of CMG Jacobian Matrix with Independent Torque Solution*

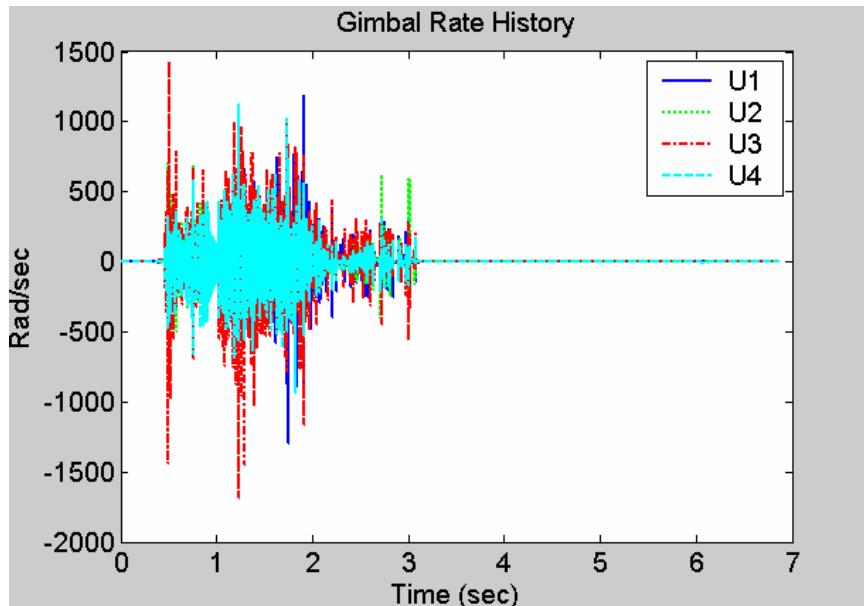


**Figure 93** *Gimbal Angle Rates From Pseudoinverse Steering Logic*

previous section. As a result of the poor condition of this matrix the algorithm attempts to drive the gimbal angle rates to infinity. Gimbal angle rates resulting

from this simulation are shown in Figure 93. The zoomed in view of the gimbal angle rates from 4-6 seconds is shown in Figure 94.

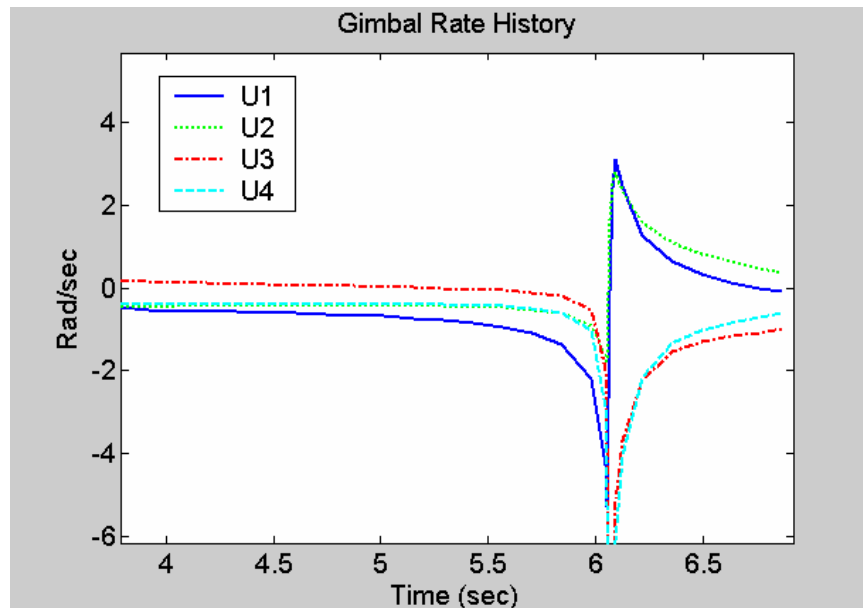


**Figure 94** *Gimbal Angle Rates from Pseudoinverse Steering Logic (Close-up)*

Gimbal angle rates are driven towards infinity as the singular states are approached. Clearly, the singularity is not caused by the bang-bang structure of the input torque. Comparing the commanded torque signal (Figure 90) with the condition number plot (Figure 92) or the gimbal angle rates (Figure 93) indicates that the singular states are encountered prior to the control switch.

Singularity avoidance is an unintended and yet significant benefit of the time-optimal control algorithm. In effect the singularity problem is avoided both mathematically and physically by requiring that the time-optimal control vector satisfy the actuator constraints in the problem formulation such that,

$$u^* = -[A(\mathbf{d})]\dot{\mathbf{d}} - \mathbf{w} \times h(\mathbf{d})$$

The actuator dynamics are solved iteratively from left to right vice right to left. The previous matrix inversion is eliminated and the solution is optimal with regard to the actuator capabilities.

In this example we have examined the CMG singularity problem since it is well known. However, the same logic could be applied to any actuator system that is *not* an ideal torque generating device. Magnetic torque rods represent a second well known system for which the actuator has known singularities. In this case, a desired torque output from the torque rod must be resolved in the magnetic dipole moment of the torque rod. The torque output of a magnetic torque rod is given by:

$$\vec{T} = \vec{m} \times \vec{B}$$

$$\vec{T} = \begin{bmatrix} 0 & B_3 & -B_2 \\ -B_3 & 0 & B_1 \\ B_2 & -B_1 & 0 \end{bmatrix} \begin{bmatrix} m_1 \\ m_2 \\ m_3 \end{bmatrix} \quad (7.1)$$

Therefore, given the desired torque output we have:

$$\vec{m} = \underbrace{\begin{bmatrix} 0 & B_3 & -B_2 \\ -B_3 & 0 & B_1 \\ B_2 & -B_1 & 0 \end{bmatrix}}_{\text{Singular}}^{-1} \begin{bmatrix} T_1 \\ T_2 \\ T_3 \end{bmatrix} \quad (7.2)$$

The inverse of equation (7.1) does not exist. Therefore it is impossible to achieve control of the three body axes by means of the created magnetic dipole vector in the satellite<sup>13</sup>. However, using the time-optimal control formulation as demonstrated in Chapter III and Chapter IV we require that the optimal control vector ( $m$ ) satisfy equation (7.1). Again, the singular condition is avoided by eliminating the matrix inversion and iteratively solving the problem from right-to-left.

### C. BELLMAN'S PRINCIPLE OF OPTIMALITY

Bellman's principle of optimality is a powerful tool when applied to closed loop time-optimal control. It states that given an optimal trajectory from a point A to a point B, the trajectory to point B from a point C lying on the optimal trajectory is also optimal<sup>14</sup>.

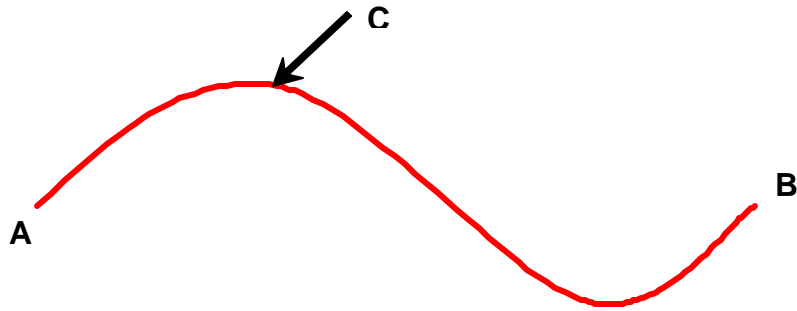


**Figure 95 Principle of Optimality**

In this work this principle serves three purposes. First, it verifies optimality in the absence of costate information. Optimal trajectories are obtained and verified by recalculating the trajectory from an intermediate point on the trajectory. Second, in the presence of a disturbance torque, this principle allows the use of previous optimal solutions as guesses for subsequent trajectories. Since the disturbed state is near the optimal state using the previously calculated state trajectory as a guess for the re-optimized state trajectory significantly reduces the computation time. Finally, it allows us to evaluate the accuracy of a solution based on a finite number of LGL points.

Shown in Figure 96 is the now familiar quaternion trajectory for the asymmetric spacecraft time-optimal slew maneuver. The intermediate point selected is on the optimal trajectory and marked with a bold **square**. The subsequent solution is overlaid with “+” marks.

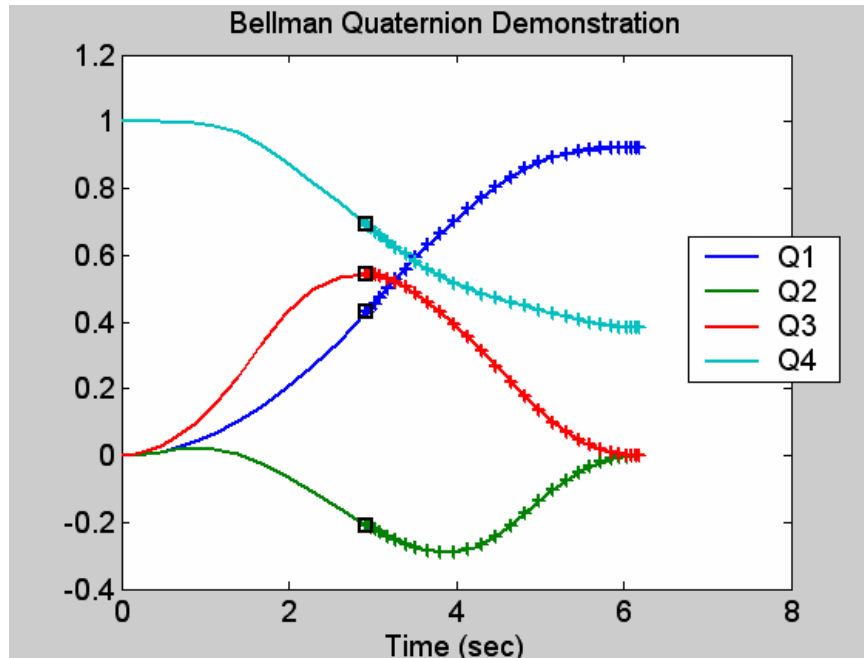


**Figure 96 Asymmetric Time-optimal Quaternion Solution – Bellman’s Principle of Optimality**

The subsequent solution clearly obeys Bellman’s Principle of Optimality. While this may not be sufficient to mathematically demonstrate the optimality of the solution it can certainly be considered a necessary condition. The original solution was obtained using 30 LGL points (nodes) and was based on a two-point guess defined by the initial and final conditions. The subsequent solution also used 30 nodes but was provided with a guess which consisted of 15 points from the previous solution. The computation times<sup>†</sup> as determined by the MATLAB tic and toc commands are shown in Table 9.

<sup>†</sup> All computations were performed on a Pentium 4 Windows based operating system at 3.06 GHz with 512 MB RAM using MATLAB 6.5.0.1 Release 13. Emphasis is placed on the relative vice absolute computational time.

Computation Time	
Original Solution	42.5310 seconds
Subsequent Solution	2.6250 seconds
Reduction, %	93.83

Table 9 *Bellman Principle Effect on Computational Time*

The accuracy of the solution obtained is related to the number of nodes used in the algorithm. The number of nodes also has a significant effect on computational time. Therefore, we strive to choose a number of nodes that meets our accuracy goal without creating excessively long computational times. As the number of nodes increases, the values returned, states, costates, etc. converge so that the difference between solutions approaches zero. Therefore, if the number of nodes is increased and the behavior of the solution changes considerably the original solution is shown to be inaccurate. In Figure 97, a low node (6 nodes) solution is overlaid with a high node solution (30 nodes) from an

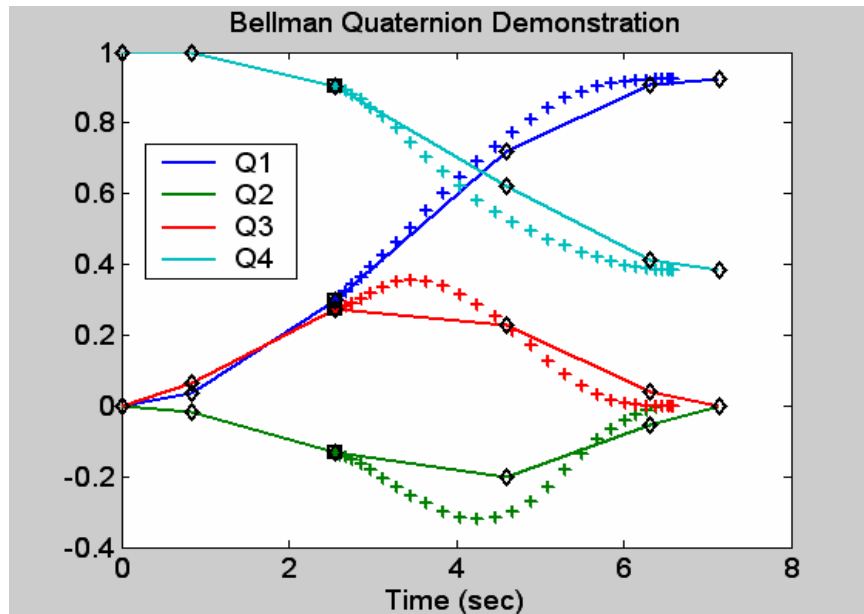
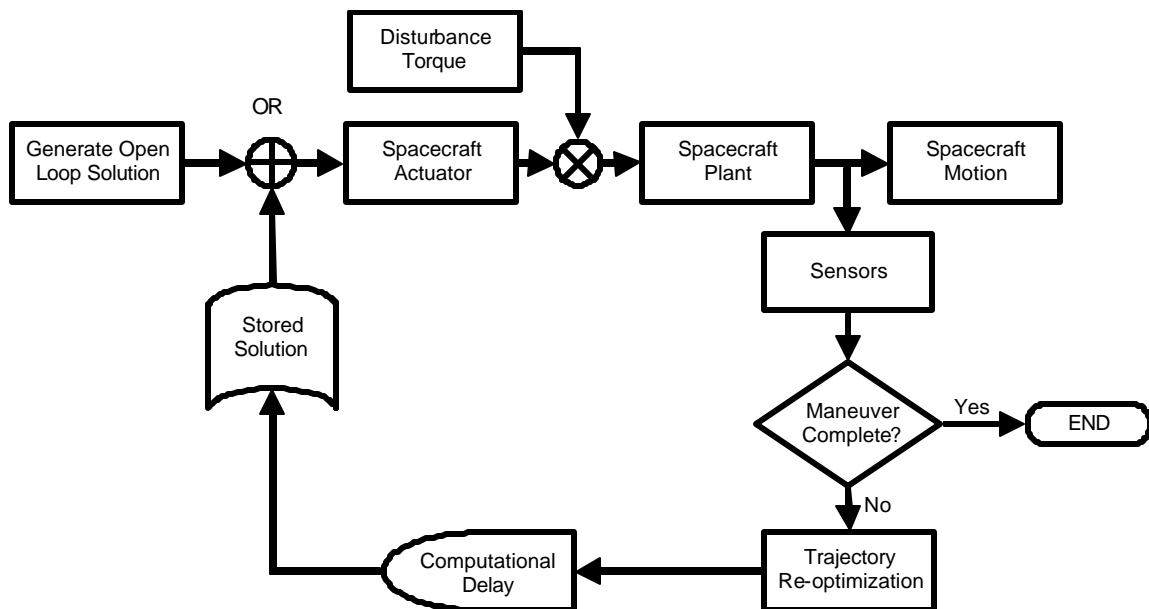


Figure 97 *Effect of Increasing Nodes on Quaternion Solution*

intermediate point on the optimal trajectory. The significant change visible in the state trajectory and final time are indications that the low node solution has questionable accuracy.

#### D. REAL-TIME OPTIMAL CONTROL

In this section we provide two examples of closed loop time-optimal control. In each case the simulation is as shown in Figure 98. The primary tuning parameter for spacecraft performance is the open-loop propagation interval. Ignoring computational delay, the state is sampled and an open loop control solution is generated time-indexed to the predicted spacecraft state. This solution is propagated for a set interval, the propagation interval, after which the state is re-sampled and a re-optimized trajectory is computed. Currently, computation times are recorded for comparison and evaluation but ignored in the simulation.



**Figure 98 Closed Loop Simulation Model**

##### 1. Asymmetric Spacecraft with Idealized Actuator Control

The time-optimal reorientation of an asymmetric spacecraft with idealized actuator control was addressed in detail in Chapter III. The spacecraft and orbital parameters remain unchanged for the closed loop simulation and are

available in Chapter III. A constant disturbance torque has been added to the model. This disturbance torque will perturb the model off the optimal trajectory and require re-optimization. Since we know from the previous chapter that the time-optimal open loop maneuver is approximately 6 seconds the disturbance torque has been amplified from what might be considered normal for graphical visualization. The disturbance torque has been selected as:

$$M_{d_x} = 0.108 \text{ N}\cdot\text{m}$$

$$M_{d_y} = 0.108 \text{ N}\cdot\text{m}$$

$$M_{d_z} = 0.0317 \text{ N}\cdot\text{m}$$

The open loop time-optimal control solution and the propagated solution in the presence of this disturbance torque are shown in Figure 99. The solid lines indicate the optimal trajectory; the propagated trajectory is marked as '+'. It is

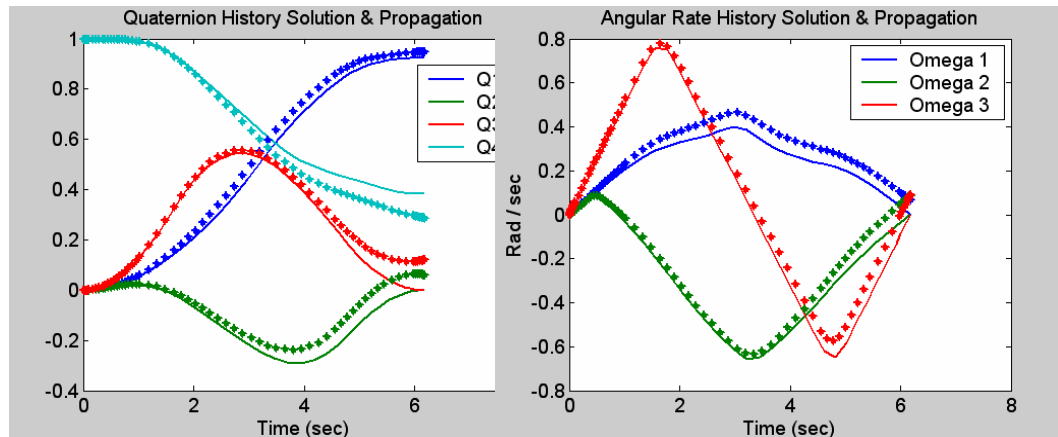


**Figure 99 Asymmetric Spacecraft Time-optimal State Solution and Propagation**

clear that in presence of a disturbance torque the open loop solution would not deliver acceptable performance.

The propagation interval for this closed loop simulation was selected as 1 second. The results of the first interval of propagation are shown in Figure 100 and Figure 101. At this time the spacecraft state is sampled and the time-optimal

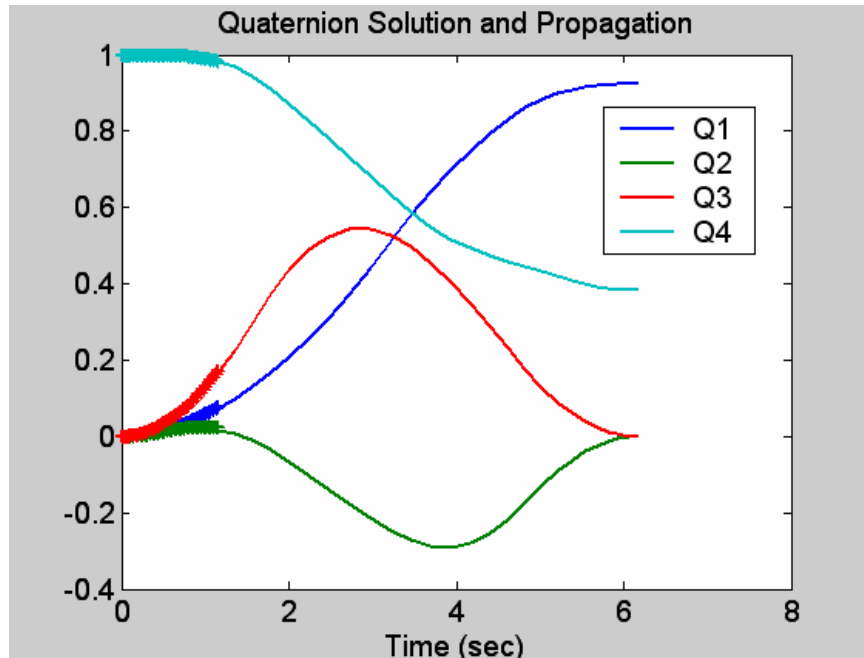


**Figure 100 Asymmetric Spacecraft Quaternion Propagation Interval 1**

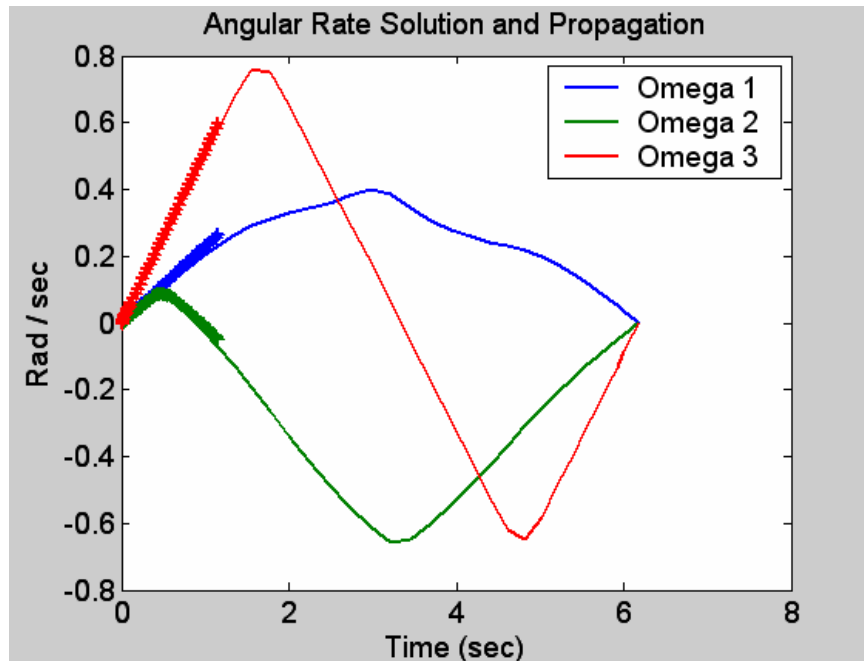


**Figure 101 Asymmetric Spacecraft Angular Rate Propagation Interval 1**

solution is computed from the current attitude and rate to the desired attitude and rate. In the next two figures, (Figure 102 and Figure 103) the re-optimized trajectory is shown along with the original trajectory. The basic structure of the optimal state trajectories is the same and the end point conditions are met.

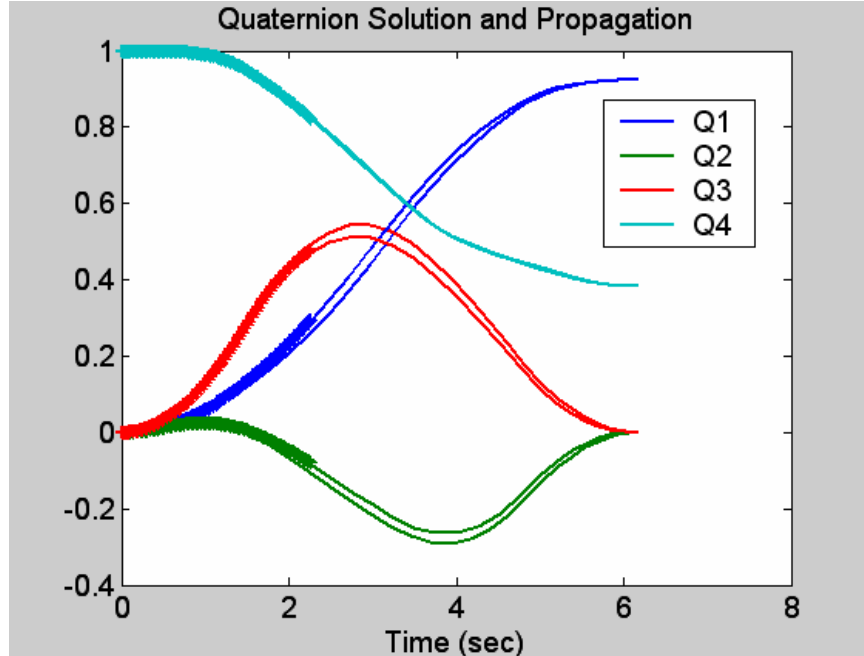


**Figure 102 Asymmetric Spacecraft Quaternion Propagation Interval 2**

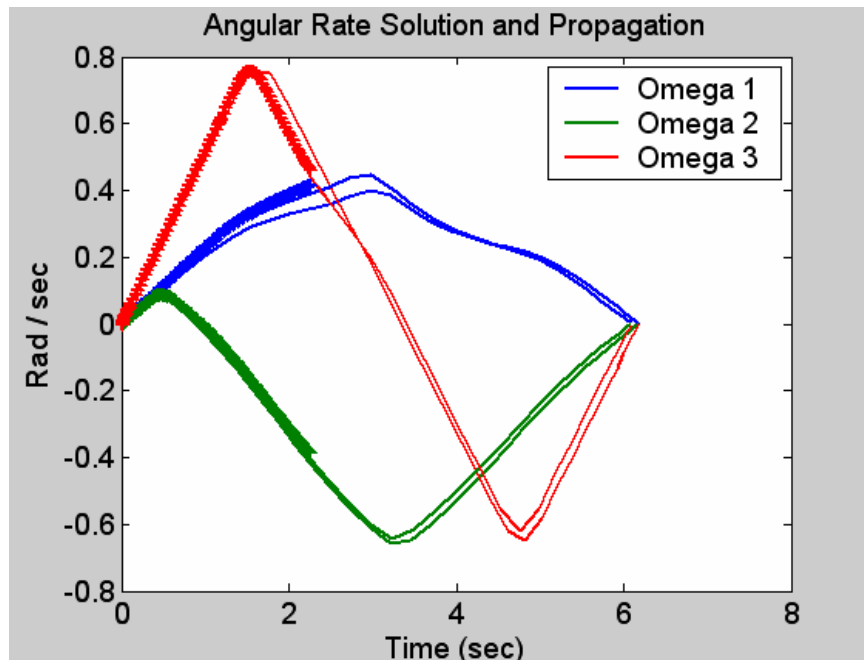


**Figure 103 Asymmetric Spacecraft Angular Rate Propagation Interval 2**

The sample and update cycle continues from Figure 104 through Figure 113. Each time the state is sampled the time-optimal solution is generated and propagation continues with the updated solution.

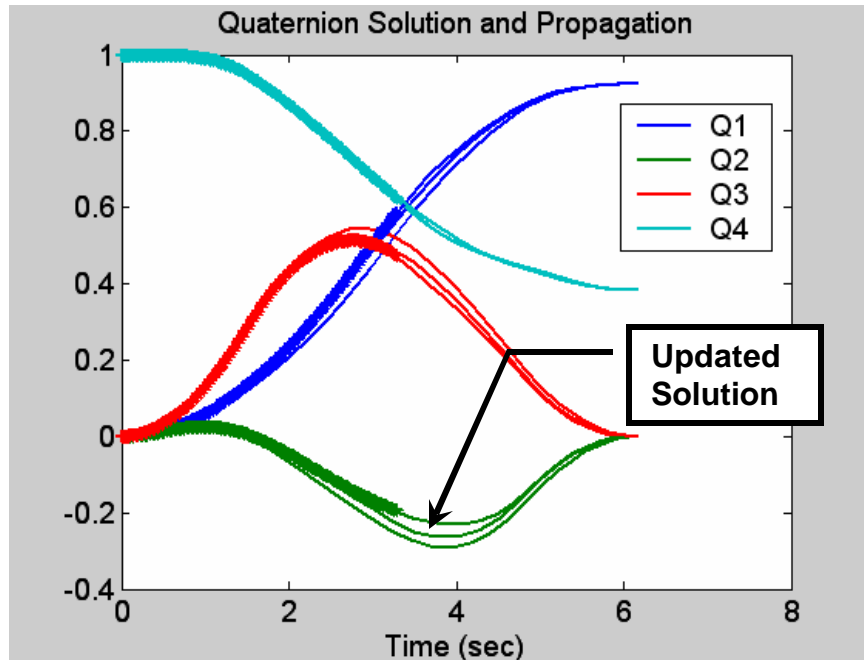


**Figure 104** *Asymmetric Spacecraft Quaternion Propagation Interval 3*

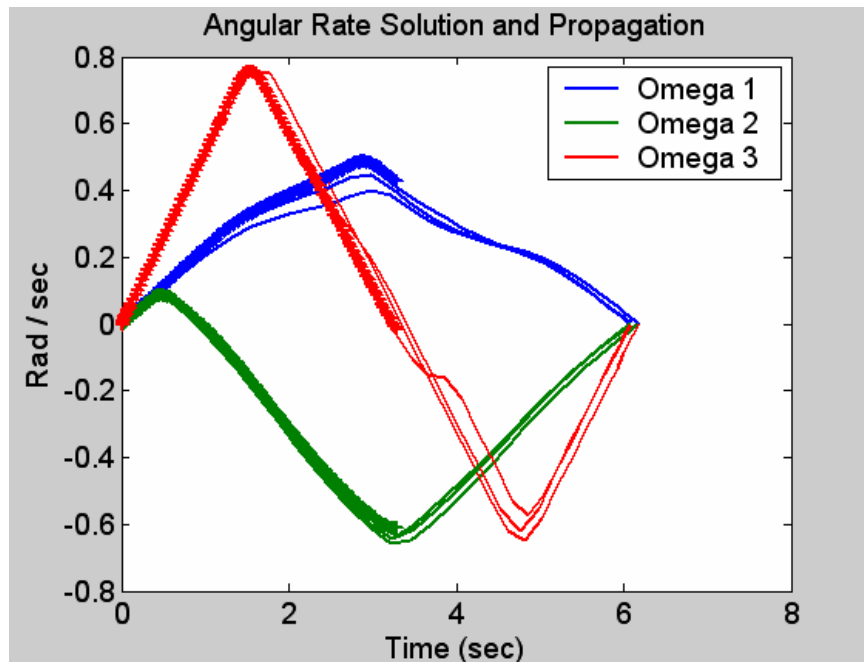


**Figure 105** *Asymmetric Spacecraft Angular Rate Propagation Interval 3*

With each update it is clear that a re-optimized trajectory is generated from the current state of the spacecraft to the final state which remains a constant.

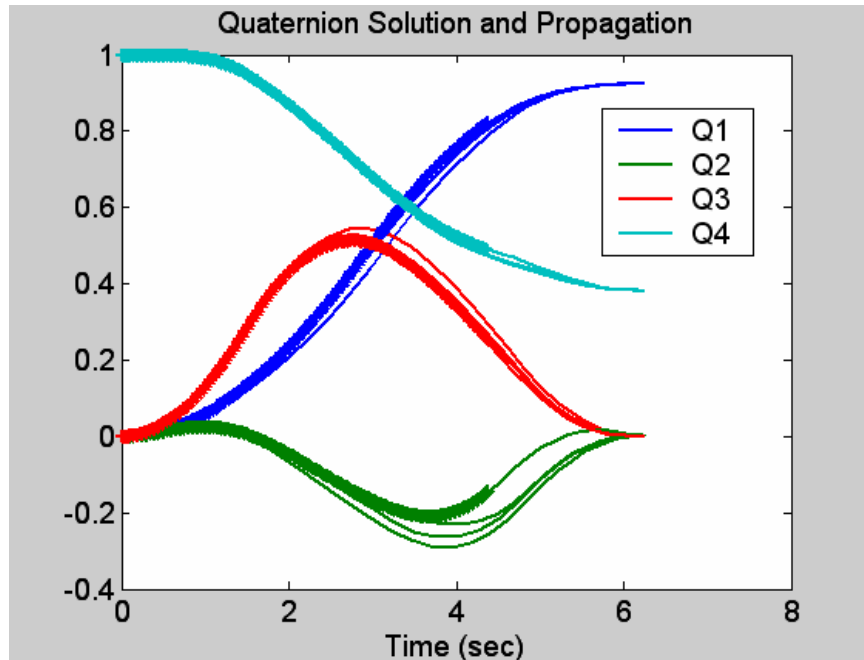


**Figure 106** Asymmetric Spacecraft Quaternion Propagation Interval 4

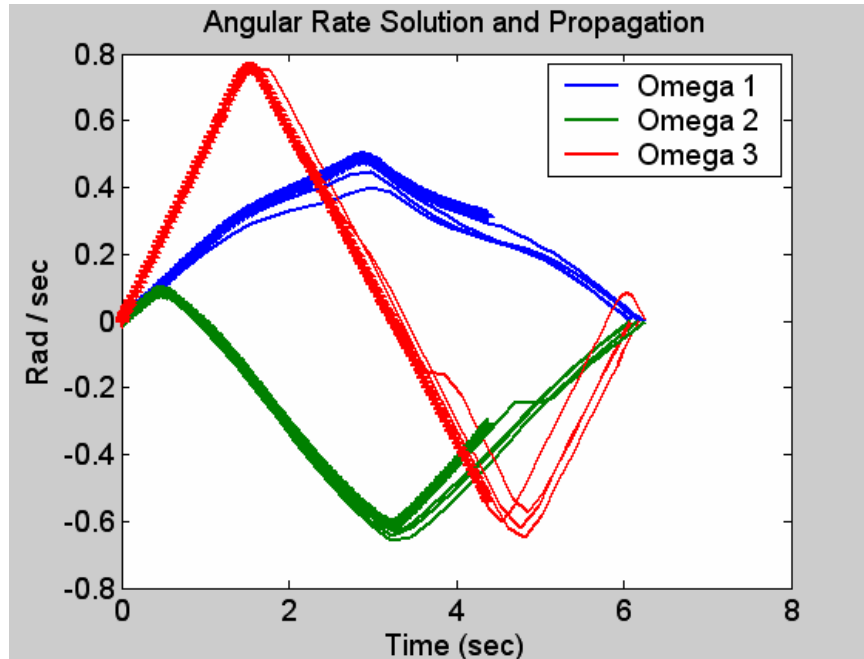


**Figure 107** Asymmetric Spacecraft Angular Rate Propagation Interval 4

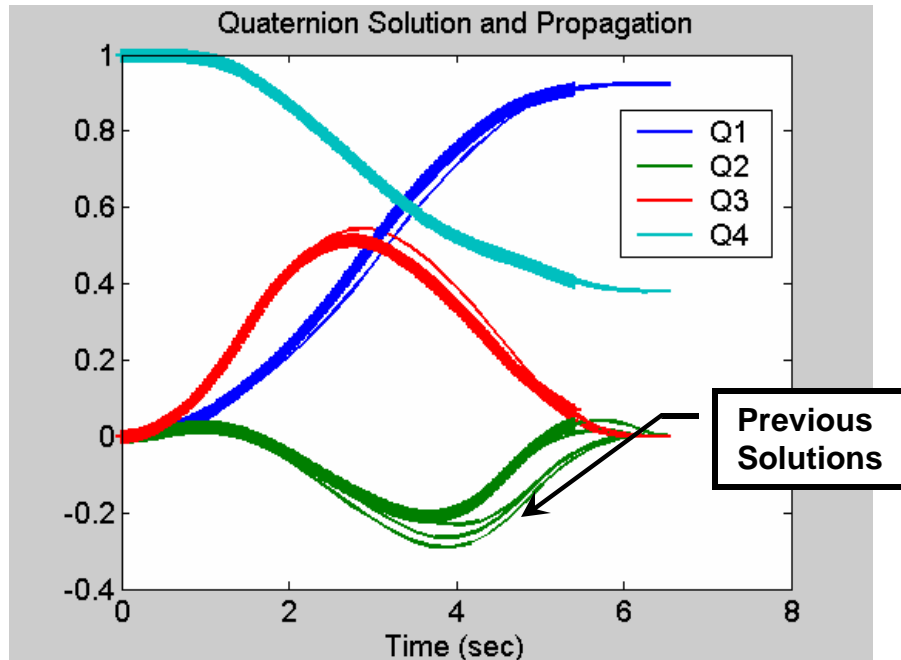


**Figure 108** Asymmetric Spacecraft Quaternion Propagation Interval 5

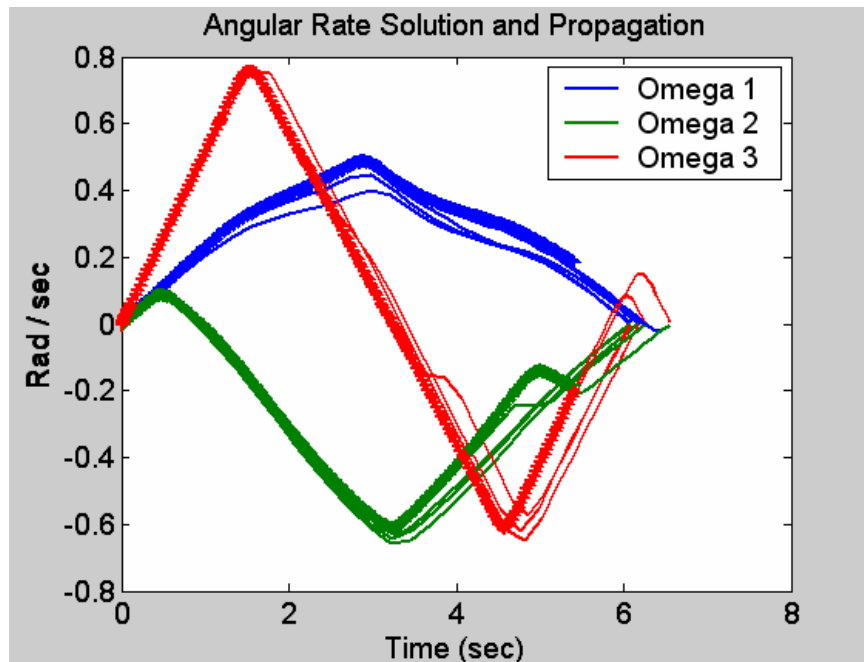


**Figure 109** Asymmetric Spacecraft Angular Rate Propagation Interval 5

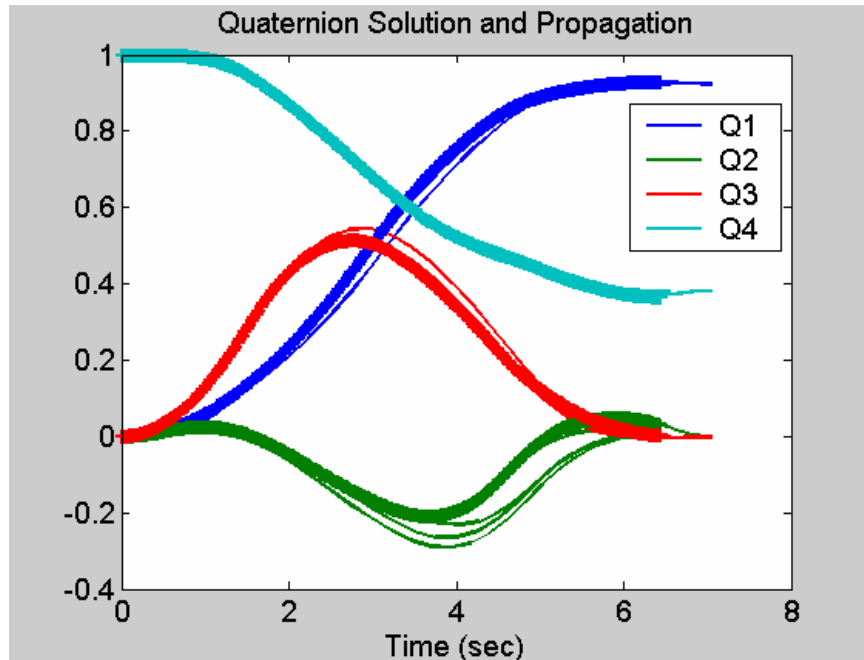


**Figure 110** *Asymmetric Spacecraft Quaternion Propagation Interval 6*

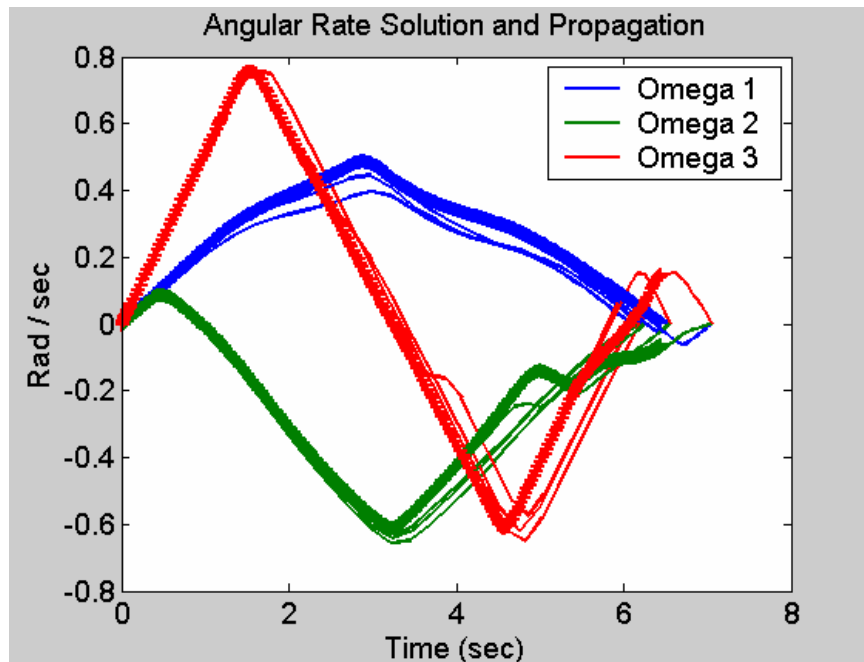


**Figure 111** *Asymmetric Spacecraft Angular Rate Propagation Interval 6*

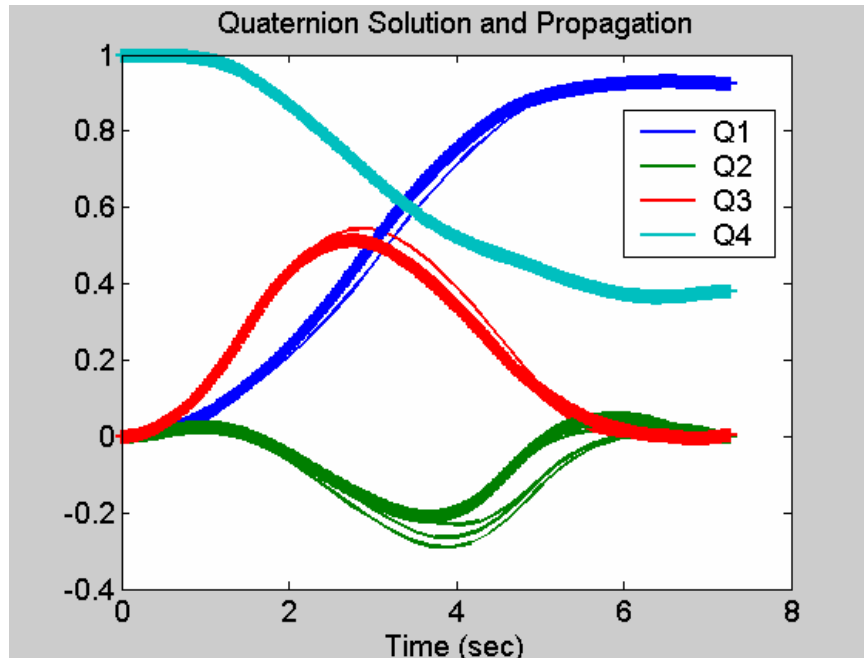


**Figure 112 Asymmetric Spacecraft Quaternion Propagation Interval 7**

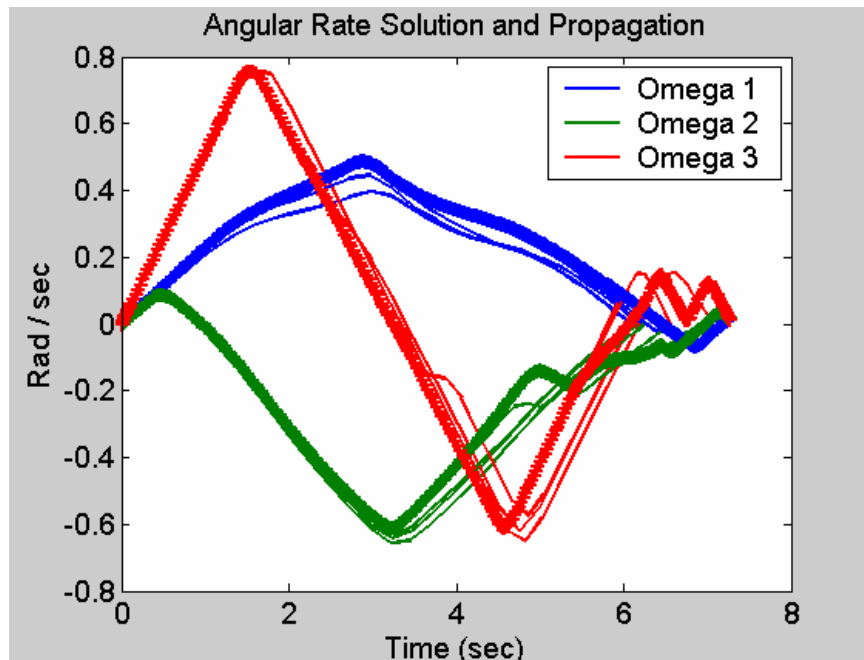


**Figure 113 Asymmetric Spacecraft Angular Rate Propagation Interval 7**

The completed maneuver is shown in Figure 112 and Figure 113. The time required to complete the 135 degree reorientation about the x-axis in the

presence of the disturbance torque is 7.2652 seconds. The original solution time, modeled without a disturbance was 6.1825 seconds. Each subsequent solution calculated from the sampled state met the feasibility and optimality criteria that were established for this problem formulation in Chapter III.

Computation time is related to propagation interval in that longer propagation intervals in the disturbance field cause the spacecraft to deviate further from the optimal trajectory. This results in longer computation times. The computation times for the simulation are shown in Figure 114. The average value of the update solutions (solutions 2 through 7) is 11.9296 seconds. This is due to the large disturbance torque modeled to aid in the visual clarity of the graphics. When the disturbance torque is modeled as something more realistic for the spacecraft and orbital parameters the previous disturbances are reduced by 5 orders of magnitude. The resulting update computation times then decrease to an average value of 4.0566 seconds.

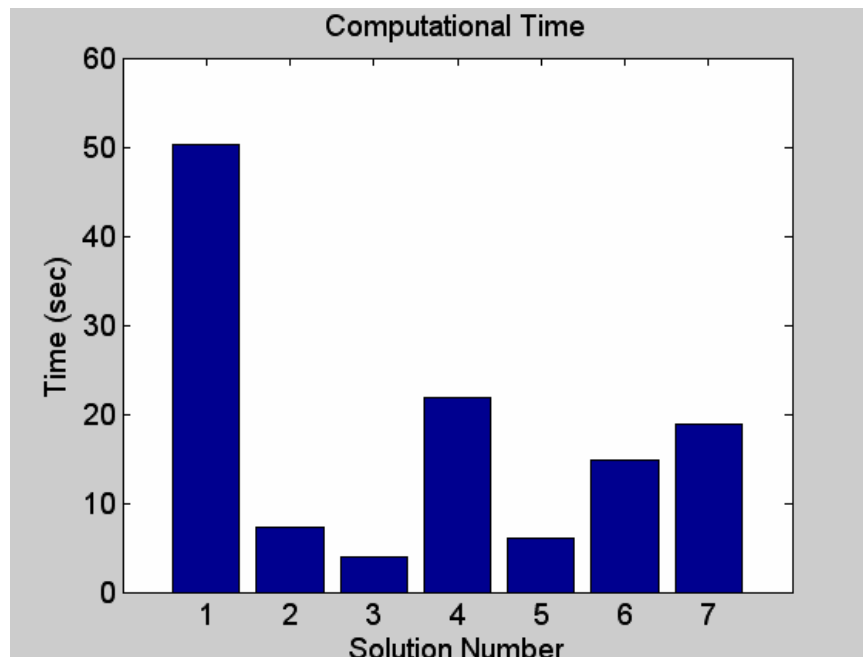


**Figure 114** *Asymmetric Spacecraft Idealized Actuator Time-optimal Solution Computation Time*

**a. Numerical Considerations and Notes**

Simulated spacecraft states were numerically generated by a MATLAB ODE45 propagation subroutine. The generated control vector plus the disturbance torque were used as input; the spacecraft state was extracted following propagation to simulate a sensor reading. In some cases due to numerical approximations and truncation errors the norm of the quaternion was not equal to one to the precision required for the optimization algorithm (DIDO) to determine a feasible solution. In order to resolve this problem the sampled-state quaternion vector was normalized as follows:

$$q_{i_{\text{normal}}} = \frac{q_{i_{\text{sample}}}}{\|q\|_2}$$

Additionally, Figure 114 indicates, and it was observed, that the computation time for the final re-optimization of a trajectory was in general longer than previous computation times. Since this algorithm was originally conceived for large angle slew maneuvers constant scaling parameters were applied based on the maneuver open loop solution. As the maneuver approaches completion and the trajectory is re-optimized the magnitude of the problem has changed to the extent that the original scaling parameters are poorly chosen. The problem requires a scaling parameter adjustment based on the remaining horizon.

**2. Asymmetric Spacecraft with Magnetic Torque Rod Control**

The time-optimal reorientation of an asymmetric spacecraft under magnetic torque control was treated in detail in Chapter IV. Once again the spacecraft and orbital parameters are based on the NPSAT 1 small satellite program and found in Table 5.

The closed loop simulation, while made more complex by the time-varying magnetic field, is accomplished as shown in Figure 98. The constant disturbance torque selected for propagation is:

$$M_{d_x} = 5.4 \times 10^{-6} \text{ N}\cdot\text{m}$$

$$M_{d_y} = 5.508 \times 10^{-6} \text{ N}\cdot\text{m}$$

$$M_{d_z} = 6.34 \times 10^{-7} \text{ N}\cdot\text{m}$$

The larger disturbance torque, used in the previous example for visual clarity, would overpower the torque available from the system and make the spacecraft uncontrollable. Recall that the time-optimal open-loop maneuver required approximately 273 seconds. The state trajectories resulting from the propagation of the open loop solution in the presence of the disturbance torque are shown in Figure 115 and Figure 116. The end point error, although difficult to see in the graphical presentation is significant enough to warrant correction. A comparison of the actual vs. desired state is shown in Table 10.

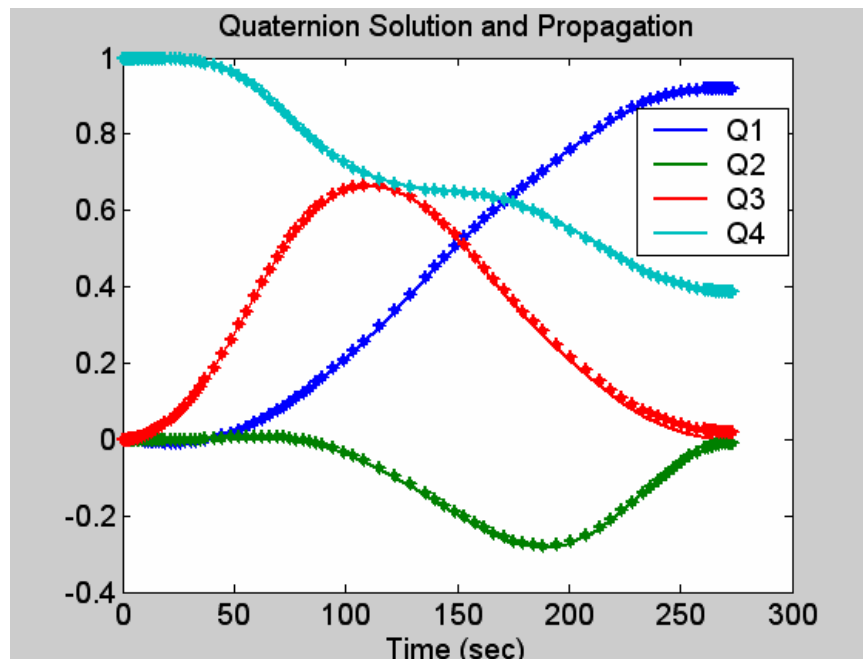


**Figure 115** *Magnetic Torque Open Loop Solution Propagated with Disturbance Torque*

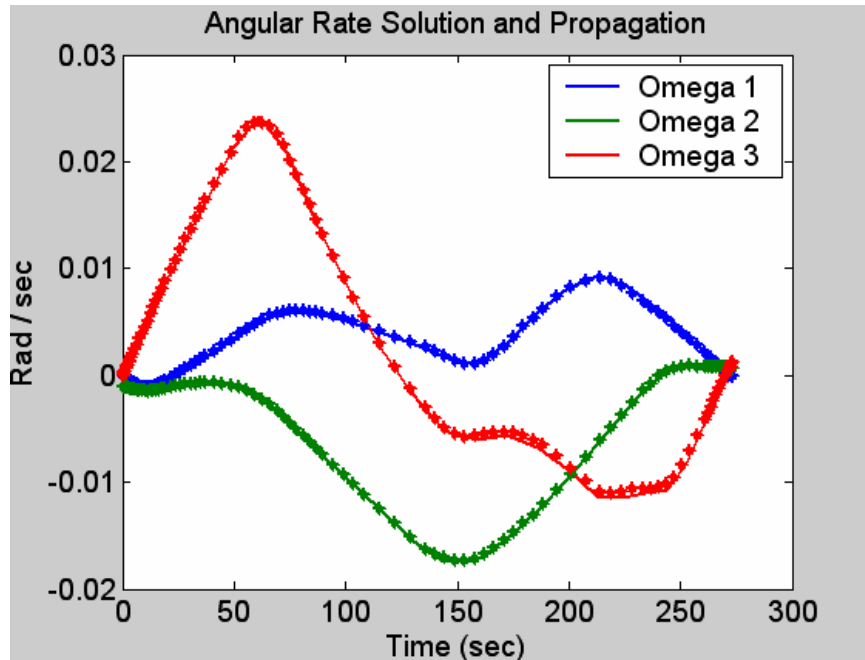


**Figure 116** *Magnetic Torque Open Loop Solution Propagated with Disturbance Torque (2)*

<b>Propagation Error with Disturbance</b>			
State	Desired	Actual	Error
q1	0.9239	0.9216	0.0023
q2	0	-0.01	0.01
q3	0	0.0206	0.0206
q4	0.3827	0.3879	0.0052
Omega 1	0.00	-1.00E-04	1.00E-04
Omega 2	7.72E-04	7.00E-04	7.25E-05
Omega 3	7.72E-04	1.30E-03	5.28E-04

**Table 10** *State Trajectory Propagation Error with Disturbance*

A propagation interval of 15 seconds was selected for this simulation based on the open loop maneuver time and the magnitude of the disturbance torque. As before, following propagation the spacecraft state is sampled and the trajectory is re-optimized from the current state.

DIDO has internal constraints which define the accuracy with which the optimal trajectory must reach the defined end points. In order to facilitate the solution, box constraints were applied to the desired end state. These form an upper and lower bound on the end state such that an acceptable end state is  $\pm$  epsilon from the exact end state. For this simulation epsilon was set as,

$$q_e = 0.006$$
$$w_e = 0.0001$$

The end state box constraints appeared to increase computational speed. In Figure 117, the first update to the disturbed quaternion trajectory is shown and appears to complete the maneuver faster than the original undisturbed solution. This is not surprising. The open loop solution was formulated to the end point and the subsequent solution was formulated to the end point with the addition of the box constraint. Additionally, it is possible that the constant disturbance torque is initially providing some benefit to maneuver speed. However, the final closed loop state trajectories (Figure 118 and Figure 119) demonstrate that to meet the established accuracy requirements in the presence of the disturbance torque requires additional time.

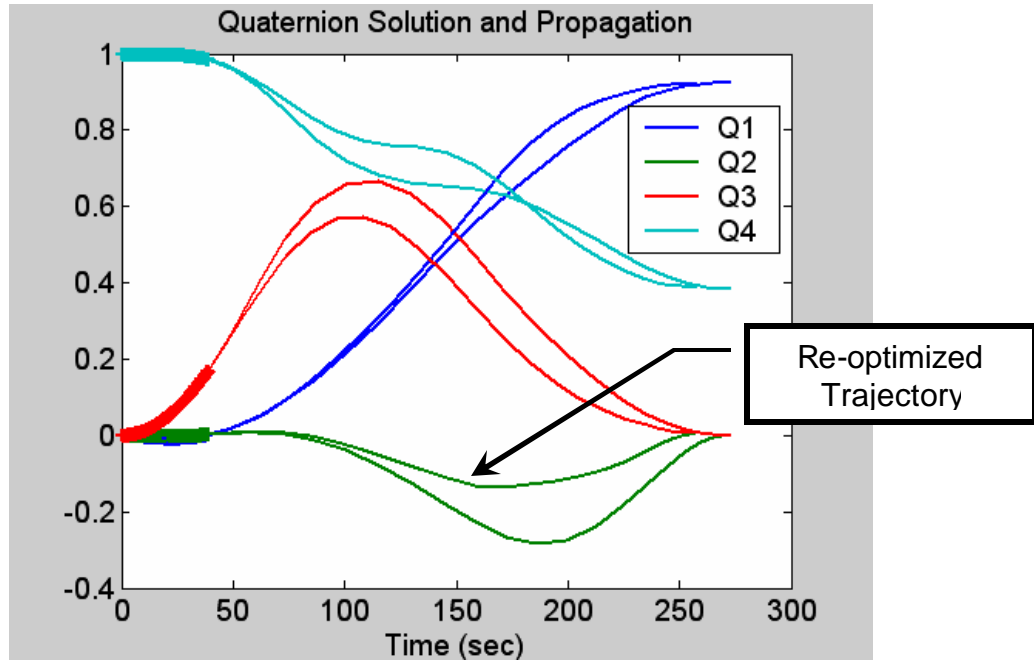


**Figure 117** *Magnetic Torque Quaternion Propagation Interval 2*

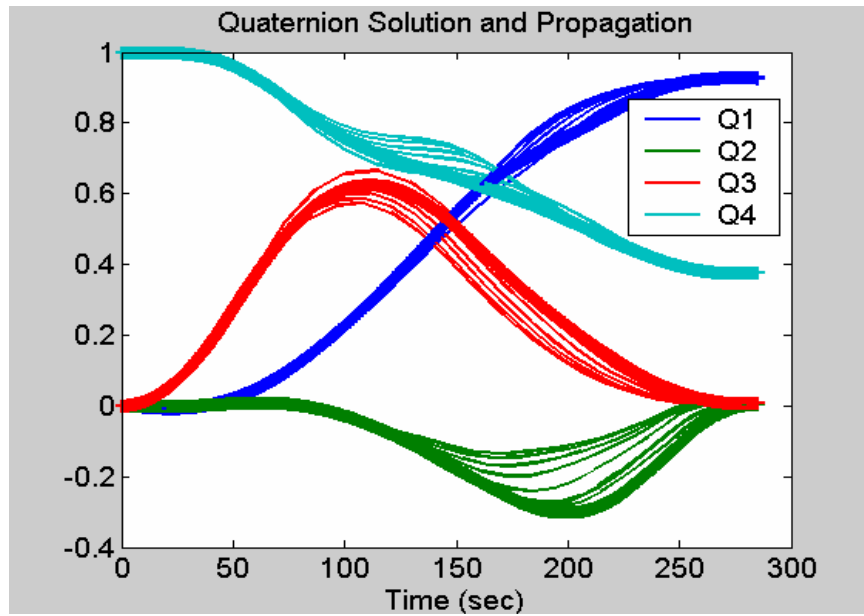


**Figure 118** *Magnetic Torque Quaternion Propagation – Maneuver Completion*

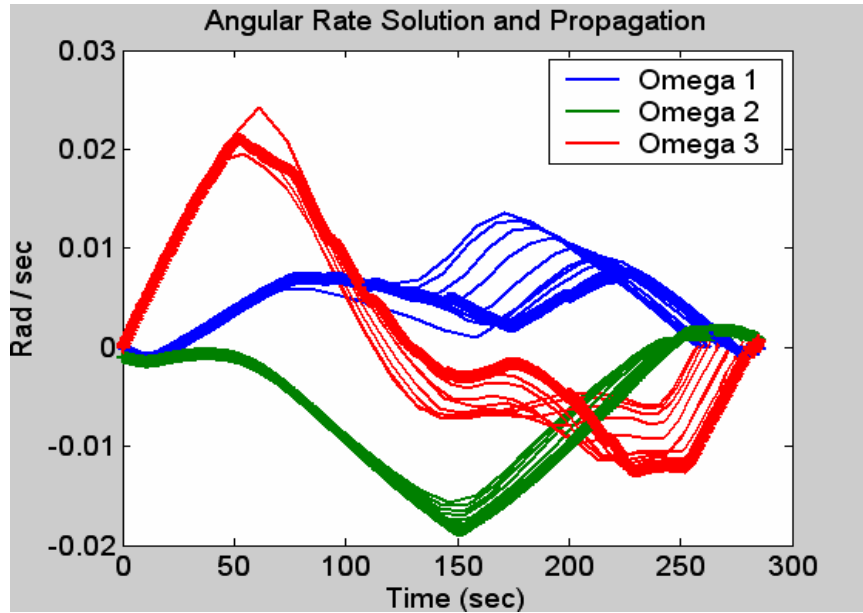


**Figure 119 Magnetic Torque Angular Rate Propagation – Maneuver Completion**

A comparison of the open loop maneuver with the disturbed closed loop maneuver shows that the disturbance increases the overall maneuver time.

The disturbance free simulation required 273.4117 seconds to complete the 135 degree x-axis slew. The close loop maneuver in the presence of the disturbance torque required 285.3174 seconds. The overall accuracy improvement is shown in Table 11. The improvement appears significant enough to warrant the application of closed loop control. Again, all subsequent solution updates met the feasibility and optimality necessary conditions that were established in Chapter IV.

<b>Closed Loop Propagation Error</b>				
State	Desired	Actual	Error	Error Reduction, %
<b>q1</b>	0.9239	0.9263	0.0024	4.35
<b>q2</b>	0	0.0042	0.0042	58.00
<b>q3</b>	0	0.006	0.006	70.87
<b>q4</b>	0.3827	0.3767	0.006	15.38
<b>Omega 1</b>	0.00	-1.00E-04	1.00E-04	0.00
<b>Omega 2</b>	7.72E-04	8.00E-04	2.75E-05	62.01
<b>Omega 3</b>	7.72E-04	7.00E-04	7.25E-05	86.26

Table 11 **Closed Loop State Propagation Results**

As before, computation time is the key to establishing the feasibility of closed loop real-time optimal control. The computation of magnetic torque time-optimal maneuvers is significantly complicated by the time-varying magnetic fields. This is illustrated by the long computation time required for the open loop solution shown in Figure 120. The open loop solution was based on a two-point guess, the end points, and calculated over 30 nodes. The subsequent solutions

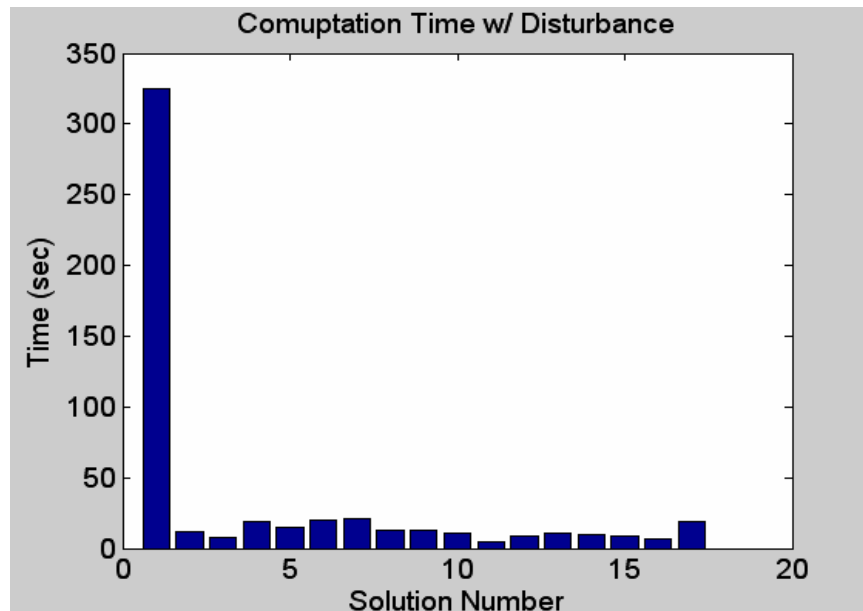


**Figure 120** *Magnetic Torque Time-optimal Maneuver Computation Time*

were also calculated over 30 nodes but used the previous state, control solution as a guess. The time required for the open loop solution was 324.9680 seconds, subsequent solutions had an average time of 12.3407 seconds. This represents a computation time reduction of 96.2 percent.

## E. CONCLUSIONS

This section has demonstrated that classical feedback control theory is ill equipped to handle time-optimal maneuvers. More recent techniques employing neighboring optimal control laws have improved slew performance but still require inverting the actuator dynamics and therefore require singularity

avoidance. By requiring that the control solution satisfy the actuator dynamic constraint equations singularity avoidance is automatically eliminated.

Strizzi et al.<sup>15</sup> noted, and engineering common sense agrees, that if open loop control solutions can be generated in real-time they become equivalent to feedback control laws. Computational power and numerical methods have come together to make this a reality.

The two numerical examples presented in this section illustrate the concept of fast and slow dynamics. In the idealized actuator example, a computational time of 10 seconds would not suffice for real-time control. However, that computation time applied to the magnetic torque example would seem an excessive requirement. The computational speed required to achieve real-time optimal control is a product of both the plant dynamics and desired performance characteristics.

Empirically it was observed that the time required to calculate the subsequent trajectories is a function of two factors, deviation from optimal trajectory and amount maneuver remaining. As the frequency at which updates are made increases, the amount of deviation from the optimal trajectory due to disturbance torques and plant uncertainties necessarily decreases. Therefore, computation time required decreases as update frequency increases. Second, as the maneuver approaches completion the computation time required asymptotically approaches a minimum value.

Using previous solutions to jump start the updated solution was shown to significantly reduce solution computation time. Further reductions in actual computation time are predicted by reducing operating system overhead and employing field programmable gate arrays.

---

## ENDNOTES

- <sup>1</sup> Wie, B., Bailey, D., and Heiberg, C. (2002). "Rapid Multitarget Acquisition and Pointing Control of Agile Spacecraft." *Journal of Guidance, Control, and Dynamics*, Vol. 25, No. 1. American Institute of Aeronautics and Astronautics, Reston, VA.
- <sup>2</sup> Ford, K.A., and Hall, C.D. (2000). "Singular Direction Avoidance Steering for Control-Moment Gyros." *Journal of Guidance, Control, and Dynamics*, Vol. 23, No. 4. American Institute of Aeronautics and Astronautics, Reston, VA.
- <sup>3</sup> Heiberg, C.J., Bailey, D., and Wie, B. (2000). "Precision Spacecraft Pointing Using Single-Gimbal Control Moment Gyroscopes with Disturbance." *Journal of Guidance, Control, and Dynamics*, Vol. 23, No. 1. American Institute of Aeronautics and Astronautics, Reston, VA.
- <sup>4</sup> Kurokawa, H. (1997). "Constrained Steering Law of Pyramid-Type Control Moment Gyros and Ground Tests." *Journal of Guidance, Control, and Dynamics*, Vol. 20, No. 3. American Institute of Aeronautics and Astronautics, Reston, VA.
- <sup>5</sup> Wie, B. (2004). "Singularity Analysis and Visualization for Single-Gimbal Control Moment Gyro Systems." *Journal of Guidance, Control, and Dynamics*, Vol. 27, No. 2. American Institute of Aeronautics and Astronautics, Reston, VA.
- <sup>6</sup> Bryson, A.E. & Ho, Y. (1975). *Applied Optimal Control*. Hemisphere Publishing. New York, NY.
- <sup>7</sup> Speyer, J.L. & Bryson, A.E. (1968). "A Neighboring Optimum Feedback Control Scheme Based on Time-to-Go with Application to Re-Entry Flight Paths." *AIAA Journal*, Vol. 6. American Institute of Aeronautics and Astronautics, Reston, VA.
- <sup>8</sup> Strizzi, J., Ross, I.M. and Fahroo, F. (2002). "Towards Real-Time Computation of Optimal Controls for Nonlinear Systems." *Proceedings of the AIAA Guidance, Navigation, and Control Conference*, Monterey, CA, August 2002, AIAA Paper No. 2002-4945.
- <sup>9</sup> Yan, H., Fahroo, F., and Ross, I.M. (2002). "Real-Time Computation of Neighboring Optimal Control Laws." *Proceedings of the AIAA Guidance, Navigation, and Control Conference*, Monterey, CA, August 2002, AIAA Paper No. 2002-4657.
- <sup>10</sup> Bryson, A.E. & Ho, Y. (1975). *Applied Optimal Control*. Hemisphere Publishing. New York, NY.
- <sup>11</sup> Sidi, M.J. (1997). *Spacecraft Dynamics and Control*. Cambridge University Press, New York, NY.
- <sup>12</sup> Wie, B. (1998). *Space Vehicle Dynamics and Control*. AIAA Education Series, American Institute of Aeronautics and Astronautics, Inc. Reston, VA.
- <sup>13</sup> Sidi, M.J. (1997). *Spacecraft Dynamics and Control*. Cambridge University Press, New York, NY.
- <sup>14</sup> Ross, I.M. (2004). *Lecture Notes in Control and Optimization*. US Naval Postgraduate School, Monterey, CA.
- <sup>15</sup> Strizzi, J., Ross, I.M. and Fahroo, F. (2002). "Towards Real-Time Computation of Optimal Controls for Nonlinear Systems." *Proceedings of the AIAA Guidance, Navigation, and Control Conference*, Monterey, CA, August 2002, AIAA Paper No. 2002-4945.

## VIII. FUTURE WORK

The work in this thesis is by no means ready for on-orbit testing. What follows are areas of improvement and future research that time precluded.

### A. ALGORITHM IMPROVEMENT AND OPTIMIZATION

This algorithm was originally conceived for large angle slew maneuvers. To that end, numerical scaling was used to adjust all parameters to within the same order of magnitude. This improved the accuracy of results and reduced computational time. However, as the spacecraft moment of inertia was varied there were conditions under which separate scaling for the angular rates of the body axes would have improved performance. A scaling format based on structure array variables<sup>1</sup> would simplify coding and allow separate scaling for each variable.

Additionally, the time scaling was designed for the initial open loop solution and held constant throughout the closed loop simulation. Therefore, as the time-to-go horizon decreased, the problem was poorly scaled in some cases. As the spacecraft state is sampled for each re-optimization the time scale should be adjusted so as to ensure that subsequent solutions are well scaled for accuracy and to reduce computational time.

Though great emphasis has been placed on computational time in the realization of real-time optimal control, the algorithms used in this work were not designed to be time-efficient. Some reconfiguration of the loops and control structure of the algorithms would undoubtedly result in additional computational speed.

Finally, though not the subject of this work, increasing the speed of the reusable software package DIDO is being investigated. Through encoding analytic Jacobian significant computational speed enhancements are possible.<sup>2,3</sup>

## B. COMPUTATIONAL DELAY MODELING

Key to the implementation of this algorithm is the computational delay associated with the solution to the optimal control problem. As shown in Figure 121 the computational delay ( $d_c$ ) is the time from when the state is observed at  $t_1$  until the time when the re-optimized control solution is available at  $t_2$ . During that time the state is continuing to propagate under the previous control solution.

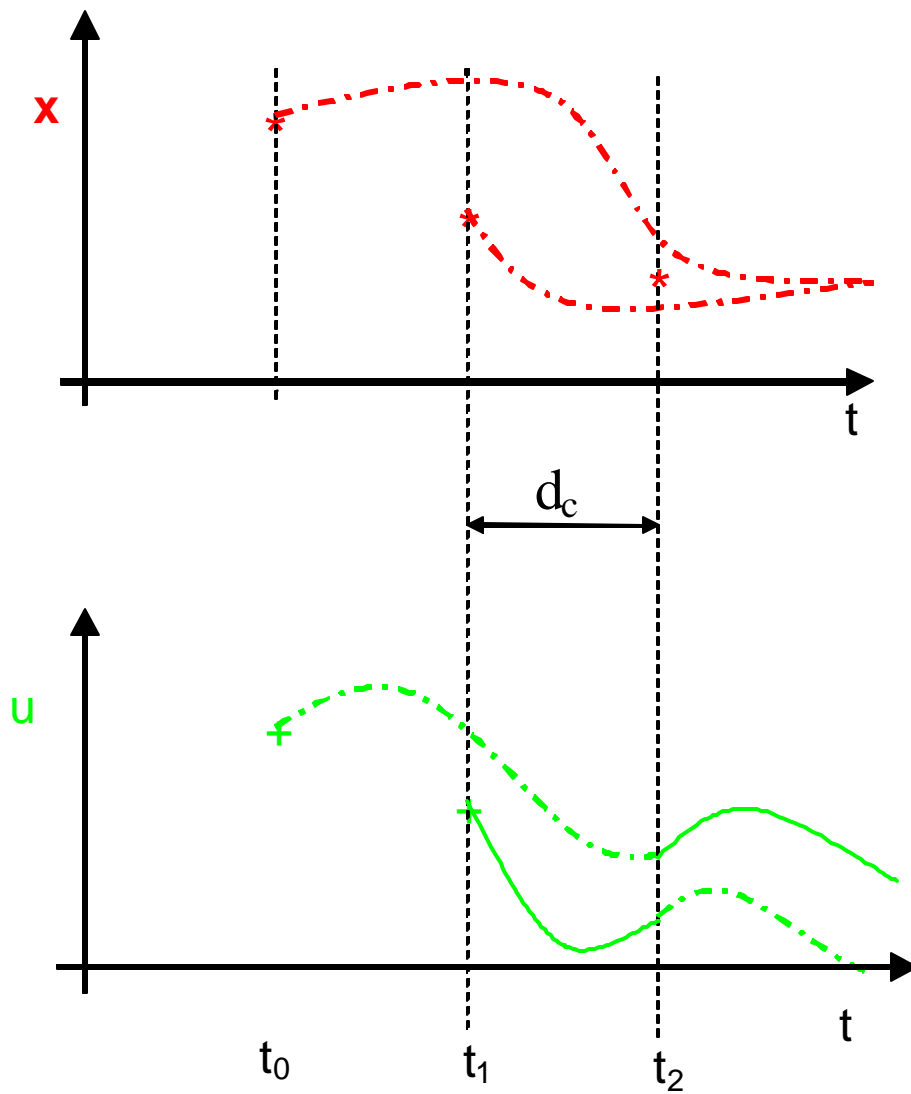


**Figure 121** *Conceptual Computational Delay Model*

Bellman's principle of optimality says that in the absence of a disturbance torque the sampled state at  $t_1$  would lie on the optimal trajectory and the updated control solution would be identical to the original solution. However, in the presence of a disturbance, the sampled state could be off the optimal trajectory and the updated control solution would not be applied until some non-zero time later. In this case, the re-optimized solution would be applied to a system whose state has propagated to another point, presumably off the re-optimized trajectory thus inducing some error into the system. In this work, the computational delay was taken to be negligibly small. In fact, the effect of the computational delay is a function of both the spacecraft dynamics and the desired performance. Numerical modeling and simulation of the effect of computational delay is necessary to determine both a sample rate and maximum acceptable computational delay.

### **C. EXTENSION TO HARDWARE**

Finally, much research is needed, and has begun, to implement these algorithms in hardware. Implementation via field programmable gate arrays (FPGA) is in ongoing. Through the efforts of others this project will see air-bearing testing and eventual on-orbit testing.

---

## ENDNOTES

<sup>1</sup> Hanselman, D. and Littlefield, B. (2001). *Mastering MATLAB 6 – A Comprehensive Tutorial and Reference*. Prentice Hall, Upper Saddle River, NJ.

<sup>2</sup> Strizzi, J., Ross, I.M., Fahroo, F. (2002). "Towards Real-Time Computation of Optimal Controls for Nonlinear Systems." *Proceedings of the AIAA Guidance, Navigation, and Control Conference*, Monterey, CA, August 2002. AIAA Paper No. 2002-4657.

<sup>3</sup> Ross, I.M. and Fahroo, F., "Issues in the Real-Time Computation of Optimal Control," *Mathematical and Computer Modeling*, An International Journal, Vol. 40, Pergamon Publication, to appear.

## INITIAL DISTRIBUTION LIST

1. Defense Technical Information Center  
Ft. Belvoir, Virginia
2. Dudley Knox Library  
Naval Postgraduate School  
Monterey, California